Next-generation reference electrodes with high potential stability towards long-term sensor measurements

by

Xinran Wang

A dissertation submitted to the graduate faculty

in partial fulfillment of the requirements for the degree of

DOCTOR OF PHILOSOPHY

Major: Electrical Engineering (Microelectronics and Photonics)

Program of Study Committee:
Meng Lu, Major Professor
Liang Dong
Jiming Song
Nathan Neihart
Michael Castellano

The student author, whose presentation of the scholarship herein was approved by the program of study committee, is solely responsible for the content of this dissertation. The Graduate College will ensure this dissertation is globally accessible and will not permit alterations after a degree is conferred.

Iowa State University

Ames, Iowa

2019

TABLE OF CONTENTS

Page

LIST OF FIGURES

Page

LIST OF TABLES

NOMENCLATURE

ISEs	Ion-Selective Electrodes
SHE	Standard Hydrogen Electrode
LJP	Liquid Junction Potential
ISM	Ion-Selective Membrane
SC	Selectivity Coefficient
PVC	Poly(Vinyl Chloride)
PVB	Poly(Vinyl Butyal)
PVA	Poly(Vinyl Alcohol)
REs	Reference Electrodes
WEs	Working Electrodes
PU	Polyurethane
PDMS	Polydimethylsiloxane
EGFET	Extended Gate Filed Effect Transistor
ISFET	Ion-Selective Field Effect Transistor
PCB	Print Circuit Board
PE	Polyethylene
THF	Tetrahydrofuran
TEC	Thermal Electric Cool
RT	Response Time

ACKNOWLEDGMENTS

This dissertation summarizes the research work during my Ph.D. program at Iowa State University. I want to thank many people who guided and supported me during this period.

First of all, I would like to thank my committee chair and major professor, Dr. Meng Lu, and my committee members, Dr. Liang Dong, Dr. Jiming Song, Dr. Nathan Neihart, and Dr. Michael Castellano, for their guidance and support throughout this research.

Second, I would like to express my deepest thanks and gratitude to Dr. Patrick Schnable and Dr. James Schnable for their wise guidance and valuable suggestions throughout the present study.

In addition, I would also like to thank my colleagues: Dr. Azahar Ali, Dr. Huaiwei Jiang, Dr. Satyanarayana Moru, Yueyi Jiao, Yang Tian, Yuncong Chen, Le Wei, Yifei Wang, and Hussam Ibrahim for their collaboration and helpful discussions. I also want to offer my appreciation and thanks to the department faculty and staff for making my time at Iowa State University an enjoyable experience.

Last, but not least, I also acknowledge with a deep sense of reverence, my gratitude towards my parents and my husband, who always support and believe me no matter what kind of dilemma I faced.

The research presented in the thesis was funded in part by the Advanced Research Projects Agency-Energy (ARPA-E), U.S. Department of Energy, under Award Number DE-AR0000824. This work was also partially supported by the United State Department of Agriculture (USDA) under the grant number 2017-67013-26463, and National Science Foundation under the grant number IOS-1650182.

ABSTRACT

Potentiometry provides a simple but powerful platform technology to determine the concentration of specific ion species in solutions and thus has been used in a wide range of applications such as industrial process control, biomedicine, agriculture, and environmental monitoring. However, the potential stability of the reference electrodes (REs) of potentiometric sensors needs to be improved for practical long-term measurement. Further improvement of their ability to counter the influences of interfering ions, pH and temperature variations are also required. Therefore, this thesis is focused on the development of several novel REs through design innovations in materials, structures, and fabrications towards the realization of next-generation potentiometric sensors.

Firstly, we developed a microfluidic channel based reference electrode (μcRE) consisting of a silver-silver chloride (Ag/AgCl) electrode embedded into a serpentine microfluidic channel, and a polymer-based porous fritz that separates the microfluidic channel from an external test cell. Due to an increased length between the Ag/AgCl electrode and the test cell, the rate of changing the concentration of chloride ion at the Ag/AgCl surface due to redox reaction is significantly reduced. The μcRE exhibited a drift rate of -37 μV/hr with only minor responses to environmental temperature and pH. The μcRE was integrated into an extended gate field-effect transistor (EGFET) to realize a potentiometric nitrate sensor that offered a sensitivity of -202.16±5.55 mV/decade to variations in nitrate concentration with 0.997 R-Squared value to its linear fitting.

Secondly, we investigated a unique fritz-less μcRE using an ultra-small orifice at the exit of microfluidic channel as a virtual fritz. The size reduction of the orifice size helped to decrease the rate of chloride loss from an embedded Ag/AgCl electrode to the

external environment, thus increasing potential stability of the reference electrode. Soft lithography technique was employed to form a 10 μm (width) × 50 μm (height) × 1 mm (length) microchannel integrated with a miniature potassium chloride reservoir. Similar to the fritz-based μcRE, this fritz-less reference electrode is little influenced by variations in temperature and pH and provides comparable performances with traditional bulky and expensive glass-body Ag/AgCl REs for potentiometric measurement.

Thirdly, we developed a planar refillable RE with double junctions that could further stabilize the reference potential of potentiometric sensors. The novel planar configuration of the double junctions, in conjunction with screen-printing and 3D printing technologies, allows both potential stabilization and electrode miniaturization. Magnets-assisted sealing allowed flexible replacing and refilling of the internal gels in the reference electrode chambers. The planar double-junction Ag/AgCl RE exhibited practical independence of chloride concentration, and high potential stability over a wide range of both temperature and pH. A drift rate of 75 μV/hr was obtained and a high linearity with 0.999 R-Squared value was demonstrated during potentiometric measurement of nitrate.

Lastly, we developed a sandwiched all-solid-state Ag/AgCl RE (S^3RE) on a silicon wafer by using standard thick-film processing technique. The S^3RE was formed by drop casting a mixture of polyvinyl butyral (PVB) and KCl as the ion-electron transductor and another layer of aromatic polyurethane (PU) as the protection layer by an automated fluid dispensing robot. The presented S^3RE showed a comparable performance with the traditional liquid-state REs, in terms of stability, chloride and pH susceptibility, and temperature. We demonstrated all-solid-state ion-selective electrode sensors using S^3RE as their reference electrodes for continuous monitoring of nitrate in both soils and plants.

CHAPTER 1. INTRODUCTION

1.1 Introduction to Potentiometry

Potentiometry is an electrochemical measurement method in which a signal is generated by an electrochemical reaction. It is widely employed to determine the concentration of a solute in a solution. Compared to many other analytical techniques, potentiometric measurement is relatively inexpensive and simple for use in both field and laboratory [1, 2].

1.1.1 General Principle of Potentiometry

Potentiometric measurement depends on electrode reactions, an electrochemical process in which charge transfer takes place at the interface between the electrode and electrolyte. A potentiometer consists of two basic functional units, i.e, a working electrode (WE), and a reference electrode (RE). The working electrode provides a potential due to the specific interaction with a targeted specie, thus serving as a receptor part to transfer the chemical information into a form of energy. The reference electrode should have a known, or at least, a constant potential value under the experimental conditions.

For normal operations, these working and reference electrodes are inserted into two different solutions connected by a salt bridge. The working electrode is immersed into a testing solution with the ion of interest, while the reference electrode is immersed into a solution of ions whose activities determine the reference electrode's potential. A voltmeter, with high impedance to eliminate net current flow so that the measuring system is under static condition, is used to measure the potential difference between these two electrodes. The Nernst equation is used to find the concentration of the ion of interest in the testing solution. Figure 1.1 illustrates a basic setup of a potentiometer.

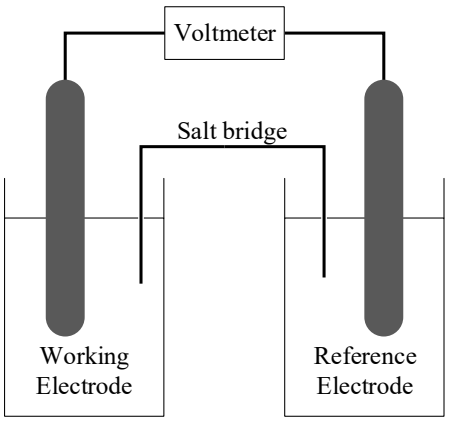

Figure 1.1 *The schematic diagram of a fundamental potentiometric measurement.*

1.1.2 Electrochemical Cells

A schematic of a typical electrochemical cell is shown in Figure 1.2, in which two half-cells are connected by a salt bridge through which ions can diffuse to maintain electroneutrality on each side and complete the electrical circuit. A spontaneous chemical reaction happens and generates electricity [3]. As an example, in Figure 1.2 the left half-cell has a zinc electrode immersed in aqueous $ZnCl_2$, while the right half-cell has a silver electrode dipped into aqueous $AgNO_3$. The salt bridge is often filled with gels containing an inert electrolyte, in this example, it is saturated aqueous KCl [4]. The two ends of the salt bridge are blocked with diaphragms, such as porous frits, which allow the electrolyte ions to freely move between the two half-cells through the salt bridge. Lastly, a voltmeter is used to measure the voltage difference between the two half-cells.

Conventionally, the left half-cell is called anode, at which oxidation occurs, and the right half-cell serves as the cathode, at which reduction occurs. The chemical reactions taking place in the exampled electrochemical cell are

Oxidation reaction: $Zn(s) \rightleftharpoons Zn^{2+}(aq) + 2e^-$ 1.1

Reduction reaction: $Ag^+(aq) + e^- \rightleftharpoons Ag(s)$ 1.2

Net reaction: $Zn(s) + 2Ag^{+}(aq) \rightleftharpoons 2Ag(s) + Zn^{2+}(aq)$ 1.3

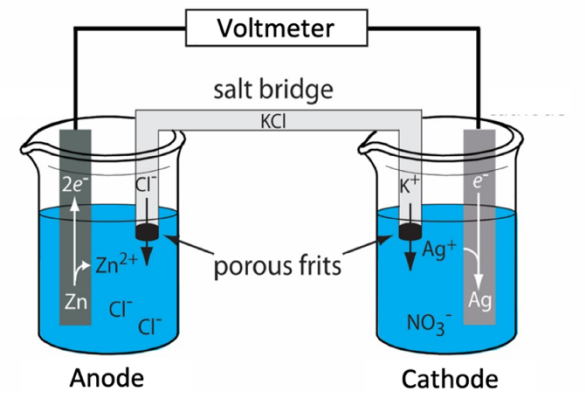

Figure 1.2 *Example of an electrochemical cell consisting of two half-cells and a salt bridge [5].*

Due to the oxidation reaction of Zn electrode at the left half-cell, aqueous Zn^{2+} is produced, and electrons flow from the Zn electrode to the Ag electrode where aqueous Ag^{+} is reduced to solid Ag through the external voltmeter. If there is no salt bridge between the two half-cells, the Zn electrode would build up positive charges due to the excess Zn^{2+}, and the Ag electrode would build up negative charges due to the depletion of Ag^{+}. Shortly, the buildup charges would prevent the chemical reaction and the process would stop. Additionally, the two electrodes in electrochemical cells cannot be placed into one solution, otherwise the electrons would directly flow from the reducing agent to the oxidizing agent without passing through the external voltmeter because the oxidation and reduction reactions could happen on the surface of one electrode.

1.1.3 Electrode Potential

The electrode potential is the electric potential difference between the left half-cell and the right half-cell of an electrochemical cell [6], which is measured by an external voltmeter. The potential is defined as:

$$E_{cell} = E_c - E_a \tag{1.4}$$

where E_c is the cathode potential (the right half-cell) attached to the positive terminal of the voltmeter, and E_a is the anode potential (the left half-cell) attached to the negative terminal. For a half-reaction:

$$aA + ne^- \rightleftharpoons bB$$

The reduction potential of a half-cell is given by the Nernst equation [3]:

$$E = E^0 - \frac{RT}{nF}\ln(\frac{[B]^b}{[A]^a}) \tag{1.5}$$

where E^0 is the standard reduction potential for each half-cell, which is measured by using the standard hydrogen electrode (S.H.E.) as the left half-cell, and the electrode of interest as the right half-cell at the standard states. The standard state means that the species are solids, liquids or their concentrations are 1 M or their pressures are 1 bar. For S.H.E. E^0 is 0 [3]. F is Faraday's constant, T is temperature in Kelvins, n is the electron's number in the reduction reaction, R is the gas constant and $\frac{[B]^b}{[A]^a}$ is defined as the reaction quotient Q ([A] and [B] is the concentration of A and B]. At 298 K temperature, equation 1.5 can be rewritten as:

$$E = E^0 - \frac{0.05916}{n}\log Q \tag{1.6}$$

It should be noticed that the Nernst equation actually is about the activity of ions, not the concentration. The activity of a species is defined as the product of the activity coefficient of the specific substance and its concentration. However, in many cases, it is impossible to calculate the activity coefficients. Also, when the species is at its standard state the activity coefficient can be approximated to 1 [3]. Therefore, the Nernst equation giving the electrode potential can be expressed in terms of ion concentration in general case.

Now we will use the potentiometric electrochemical cell in Figure 1.2 as an example to relate the electrode potential E_{cell} to the concentration of species. Using equation 1.6, the potential for each half-cell is:

$$E_c = E^0_{Ag^+/Ag} - \frac{0.05916}{1}\log\frac{1}{C_{Ag^+}} \quad 1.7$$

$$E_a = E^0_{Zn^{2+}/Zn} - \frac{0.05916}{2}\log\frac{1}{C_{Zn^{2+}}} \quad 1.8$$

where C_{Ag^+} and $C_{Zn^{2+}}$ are the concentrations of silver ion and zinc ion in the two half-cells, (pure solids, liquids, and solvent are omitted from Q). Therefore, the electrode potential of the electrochemical cell is:

$$E_{cell} = E^0_{\frac{Ag^+}{Ag}} - \frac{0.05916}{1}\log\frac{1}{C_{Ag^+}} - \left(E^0_{\frac{Zn^{2+}}{Zn}} - \frac{0.05916}{2}\log\frac{1}{C_{Zn^{2+}}}\right)$$

$$= \left(E^0_{\frac{Ag^+}{Ag}} - E^0_{\frac{Zn^{2+}}{Zn}}\right) - \frac{0.05916}{2}\log\left[\frac{C_{Zn^{2+}}}{(C_{Ag^+})^2}\right] \quad 1.9$$

The standard reduction potential for Ag and Zn are known as 0.7996 V and 0.7618 V. Therefore, the electrode potential E_{cell} only depends on the concentration of ions. If one of the concentrations of the ion is fixed and the cell potential E_{cell} could be measured, then the concentration of the other ion of interest could be calculated based on equation 1.9.

When using the Nernst equation to determine the concentration of an electrolyte, there are some limitations. Firstly, the standard reduction potential for each electrode is temperature dependent. Temperature compensation is usually needed to obtain more accurate results. Secondly, the activity coefficient would be far away from 1 when the concentration of analyte is high. This problem can be efficiently overcome by diluting the testing samples. Thirdly, additional potentials will also contribute to the cell potential E_{cell}, one of the most famous one is called liquid junction potential which is discussed in the next section.

1.1.4 Liquid Junction Potential

The liquid junction potential is the potential drop at the interface of two different ionic solutions due to the difference in concentration and mobility of ions. It can be presented by two contributions induced by heterogeneous distribution of ions and polar molecules [7]. In a single solvent, such as the potentiometric measurement, only the heterogeneous distribution was considered [8, 9], so the liquid junction potential is known as diffusion potential, which results from the fact that the space separation of charge is initially induced by diffusion.

In the potentiometric electrochemical cell, such as the examples in Figure 1.2 and 1.3, the two ends of the salt bridge are separately immersed into the electrolytes of the two half-cells. Due to the concentration difference of the solutions, the k^+ and Cl^- start to diffuse from the salt bridge tube into the electrolytes. If the mobility of k^+ is greater than that for Cl^-, the solution inside the bridge tube would have an excess of Cl^- and a negative charge. Simultaneously, the electrolyte solutions would have an excess of k^+ and a positive charge. Therefore, two liquid junction potentials are developed at the surface of two ends of porous frits. These two liquid junctions can be rather high. However, the magnitude of the salt bridge's liquid junction potential can be minimized by using salt for which the mobilities of the cation and anion are approximately equal. That is the reason why saturated KCl solution is frequently used as the salt bridge. Another suitable substance is lithium acetate, which is widely employed to form the double junction reference electrode and will be discussed in the following sections.

Thus, when we measure the electrode potential of an electrochemical cell E_{cell}, the liquid junction potentials should be also included and the equation 1.4 should be modified as

$$E_{cell} = E_c - E_a + E_j \qquad 1.10$$

From the equation 1.10, if the liquid junction potential could not be measured correctly, then the ion's concentration could not be directly calculated by using equation 1.9. In fact, in a realistic situation, we do not know the junction potential's actual value. However, as long as the liquid junction potential is constant during the experiment, the same requirement for the reference electrode potential, then its effect can be eliminated so that quantitative analytical work is still possible. For example, in practical potentiometric measurement, the potentiometer will be firstly calibrated with two known solutions containing the specie of interest, then immerse the meter in any test solutions, the concentration of the specie of interest will be calculated based on the calibration graph.

After discussing the working principle of potentiometric measurement, we would like to introduce the main components of potentiometric sensors.

1.2 Introduction to Working Electrodes (WEs)

As mentioned above, a potentiometer consists of two basic functional electrodes: a working electrode and a reference electrode, which is the main topic of this thesis and will be discussed in detail in the following contents. Two classes of indicator electrodes are used in potentiometry: metallic electrodes and ion-selective electrodes.

1.2.1 Metallic Electrodes

Electrodes **in direct contact with a solution containing its own ion** [9, 10]: If a metal M is immersed into a solution of M^+, and then the half-cell potential of this electrode is determined by the concentration (more correctly of activity) of the cation ion M^+. Like the example in Figure 1.2, the two electrodes used in the electrochemical cell are both electrodes of the kind. However, due to purity, metal oxidation, etc., the electrodes of the kind are limited

to a few metals, including Ag, Zn, Cu, Hg, Bi, Pb, Sn, Ti and Cd, and some of them cannot be used as a working electrode in acidic solutions due to possible oxidization by H^+.

Electrodes **responding to the activity of another species in equilibrium with its own cation ion** [10, 11]: This kind of electrode links the redox reaction and the solubility reaction. Because there is an equilibrium between the metal ion and the analyte, the half-cell potential for this kind of electrodes can be expressed in terms of that analyte of interest. The most common example of this type of electrode is silver-silver chloride electrodes.

Redox electrodes [12, 13]: The potential of redox electrodes usually responds to the concentration of more than one ion. For example, a platinum electrode is dipped into a solution containing Fe^{2+} and Fe^{3+}. The redox reaction takes place between Fe^{2+} and Fe^{3+}, and there is nothing to do with the inert electrode. Because the redox electrodes can respond to the activity of multiple ions, its application for potentiometry is greatly restricted.

1.2.2 Ion-Selective Electrodes (ISEs)

An ion-selective electrode (ISE) responds preferentially to one species in a solution with the help of an ion-selective membrane (ISM). A voltage difference across the ISM is produced due to the concentration difference of the selected ion inside and outside the membrane. In general, the ISM is fixed at one end of the ISEs so that the external test solution can only come into contact with the outer surface of the ISM, and the other end of the ISEs is fitted with a gold-plated pin for connection to a voltmeter. Based on the utilized material, ISEs can be grouped into three categories: glass ISEs, liquid-state ISEs, and solid-state ISEs [14, 15]. As the most important component in ISEs, we will introduce the ISM.

ISM**:** ISM is responsible for the potential response and selectivity (quantified by Selectivity Coefficient or SC). In general, there are four main types of ISM, including glass membrane, crystalline membrane, polymeric membrane and enzyme membrane [16, 17].

Glass membrane: Glass membrane is made from an ion-exchange type of glass, such as silicate or chalcogenide. It has good selectivity and excellent chemical durability; however, its application is limited to a few cations, including H^+, Na^+, Ag^+, Pb^{2+} and Cd^{2+}. The most commonly used ISEs based on the glass membrane is the pH glass electrode.

Crystalline membrane: This type of membrane is made from mono- or polycrystals of a single substance, where only the ions that can introduce themselves into the crystal structure can interfere with the electrode response; therefore, the crystalline membrane also has high selectivity. Moreover, it can be used for selecting both cation and anion. The ISEs using crystalline membranes could eliminate internal solutions, thus reducing the junction potential.

Polymeric membrane: The most widespread type of ISM is the polymeric membrane, which contains a specific ion-exchange resin. Typically, this type of membrane is made of hydrophobic organic polymer, such as poly(vinyl chloride) (PVC), and poly(vinyl butyal) (PVB) impregnated with an organic liquid containing hydrophobic anion or cation, and ligand (ionophore) which is soluble inside the membrane and selectively binds analyte cation or anion of interest. The hydrophobic ion is an ion exchanger that is soluble in the organic phase, but not in water, so it is confined to the membrane. The ionophore is chosen to have a high affinity for the analyte ion of interest and low affinity for other ions. ISEs based on the polymeric membrane can be used for detecting many different types of ions by choosing appropriate ion-exchange substances. However, polymeric membranes have relatively low selectivity, which may cause the ionic interference problem and suffer from low chemical and physical durability.

Enzyme membrane: Enzyme membrane has a double reaction mechanism. Usually, this type of membrane needs to work together with another ISE. The enzyme reacts with a specific species and the product of this reaction (usually H^+ or OH^-) is detected by the

combined ISEs, such as the pH electrode. This type of membrane is widely used in gas detection [18].

In the next section, we will use the liquid-state ISEs based on the polymeric membrane as an example to explain the working principle for the potentiometric ISEs measurement.

General principle of ISEs**:** Figure 1.3 shows a schematic diagram of a liquid-state based ISE. In this electrode, a membrane made of PVC is placed at the bottom of the working electrode which directly contact with the outside analyte solution containing the cation of interest C^+ and anion A^-. The concentration of the outside analyte is unknown. The aqueous filling solution with fixed concentration inside the electrode containing the ion of interest C^+ and anion B^-. Ideally, A^- and B^- will not affect the potential drop across the ISM due to the selectivity of the membrane.

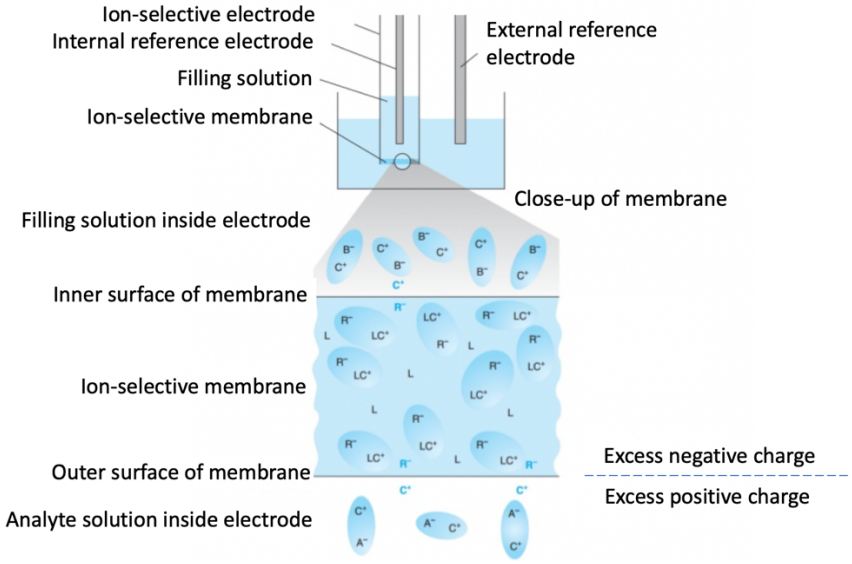

Figure 1.3 *A diagram of an ion-selective electrode immersed in aqueous solution containing analyte cation of interest C^+, ionophore L and hydrophobic anion R^- [3].*

In general, almost all the analyte ions inside the membrane are bonded with ionophore L, forming the complex pair of LC^+. Excess free L and a few amounts of free C^+ are inside the

membrane at the equilibrium state. If the concentration of C^+ inside the membrane is higher than that of C^+ outside the membrane, then the C^+ can diffuse from the membrane into the aqueous phase across the interface of the membrane, which results in an excess positive charge in the first few nanometer of the aqueous phase and simultaneously an excess negative charge in the outer few nanometers of the membrane. Therefore, an electric potential difference is produced across the membrane, which opposes the diffusion of more C^+ and then a new equilibrium is created [3, 10]. This potential drop across the membrane also contributes to the electrode cell potential, thus, equation 1.10 should be rewritten as

$$E_{cell} = E_c - E_a + E_j + E_m \tag{1.11}$$

where E_m represents the potential across the membrane, which is given by the Nernst equation

$$E_m = \frac{0.05916}{n}\log(\frac{[C^+]_{outer}}{[C^+]_{inner}}) \tag{1.12}$$

where n is the charge of the analyte ion, $[C^+]_{outer}$ is its concentration in the outer analyte solution (unknown), and $[C^+]_{inner}$ is its concentration in the inner analyte solution which is fixed. In ISEs, E_a and E_c are the internal and external reference electrodes which have constant electric potential, and we also assume that the liquid junction potential is constant at ideal case. Therefore, any change in cell potential E_{cell} is a result of a change in the membrane's potential which is determined by the concentration of analyte ion outside the ISEs.

In the following contents, all the potentiometric sensors discussed, without no special mention, will refer as the ISE-based potentiometric sensors and for simplify, we will call them ISE sensors.

1.2.3 State-of-art ISE sensors

The ISEs were presented for the first time in 1906 [14] after the discovery that there was a potential change across a glass membrane when its two sides were exposed to two

different solutions with different acidity. This discovery led to the development of a totally new class of working electrodes, called ISEs. Since the first practical ISEs was invented in 1932 [20], a pH-sensitive electrode based on a glass membrane, ISEs entered the period of rapid development, especially the 1960s and 70s, in this two decades ISEs experienced an exponential growth due to a new discovery that some antibiotics [21-23] and compounds [24] are able to selectively bind with some particular ions through appropriate synthesizing. At that time a new word 'ionophore' was created, which is still in use today. The development of ionophore extremely expanded the usage of ISEs. Suitable sensitivity and quick response time made the ISEs become a significant tool in clinical analysis [25]. After a short sleep time [2], ISEs welcomed a second spring of life. The revolution of ISEs took place in the late 1990s and early 2000s. It was realized the determination of selectivity coefficient and limits of detection was underestimated. [14, 26] Consequently, selectivity and sensitivity were improved by up to 6 orders of magnitude by slight alteration of the experimental protocols, without any additional instrumentation updates [27-29, 59], which led the ISE sensors to one of the most attractive analyzing tools. ISE sensors, traditionally unbeatable in terms of low-cost, simplicity, robustness and power consumption have been further improved through the development of solid-state technology [30-33] and more recently nanotechnology. In the last twenty years ISEs have gone through another revolution period. The state of the art and current development activities can be characterized by 1) miniaturization of sensors; 2) development of new and improved sensor materials; 3) application of multi-sensor setups and sophisticated measuring procedure; 4) development of fast response sensors; and 5) development of all-solid-state ISEs.

1.3 Introduction to Reference Electrodes (REs)

The reference electrode is one half-cell with a fixed composition in a potentiometric electrochemical cell. Ideally, it should provide a stable and known potential so that any change in the net cell potential E_{cell} in equation 1.10 will be only contributed to the analyte's effect on the potential of the working electrode. Therefore, REs have to meet several requirements for their reference potential: 1) stable and reproducible; 2) independent of the composition of other ions in the testing analytes; 3) insensitive to changes in local pH, temperature, and concentration of redox species [34]. Even though numerous efforts have been made to improve the performance of ISEs, REs have not always been paid attention with the same intensity despite the important role of REs in potentiometric sensors.

1.3.1 Importance of REs

It is generally accepted that long-term stability of ISE sensors used for determination of aqueous ions is significantly determined by the potential stability of REs [34]. Without a suitable reference electrode, none of the above-mentioned advantages of ISEs, such as simplicity, fast response, portable, robustness and low-cost, can be gained. There has been a considerable interest in the development of miniature electrochemical sensors for biomedical and environmental monitoring. However, insufficient stability of the sensing interface has imposed a major issue in electrochemical sensors [35, 36-37]. For example, ±1mV potential change would result in a ±4% change in the estimated activity for a monovalent ion and ±8% for a divalent one [38]. Although improving the performance of ISEs is the eternal theme for potentiometry, it is recognized that the real challenge is REs, because without a reference to compare against, the response of any other type of ISEs is meaningless [39-41].

1.3.2 Types of REs

Different types of REs have been developed in terms of different metal materials and different structures. In general, they can be grouped into two categories: conventional liquid-state and solid-state REs.

Conventional liquid-state REs

Standard hydrogen electrode: The standard hydrogen electrode (SHE) is a primary reference in electrochemical area. All the standard reduction potentials for other types of REs are measured against the SHE at the same temperature. The SHE potential is set to 0V.

A common design of SHE is shown in Figure 1.4. It consists of a catalytic Pt wire or plate, the surface of which is in contact with an acidic solution in which the concentration of H^+ is 1 M. A stream of hydrogen gas (1 bar) continues bubbling over the Pt surface [42] where the following reaction takes place:

$$H^+(ag, 1\ M) + e^- \rightleftharpoons \frac{1}{2}H_2(g, 1\ bar)$$

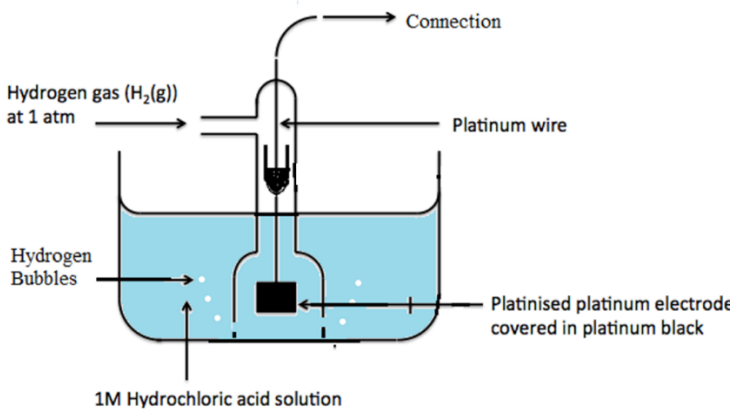

Figure 1.4 *Schematic representation of the platinum SHE [42].*

In most cases, the hydrogen gas needs to continuously flowing from a hydrogen generator or gas cylinder to the metal plate in the acid solution, which makes the handling and

maintenance of SHE cumbersome. Therefore, the applications of the SHE are restricted to only several ones, such as for characterizing other REs.

Silver-silver chloride electrode: The most common REs is the Ag/AgCl electrode due to its advantages, including simplicity, capacity and stability [43]. The conventional Ag/AgCl RE has a relatively simple structure, as shown in Figure 1.5. A silver wire coated with silver chloride paste is immersed into a saturated or 3.5 M potassium chloride solution. A porous plug, such as a glass frit at the base of the electrode works as a salt bridge to allow ion exchange. In most cases, high concentration of KCl solution is chosen as the inner filling analyte, which will bring three advantages: 1) the chloride and potassium ions have similar high ion mobilities which will reduce the liquid junction potential [6]; 2) high ion mobilities will ensure a low impedance path for ionic current between the inner and external solutions which improve the transient response of the sensor [41]; and 3) the chloride concentration does not change even though some of the liquid evaporates if saturated KCl solution is chosen [3].

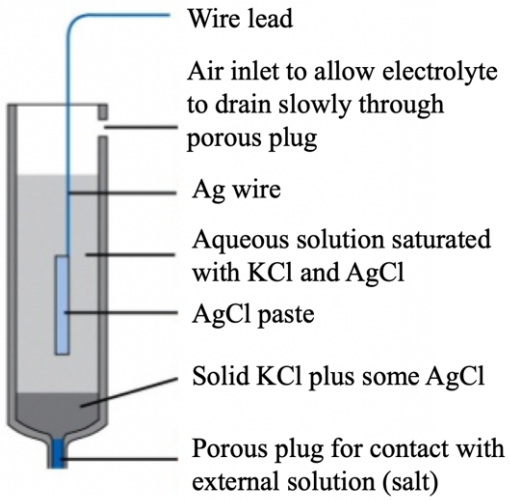

Figure 1.5 *Schematic of silver-silver chloride reference electrode (Quantitative Chemical Analysis, Seventh Edition @ 2007 W.H.Freeman and Company).*

The reaction happens on the electrode is $A_gCl(s) + e^- \rightleftharpoons A_g(s) + Cl^-(aq)$, and the electrode potential at 25°C is given by the Nernst equation

$$E_{Ag/AgCl} = E_{Ag/AgCl}{}^0 - 0.05916 \log(C_{Cl^-}) \quad 1.13$$

where $E_{Ag/AgCl}{}^0$ is the standard reduction potential of the silver-silver chloride electrode at 25°C (constant) and C_{Cl^-} represents the concentration of free chloride ions (at moderate concentration activity can be replaced by concentration, previously discussed). With 3.5 M KCl inner filling solution, the potential value of the Ag/AgCl RE is close to 0.205 V at 25 °C.

Because the net reaction on the surface of Ag/AgCl electrode depends on the solubility of AgCl in KCl solution, which means the temperature has big influence on the potential value of Ag/AgCl RE. Therefore, the Ag/AgCl RE needs a careful control of the working conditions.

Calomel electrode: Calomel RE contains a pure mercury wire and a sparing soluble mercury salt, such as Hg_2Cl_2 [44]. Figure 1.6 shows a typical construction. There are two glass tubes, an inner tube contains a paste of mercury and mercury chloride dispersed in a saturated KCl solution is situated within an outer tube containing saturated KCl solution. Glass wool is filled at the bottom of the inner tube to allow electrical contact and a porous plug is placed at the bottom of the outer tube to serve as a salt bridge.

The reaction happens on the electrode is

$$Hg_2Cl_2(s) + 2e^- \rightleftharpoons 2Hg(s) + 2Cl^-(aq)$$

The electrode potential at 25°C is given by the Nernst equation

$$E_{Hg/Hg_2Cl_2} = E_{Hg/Hg_2Cl_2}{}^0 - \frac{0.05916}{2} \log(C_{Cl^-})^2 \quad 1.14$$

where $E_{Hg/Hg_2Cl_2}{}^0$ is the standard reduction potential of standard potential Hg/Hg_2Cl_2 electrode at 25°C (constant) and C_{Cl^-} represents the concentration of free chloride ions. With

the saturated KCl inner filling solution, the potential value of the calomel RE is close to 0.268 V at 25°C.

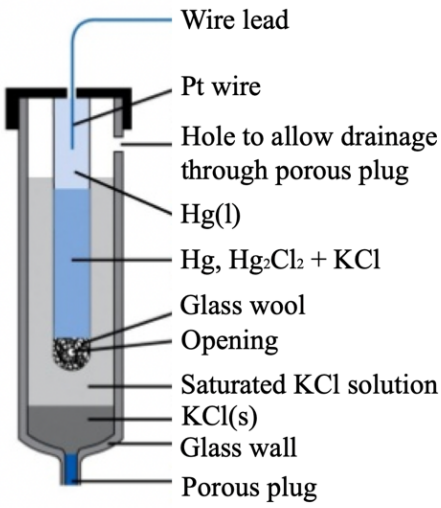

Figure 1.6 *Schematic diagram of saturated calomel electrode constructions (Quantitative Chemical Analysis, Seventh Edition @ 2007 W.H.Freeman and Company).*

While calomel electrodes are not widely used due to the environmental compatibility issue, its advantages include insensitivity to light and relatively high reproducibility [45]. The calomel electrode also has a high dependence on temperature.

Besides the three commonly used REs mentioned above, other REs include silver-silver bromide electrode, silver-silver iodide electrode, mercury-mercury sulfate electrode, mercury-mercury sulfide electrode, thallium-thallium chloride electrode, iodine-iodide electrode, silver-silver oxide electrode and mercury-mercury electrode.

Although the performances of the conventional REs have been proved sound in many practical applications, some drawbacks related to the use of the aqueous inner filling solution in these electrodes have restricted their applications: 1) the concentration of electrolyte ions, which determine the electrode potential, can easily vary due to the outflow of the ions through the porous plug; 2) the use of glass tube makes it mechanical fragile and hard for device

miniaturization; 3) the liquid filling solution makes it impossible for high temperature and high pressure applications. Therefore, considerable efforts have been paid to develop another kind of reference electrode, namely solid-state reference electrode.

Advanced solid-state REs

For a long time, combining solid-state working electrodes with equivalent reference electrodes to take fully advantage of the liquid absence sensing system has been an attractive topic in potentiometry. The term 'solid-state' is interpreted by different people. In this thesis, we define the solid-state electrode as an electrode in which no aqueous inner filling solution existed. In this section, we will discuss a few typical solid-state REs.

Gel-solidified RE: In conventional REs, the electrolyte salts (mostly, KCl) are dissolved into deionized (DI) water to form the inner filling solution in which the concentration of Cl^- determines the potential of the reference electrode. If the electrolyte salts are dissolved into gels (agar and gelatin [46-48]), then the electrode is identified as gel-solidified RE. These sealers can form a relatively raw network so that the electrolytes can freely move and interact within the gel's framework. Compared with the aqueous filling solutions, the gel fillings have higher temperature stability (up to 130 ^oC without melting) and higher pressure resistance [45].

The gel-solidified REs generally have a shorter lifetime than the conventional REs with the aqueous filling solutions, which is caused by the limited and non-refillable electrolytes in the gels. Because the existence of flexibiliser in gels, the amount of solvable electrolyte salts is largely limited. Therefore, the concentration of electrolyte in the gel fillings is much lower than that of in aqueous solutions. However, the gel-solidified REs have nearly identical and highly reproducible potentials. Moreover, the maintenance of the type of REs becomes easy due to the reduced outflow of electrolyte to the outside of electrode.

Polymer-solidified RE: If inserting the electrolyte salts into strong hardening polymers, such as polyvinyl chloride, polyvinyl alcohol, polyvinyl butyral, polyethylene, epoxy resins and vinylesters, then the electrodes are called polymer-solidified REs (Figure 1.7). In addition to the same advantages with the gel-solidified REs, the polymer-solidified REs have a planar structure that makes it suitable for miniaturization, and can provide higher temperature stability and pressure tolerance [34, 48-50]. However, the polymer-solidified REs also have the issue of the loss of electrolyte due to its low content.

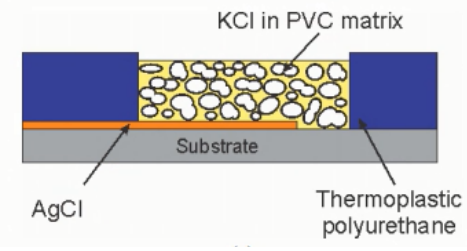

Figure 1.7 *A schematic illustration of a solid-state reference electrode based on PVC which premixed with KCl [51].*

In the example shown in Figure 1.7, the electrode AgCl was screen printed on the substrate of polyethylene terephthalate foil and then a thick thermoplastic polyurethane (TPU) layer was patterned to form a reservoir for the solid inner electrolyte which is plasticized PVC premixed with KCl. The KCl crystals were uniformly distributed inside the PCV mixture. After immersing this reference electrode into testing solution, the KCl crystals can partially dissolve due to the quick penetration of the solution into the solid contact layer, which provides a stable chloride concentration around the AgCl electrode resulting in a stable reference electrode potential. However, due to the small amount of KCl contained in the PVC, the long-term stability of this RE is relatively shorter than that of the liquid- or gel-state REs.

All-solid-state RE: An all-solid-state RE, also called liquid-junction free electrode, consists of a metallic wire in close contact with a mixed ionic electronic conductor. A porous

plug is not needed in this type of electrodes. A typical design [52] is shown in Figure 1.8, where ionic liquid (1-dodecyl-3-methylimidazolium chloride) was premixed with plasticized PVC membrane. After the evaporation of all the solvents, the solid contact is formed between the outer analyte solution and the metal layer.

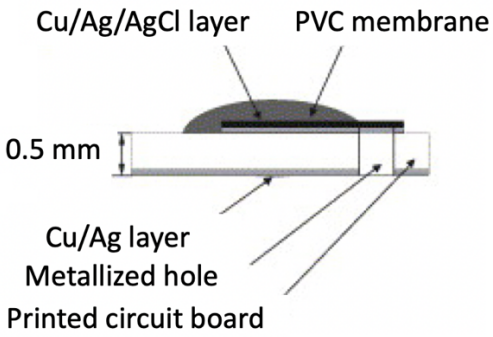

Figure 1.8 *A schematic cross-section view of the all-solid-state reference electrode [52].*

As the matter of fact, the solid contact of all-solid-state REs make it easy to design planar-structure devices or miniaturized sensors by employing microsystem technology. The absence of liquids or solidified liquids allows the measurements into broader temperature and pressure ranges. However, one main problem in the all-solid-state REs is to connect the ionic conducing solution with the electronic conductor. To maintain a stable and constant electrode potential, the redox reaction of the components in the electrolyte (solid contact) must be avoided or at least reduced. Therefore, an electrode material with mixed ionic and electronic conductivity is required. Suitable materials include oxides, mixed oxides and salts of oxo-anions of the transition elements.

The investigation of all-solid-state references is still in an early state. Although several examples of solid contacts using mixed conductors were reported [53-57], the understanding of electrode processes is insufficient. Basic research on electrochemical kinetics is necessary

to clarify the role of charge carriers in the mixed conductor, such as the concentration of ions and electrons, their mobility and the exchange processes between the surface of solids and dissolved ions.

1.3.3 State-of-Art REs

The Ag/AgCl reference electrode with aqueous 3 M KCl inner filling solution has been proved as a powerful but delicate referencing structure that requires careful control of the working conditions. The imperfection of this type of reference electrode is due to the use of aqueous electrolyte solutions. Therefore, many methods have been proposed to replace this aqueous inner filling solutions to form a solid-state reference electrode, such as dissolving KCl crystal in gels [45-51]. Nevertheless, the gel-state electrodes are not suitable for all kinds of potentiometric measurements. The most promising approach reported so far involves coating a polymer membrane containing ionic liquid or mixed oxides and salts on the top of a screen-printed Ag/AgCl electrode [34, 58-64]. The membrane has a high and constant chloride concentration. Many planar solid-state REs have been fabricated using microsystems technologies, showing good performance in terms of stability and reproducibility. But these solid-state electrodes are not free from interferences caused by other species and leakage of chloride ions. Therefore, an additional membrane, made from materials such as polyacrylate microspheres, Nafion, polypyrrole microcapsules, etc., is used to serve as a protection layer to increase the stability of the potential and reduce the interferences from other species. Recently, all-solid-state REs have attracted much attention due to their all solid-state features favorable for miniaturization and integration, although batch reproducibility needs to be optimized. [48, 50, 52, 57]. Designing and manufacturing of miniature planar REs with high performance and cost efficiency are still an ambitious challenge.

1.4 Applications of Potentiometric Sensors

A potentiometric sensor with a working electrode which only responds to the activity of hydrogen ions is defined as the pH electrode. The most widely used pH electrode is the glass combination electrode with a silver-silver chloride reference electrode, shown in Figure 1.9. As the most widely employed ISEs, the pH membrane of the sensor has high sensitivity and selectivity, which means that the activity measurement of H^+ is not likely to be affected by other interfering ions. Additionally, the pH depends on the order of magnitude of the concentration rather than the precise values, therefore, the pH electrode has more error tolerance compared with other ISEs [65-68].

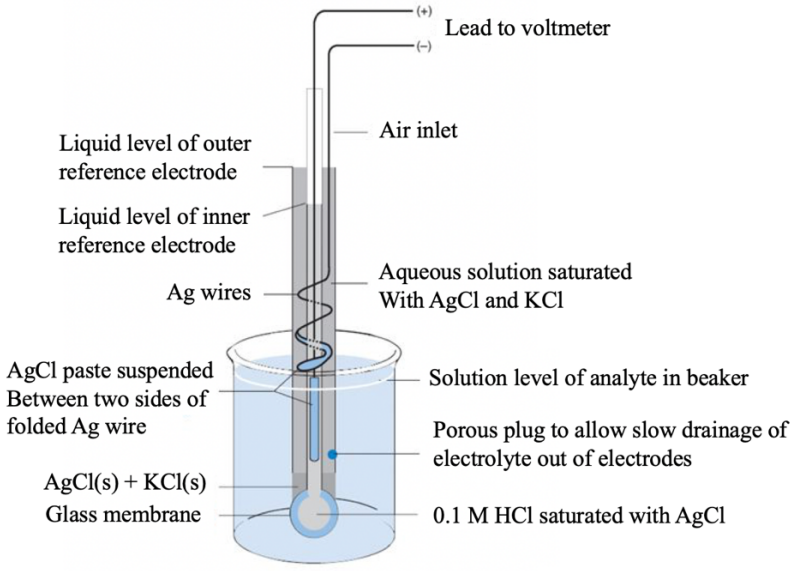

Figure 1.9 *Glass combination electrode with a silver-silver chloride reference electrode (Quantitative Chemical Analysis, Seventh Edition @ 2007 W.H.Freeman and Company).*

The ability of ISEs to directly sense analytes in complex matrices and fast turnaround time allow many traditional laboratory testings to move closer to the patient for improved patient care. They are routinely used for the determination of electrolytes in body fluids (blood,

plasma, serum and sweat), such as potassium (K) [69, 70], sodium (Na) [71], calcium (Ca) [72], chloride (Cl) [73], lithium (Li) [74-76], and glucose [77]. For medical applications, the ISEs face many challenges such as reliability, sample size, throughput, stability, selectivity, lifetime, miniaturization, etc. [78-80].

ISE sensors have been used to optimize the management of agriculture inputs to increase the profitability of crop production and protect the environment. The most popular application for ISEs in agriculture is to measure key macronutrients in soils, such as K, phosphorus (P), and nitrogen (N) [81-89].

In addition to the above-mentioned applications, ISEs can be used to monitor environmentally important traces of species in water and food productions [90-95].

1.5 Problems, Objective, Goal and Approach

ISE-based potentiometric sensors represent a simple, rapid and accurate analytical approach to measure ionic constituents in complex samples. While the selectivity and detection limit of ISEs have been improved by orders of magnitude to detect micromolar and even nanomolar concentration of specific targets, long-term measurements using ISEs is a challenge due to the inability of the current REs to provide stable potentials under different environments (e.g., temperature, pH, compositions of test solutions, etc.). Without a reference potential to compare against, any potentiometric measurement would be meaningless. Despite the progress in the development of REs, we are still far away from practical long-term measurement applications and there are many limitations and challenges to be overcome.

1.5.1 Problems to Be Solved

The first problem that needs to be solved is instability of REs. The conventional glass body REs with aqueous inner filling solutions have better stability compared to solid-state REs.

Therefore, almost all commercial REs use aqueous electrolyte solutions. Some of the liquid-state sensors have a second liquid junction to form double junction REs, thus reducing the effect of the instable liquid junction on potential stability. These traditional REs, however, are quite expensive (e.g., $100-200 each unit) and bulky in general. These limitations become evident in the development of compact, stable, and cost-effective potentiometric sensors.

The second problem relates to the miniaturization of REs. The tendency of developing new ISE sensors for an increasing number of applications for field measurements (e.g., point-of-care medical diagnosis, and on-site environmental monitoring) requires miniaturizing ISE sensors further. Although planar solid-state REs [58-64] represents a promising approach to sensor miniaturization, achieving long-term stability for this type of REs remains challenging.

The third problem relates to the high manufacturing cost of REs that have hindered mass production of REs. This limitation is a major issue for many applications that require a large number of ISE sensors for increasing spatial resolution [96]. Recently, screen-printed sensors using a thick-film technology provide a possible solution for this problem.

The last problem relates to the anti-interference ability of REs to other species existing in analyte solutions. Because the potential of Ag/AgCl REs is determined by the chloride ion concentration, any outflow or inflow of Cl^- through the liquid junction will change the electrode potential resulting in REs' instability. In addition, the leakage of Cl^- from the inner filling solutions of REs may contaminate the analyte solutions because of the introduction of interfering ions onto the ISEs.

1.5.2 Objectives and Basic Approaches of This Thesis

The goal of this dissertation is to develop novel REs with improved stability, miniaturization, cost-effectiveness, and anti-interference through new designs, materials, and structures.

The first objective is to develop a microfluidics-based Ag/AgCl RE with a miniature polymer frit at the exit of a long serpentine channel filled with gelatin containing KCl. Due to an increased diffusion length between the Ag/AgCl electrode and the testing samples, the changing rate of the concentration of chloride ion at the electrode surface is significantly reduced, thus the long-term stability of the presented microfluidics-based Ag/AgCl RE can be effectively improved. Also, due to the microfluidics channel structure, a long diffusion path can be easily obtained in a limited volume. Owing to easy manufacturing, cost efficiency and high long-term stability, this electrode could be a possible alternative to traditional glass body Ag/AgCl REs with similar performances.

The second objective is to develop a miniaturized frit-free Ag/AgCl RE by using a microfluidic channel with an ultra-small orifice serving as a virtual frit. Traditional soft lithography technique is employed to form the microchannel integrated with a miniature potassium chloride reservoir made from polydimethylsiloxane (PDMS). Similar to the frit-based μcRE, the leaching rate of chloride ions from the mini KCl reservoir to the external solutions can be effectively reduced due to the ultra-small virtual frit so that good potential stability and high resistance to the environmental changes can be achieved. The performance exhibited by the presented frit-free Ag/AgCl reference electrode should be comparable with traditional bulky and expensive glass-body Ag/AgCl REs for potentiometric measurements.

The third objective is to develop a refillable planar Ag/AgCl reference electrode with double junction. The stability and anti-interference ability of this planar Ag/AgCl RE is further improved by introducing a second liquid junction with lithium acetate (CH_3COOLi) in which CH_3COO^- and Li^+ have similar ion mobility so that the liquid junction and the ion contamination from the filling electrolyte can be effectively suppressed. Screen-printing and

3D printing techniques are utilized to make the novel planar reference electrode. Flexible replacing and refilling the internal gels electrolyte can be easily accomplished by using four pairs of mini magnets. The planar structure can be easily integrated with solid-state ISEs to build a miniature ISE sensor with good performance.

The fourth objective of this thesis is to develop a sandwiched all-solid-state Ag/AgCl reference electrode (S^3RE). By using the thick-film manufacturing technology and an automatic dispensing robot, a miniature S^3RE can be formed by coating the functional materials (e.g. Ag/AgCl paste, PVB mixed with KCl and PU) layer-by-layer. The micro-scale feature of the S^3RE is suitable for some specific applications. Therefore, a miniature ISE sensor for continuous monitoring of nitrate in both soils and plants is going to be built to demonstrate the performances of the presented S^3RE.

References

1. Stanic, Z., and Stella Girousi. "Carbon paste electrodes in potentiometry: the state of the art and applications in modern electroanalysis (A review)." *Sens. Electroanal* 6 (2011): 89-128.

2. Bakker, Eric, and Ernö Pretsch. "Modern potentiometry." *Angewandte Chemie International Edition* 46.30 (2007): 5660-5668.

3. Harris, Daniel C. *Exploring chemical analysis*. Macmillan, 2012.

4. Grønneberg, Truls, Lise Kvittingen, and Per-Odd Eggen. "Small-scale and low-cost galvanic cells." *Journal of chemical education* 83.8 (2006): 1201.

5. Chemistry LibreTexts™: Potentiometric Methods. https://chem.libretexts.org/Courses/Northeastern_University/11%3A_Electrochemical_Methods/11.2%3A_Potentiometric_Methods.

6. Inzelt, György, Andrzej Lewenstam, and Fritz Scholz. Handbook of reference electrodes. Heidelberg: Springer, 2013.

7. Izutsu, Kosuke. "Liquid junction potentials between electrolyte solutions in different solvents." *Analytical Sciences* 27.7 (2011): 685-685.Izutsu K (2008) Bull Chem Soc Jpn 81:703.

8. Izutsu, Kosuke. "Liquid Junction Potential between Electrolyte Solutions in Different Solvents: Some Consideration on the Component Due to Solvent–Solvent Interactions." *Bulletin of the Chemical Society of Japan* 83.1 (2009): 39-41.

9. Generalic, Eni. "Electrode of the first kind." *Croatian-English Chemistry Dictionary & Glossary*. 20 Oct. 2018. KTF-Split. 28 Apr. 2019. <https://glossary.periodni.com>.

10. Koryta, Jiří, Jiří Dvořák, and Ladislav Kavan. *Principles of electrochemistry*. John Wiley & Sons Inc, 1993.

11. Mirčeski, Valentin, et al. "Electrocatalysis of the first and second kind: Theoretical and experimental study in conditions of square-wave voltammetry." *Electrochimica Acta* 55.28 (2010): 8696-8703.

12. Peiffer, Stefan, et al. "Redox measurements in aqueous solutions—a theoretical approach to data interpretation, based on electrode kinetics." *Journal of contaminant hydrology* 10.1 (1992): 1-18.

13. Thévenot, Daniel R., et al. "Electrochemical biosensors: recommended definitions and classification." *Analytical Letters*34.5 (2001): 635-659.

14. Radu, Aleksandar, et al. "Ion-selective electrodes in environmental analysis." (2013).

15. A. J. Bard and L. Faulkner (2000). *Electrochemical Methods: Fundamentals and Applications*. New York: Wiley. ISBN 978-0-471-04372-0.

16. Buck, Richard P., and E. Lindner. "Recommendations for nomenclature of ionselective electrodes (IUPAC Recommendations 1994)." *Pure and Applied Chemistry* 66.12 (1994): 2527-253.

17. Schaefer, Tim, and Detlef Dieball. "Electrochemical energy storage device with data transmission, arrangement and method." U.S. Patent Application No. 14/079,372.

18. Cortón, Eduardo, et al. "Potentiometric determination of CO2 concentration in the gaseous phase: applications in different laboratory activities." *Journal of Chemical Education* 77.9 (2000): 1188.

19. Pranitis, David M., et al. "Potentiometric ion-, gas-, and bio-selective membrane electrodes." *Critical Reviews in Analytical Chemistry* 23.3 (1992): 163-186.

20. Frant, Martin S. "Historical perspective. History of the early commercialization of ion-selective electrodes." *Analyst* 119.11 (1994): 2293-2301.

21. Stefanac, Z., and W. Simon. "Highly selective cation electrode systems based on in-vitro behavior of macrotetrolides in membranes." *Chimica* 20 (1966): 436-440.

22. Pioda, Lavinia AR, et al. "Komplexe von Nonactin und Monactin mit Natrium-, Kalium- und Ammonium-Ionen." *Helvetica Chimica Acta* 50.5 (1967): 1373-1376.

23. Lutz, W. K., H. K. Wipf, and W. Simon. "Alkali-cation specificity and carrier qualities of the antibiotics nigericin and monensin." *Helvetica chimica acta* 53.7 (1970): 1741-1746.

24. Frant, M-S_, and J. W. Ross. "Potassium ion specific electrode with high selectivity for potassium over sodium." *Science* 167.3920 (1970): 987-988.

25. vitro Diagnostics, In. "Market (Applications, End-users & Types) Trends & Global Forecasts (Major & Emerging Markets-G7, Japan & BRIC)." *Markets and Markets* (2011).

26. Bakker, Eric, Philippe Bühlmann, and Ernö Pretsch. "Polymer Membrane Ion-Selective Electrodes–What are the Limits?." *Electroanalysis: An International Journal Devoted to Fundamental and Practical Aspects of Electroanalysis* 11.13 (1999): 915-933.

27. Sokalski, Tomasz, et al. "Large improvement of the lower detection limit of ion-selective polymer membrane electrodes." *Journal of the American Chemical Society* 119.46 (1997): 11347-11348.

28. Bobacka, Johan, Ari Ivaska, and Andrzej Lewenstam. "Potentiometric ion sensors." *Chemical reviews* 108.2 (2008): 329-351.

29. Radu, Aleksandar, and Dermot Diamond. "Ion-selective electrodes in trace level analysis of heavy metals: potentiometry for the XXI century." *Comprehensive analytical chemistry* 49 (2007): 25-52.

30. Guinovart, Tomàs, et al. "A reference electrode based on polyvinyl butyral (PVB) polymer for decentralized chemical measurements." *Analytica chimica acta* 821 (2014): 72-80.

31. Cadogan, Aodhmar, et al. "All-solid-state sodium-selective electrode based on a calixarene ionophore in a poly (vinyl chloride) membrane with a polypyrrole solid contact." *Analytical Chemistry* 64.21 (1992): 2496-2501.

32. Sutter, Jolanda, et al. "A polypyrrole-based solid-contact Pb 2+-selective PVC-membrane electrode with a nanomolar detection limit." *Analytical and Bioanalytical Chemistry* 380.1 (2004): 7-14.

33. Sutter, Jolanda, et al. "Solid-contact polymeric membrane electrodes with detection limits in the subnanomolar range." *Analytica Chimica Acta* 523.1 (2004): 53-59.

34. Guth, U., et al. "Solid-state reference electrodes for potentiometric sensors." *Journal of Solid State Electrochemistry* 13.1 (2009): 27-39.

35. Zuliani, Claudio, and Dermot Diamond. "Opportunities and challenges of using ion-selective electrodes in environmental monitoring and wearable sensors." *Electrochimica Acta* 84 (2012): 29-34.

36. Tercier-Waeber, Mary-Lou, and Martial Taillefert. "Remote in situ voltammetric techniques to characterize the biogeochemical cycling of trace metals in aquatic systems." *Journal of Environmental Monitoring* 10.1 (2008): 30-54.

37. Tercier-Waeber, Mary-Lou, and Martial Taillefert. "Remote in situ voltammetric techniques to characterize the biogeochemical cycling of trace metals in aquatic systems." *Journal of Environmental Monitoring* 10.1 (2008): 30-54.

38. Unwin, Patrick R., Martin Stratmann, and Allen J. Bard. *Encyclopedia of Electrochemistry: Instrumentation and Electroanalytical Chemistry; Volume 3*. Wiley-vch, 2003.

39. Sophocleous, Marios, and John K. Atkinson. "A review of screen-printed silver/silver chloride (Ag/AgCl) reference electrodes potentially suitable for environmental potentiometric sensors." *Sensors and Actuators A: Physical* 267 (2017): 106-120.

40. Bard, Allen J., et al. *Electrochemical methods: fundamentals and applications*. Vol. 2. New York: wiley, 1980.

41. Atkinson, J. K., et al. "An investigation into the effect of fabrication parameter variation on the characteristics of screen-printed thick-film silver/silver chloride reference electrodes." *Microelectronics International* 28.2 (2011): 49-52.

42. Redefining Knowledge.
https://hemantmore.org.in/science/chemistry/reference-electrodes/14561/

43. Plieth, W. J., and A. J. Bard. "Encyclopedia of Electrochemistry of the Elements." *by AJ Bard, Marcel Dekker, Inc. New York* 8 (1978).

44. Hills, G. J., and D. J. G. Ives. *The calomel electrode and other mercury-mercurous salt electrodes*. Academic Press: New York, 1961.

45. Dörfler, Hans-Dieter. *Grenzflächen und kolloid-disperse Systeme: Physik und Chemie*. Springer, 2002

46. Vonau W, Gabel J, Teichmann P, Lange R (2000) DE10047825

47. Vonau W, Bachmann T, Gabel J, Lange R (2002) pH-Elektroden für den Einsatz in der Prozesschemie und Biotechnologie. In: Baselt JP, Gerlach G (eds) Dresdner Beiträge zur Sensorik, Vol. 12: Sensoren im Fokus neuer Anwendungen. Verbraucherschutz und Lebensmittelkontrolle, Biosysteme und Nanobiotechnologie, Umweltmesstechnik, neue Sensormaterialien, Mess-und Eichwesen. w.e.b. Universitätsverlag, Dresden, pp 13–16.

48. Vonau, W., et al. "An all-solid-state reference electrode." *Sensors and Actuators B: Chemical* 144.2 (2010): 368-373.

49. Blaz, Teresa, Jan Migdalski, and Andrzej Lewenstam. "Junction-less reference electrode for potentiometric measurements obtained by buffering pH in a conducting polymer matrix." *Analyst* 130.5 (2005): 637-643.

50. Kisiel, Anna, et al. "All-solid-state reference electrodes based on conducting polymers." *Analyst* 130.12 (2005): 1655-1662.

51. Dam, Van Anh T., Martijn Goedbloed, and Marcel AG Zevenbergen. "Solid-Contact Reference Electrode for Ion-Selective Sensors." *Multidisciplinary Digital Publishing Institute Proceedings*. Vol. 1. No. 4. 2017.

52. Mamińska, Renata, Artur Dybko, and Wojciech Wróblewski. "All-solid-state miniaturised planar reference electrodes based on ionic liquids." *Sensors and Actuators B: Chemical* 115.1 (2006): 552-557.

53. Chou JC, Tzeng DJ (2007) US 20070155037

54. Young-Chul, Lee, and Sohn Byung-Ki. "Development of an FET-type reference electrode for pH detection." *Journal of Korean Physical Society* 40 (2002): 601.

55. Han, Ji-Hyung, et al. "Solid-State Reference Electrode Based on Electrodeposited Nanoporous Platinum for Microchip." *Electroanalysis: An International Journal Devoted to Fundamental and Practical Aspects of Electroanalysis* 19.7-8 (2007): 786-792.

56. Chudy, Michal, Wojciech Wróblewski, and Zbigniew Brzózka. "Towards REFET." *Sensors and Actuators B: Chemical* 57.1-3 (1999): 47-50.

57. Kwon, Nak-Hyun, et al. "An all-solid-state reference electrode based on the layer-by-layer polymer coating." *Analyst* 132.9 (2007): 906-912.

58. Cranny, Andrew, et al. "Screen-printed potentiometric Ag/AgCl chloride sensors: Lifetime performance and their use in soil salt measurements." *Sensors and Actuators A: Physical* 169.2 (2011): 288-294.

59. Sophocleous, Marios, and John K. Atkinson. "A review of screen-printed silver/silver chloride (Ag/AgCl) reference electrodes potentially suitable for environmental potentiometric sensors." *Sensors and Actuators A: Physical* 267 (2017): 106-120.

60. Andreescu, Silvana, et al. "Screen-printed electrode based on AChE for the detection of pesticides in presence of organic solvents." *Talanta* 57.1 (2002): 169-176.

61. Carrara, Sandro, et al. "Screen-printed electrodes based on carbon nanotubes and cytochrome P450scc for highly sensitive cholesterol biosensors." *Biosensors and Bioelectronics* 24.1 (2008): 148-150.

62. Musa, Arnaud Emmanuel, et al. "Disposable Miniaturized Screen-Printed pH and Reference Electrodes for Potentiometric Systems." *Electroanalysis* 23.1 (2011): 115-121.

63. Glanc, M., et al. "The effect on performance of fabrication parameter variations of thick-film screen printed silver/silver chloride potentiometric reference electrodes." *Sensors and Actuators A: Physical* 197 (2013): 1-8.

64. Glanc, M., et al. "The effect on performance of fabrication parameter variations of thick-film screen printed silver/silver chloride potentiometric reference electrodes." *Sensors and Actuators A: Physical* 197 (2013): 1-8.

65. Cremer, Max. *Über die Ursache der elektromotorischen Eigenschaften der Gewebe, zugleich ein Beitrag zur Lehre von den polyphasischen Elektrolytketten*. R. Oldenbourg, 1906.

66. Cremer, M. "The cause of the electromotor properties of tissue, and a contribution to the science of polyphasic electrolytes." *Zeitschrift Fur Biologie* 29 (1906): 562-608.

67. Haber, Fritz, and Z. Hlemensiewicz. "Über elektrische phasengrenzkräfte." *Zeitschrift für physikalische Chemie* 67.1 (1909): 385-431.

68. NICO 2000.
http://www.nico2000.net/Book/Guide4.html

69. Lev, A. A., and W. McD Armstrong. "Ionic activities in cells." *Current topics in membranes and transport*. Vol. 6. Academic Press, 1975. 59-123.

70. Pioda, Lavinia AR, V. Stankova, and W. Simon. "Highly selective potassium ion responsive liquid-membrane electrode." *Analytical Letters* 2.12 (1969): 665-674.

71. Eisenman, George, Donald O. Rudin, and James U. Casby. "Glass electrode for measuring sodium ion." *Science*126.3278 (1957): 831-834.

72. Ross, James W. "Calcium-selective electrode with liquid ion exchanger." *Science* 156.3780 (1967): 1378-1379.

73. Coetzee, C. J., and Henry Freiser. "Anion-responsive electrodes based on ion association extraction systems." *Analytical Chemistry* 40.13 (1968): 2071-2071.

74. Zhukov, A. F., et al. "Improved lithium ion-selective electrode based on a lipophilic diamide as neutral carrier." *Analytica Chimica Acta* 131 (1981): 117-122.

75. Imato, Toshihiko, Masahiro Katahira, and Nobuhiko Ishibashi. "Effects of concentration of neutral carrier and addition of organophosphorus compounds on alkali metal ion-selectivity of the dibenzo-14-crown-4 liquid-membrane electrode." *Analytica Chimica Acta* 165 (1984): 285-289.

76. Kitazawa, Sadaya, et al. "Lithium-selective polymeric membrane electrodes based on dodecylmethyl-14-crown-4." *Analyst* 110.3 (1985): 295-299.

77. Mullen, William H., et al. "Glucose enzyme electrode with extended linearity: Application to undiluted blood measurements." *Analytica chimica acta* 183 (1986): 59-66.

78. Oesch, Urs, Daniel Ammann, and Wilhelm Simon. "Ion-selective membrane electrodes for clinical use." *Clinical Chemistry* 32.8 (1986): 1448-1459.

79. Lewenstam, Andrzej, Magdalena Maj-Zurawska, and Adam Hulanicki. "Application of ion-selective electrodes in clinical analysis." *Electroanalysis* 3.8 (1991): 727-734.

80. Simon, W., et al. "Ion-Selective Electrodes and Their Clinical Application in the Continuous Ion Monitoringa." *Annals of the New York Academy of Sciences* 428.1 (1984): 279-285.

81. Farrell, Richard Edmond. "Development and application of potentiometric methods of charcterizing potassium in soils and micaceous minerals." (1985).

82. Cattrall, R. W., S. Tribuzio, and Henry Freiser. "Potassium ion responsive coated wire electrode based on valinomycin." *Analytical chemistry* 46.14 (1974): 2223-2224.

83. Fassel, V. A. "International Union of Pure and Applied Chemistry. Analytical Chemistry Division. Commission on Spectrochemical and Other Optical Procedures for Analysis. Nomenclature, symbols, units and their usage in spectrochemical analysis. II. Data interpretation.(Rules approved 1975)." *Analytical Chemistry* 48.14 (1976): 2294-2296.

84. Covington, Arthur K., and Alastair Sibbald. "Encapsulated chemoresponsive microelectronic device arrays." U.S. Patent No. 4,502,938. 5 Mar. 1985.

85. Adamchuk, V. I., et al. "Direct measurement of soil chemical properties on-the-go using ion-selective electrodes." *Computers and Electronics in Agriculture* 48.3 (2005): 272-294.

86. Santos, Emília MG, et al. "Ion-selective electrodes based on metalloporphyrins for gibberellic acid determination in agricultural products." *Analytical and bioanalytical chemistry*375.4 (2003): 511-516.

87. Kim, Hak-Jin, et al. "Simultaneous analysis of soil macronutrients using ion-selective electrodes." *Soil Science Society of America Journal* 71.6 (2007): 1867-1877.

88. Milham, P. J., et al. "Analysis of plants, soils and waters for nitrate by using an ion-selective electrode." *Analyst* 95.1133 (1970): 751-757.

89. Kim, Hak-Jin, Kenneth A. Sudduth, and John W. Hummel. "Soil macronutrient sensing for precision agriculture." *Journal of Environmental Monitoring* 11.10 (2009): 1810-1824.

90. De Marco, Roland, Graeme Clarke, and Bobby Pejcic. "Ion-selective electrode potentiometry in environmental analysis." *Electroanalysis: An International Journal Devoted to Fundamental and Practical Aspects of Electroanalysis* 19.19-20 (2007): 1987-2001.

91. Murray, Royce, ed. "Challenges in environmental analytical chemistry." (2010): 1569-1569.

92. Zuliani, Claudio, and Dermot Diamond. "Opportunities and challenges of using ion-selective electrodes in environmental monitoring and wearable sensors." *Electrochimica Acta* 84 (2012): 29-34.

93. Lin, M-J., M. J. Lewis, and A. S. Grandison. "Measurement of ionic calcium in milk." *International Journal of Dairy Technology* 59.3 (2006): 192-199.

94. On-Nom, N., A. S. Grandison, and M. J. Lewis. "Measurement of ionic calcium, pH, and soluble divalent cations in milk at high temperature." *Journal of dairy science* 93.2 (2010): 515-523.

95. Upreti, Praveen, Lloyd E. Metzger, and Philippe Bühlmann. "Glass and polymeric membrane electrodes for the measurement of pH in milk and cheese." *Talanta* 63.1 (2004): 139-148.

96. Yantasee, Wassana, et al. "Electrochemical sensors for the detection of lead and other toxic heavy metals: the next generation of personal exposure biomonitors." *Environmental health perspectives* 115.12 (2007): 1683-1690.

CHAPTER 2. SILVER-SILVER CHLORIDE REFERENCE ELECTRODE WITH SERPENTINE MICROFLUIDIC CHANNEL

A paper published at the Transducers 2019/EUROSENSORS XXXIII Conference

Xinran Wang, Yang Tian, Le Wei, and Liang Dong

Abstract

This paper reports a low-cost silver-silver chloride (Ag/AgCl) reference electrode (RE) incorporating a 3D printed serpentine microfluidic channel (μcRE). The μcRE is integrated with a MOSFET to form an extended gate filed effect transistor (EGFET) to enhance potential stability for long-term measurement. The results show that the longer diffusion length between the internal Ag/AgCl element and external analyte solutions, the slower concentration change of the chloride ion at the Ag/AgCl surface, thus resulting in improved stability of the μcRE. The μcRE exhibits a -37 μV/hr long-term drift rate with low sensitivity to changes in environmental chloride ion concentration and temperature. The EGFET nitrate sensor adopting the μcRE offers a high sensitivity of -202.16±5.55 mV per decade across a wide concentration range from 0 to 2000 ppm with 0.997 R-Squared value related to its linear fit.

2.1 Introduction

For a silver-silver chloride (Ag/AgCl) reference electrode (RE), the reaction occuring on the electrode can be described as $A_gCl(s) + e^- \rightleftharpoons A_g(s) + Cl^-(aq)$. According to the Nernst equation (1.13), the potential at the RE at 25 °C is described as $E_{Ag/AgCl} = {E_{Ag/AgCl}}^0 - 0.05916\log(C_{Cl^-})$ (see the detailed description in Section 1.3.2). To obtain a stable reference potential $E_{Ag/AgCl}$, the chloride ion concentration at the electrode needs to be constant. While

commercial glass-body aqueous Ag/AgCl REs have different shape and size, they all use high-concentration or saturated potassium chloride (KCl) solution as the inner filling electrolyte solution to react with the internal reference element for producing a stable reference potential. Also, the porous plug at the bottom of the glass body functions as a salt bridge that allows all ions to diffuse between the inner filling electrolyte solution and the analyte solution with minimal mixing. These commercial REs can provide a relatively stable reference potential but suffer from high cost and difficulty in integration and miniaturization.

This work reports a low-cost RE incorporating a zigzag microfluidic channel to improve the potential stability at the RE for long-term measurement. The microfluidic channel contains an Ag/AgCl electrode at the end of the channel, and is filled with gelatin premixed with a 1 M-concentration KCl electrolyte solution. A mini polyethylene (PE) frit is inserted into an 800 μm-diameter hole through the thin wall that separate the channel from a sample test cell. Essentially, due to osmosis, the chloride ions in the KCl electrolyte solution is leaching from the channel through the frit into the sample test cell. However, the chloride ion concentration around the Ag/AgCl electrode won't get affected unless the chloride ions leach for a long time. The long channel thus will help to increase the potential stability over time. The proposed μcRE also has a small footprint size, compared to the commercial bulky REs using a glass tube.

Further, this μcRE is applied in an extended-gate field effect transistor (EGFET) to form an ion-selective electrode (ISE)-based potentiometric sensor. The sensor consists of an ISE sensor and a metal-oxide semiconductor field-effect transistor (MOSFET) [1]. The difference between the EGFET-based ion sensor and the ion-selective field effect transistor (ISFET) is the location of ion-selective membrane. For the EGFET-based sensor, the MOSFET

is designed as part of a readout circuit and only the ion-selective membrane contacts the analyte solution. Also, in contrast to the ISFET, no extra semiconductor fabrication process is needed for the EGFET by integrating a commercial low-cost MOSFET. Thus, using the EGFET to structure the sensor can not only reduce the fabrication cost of the sensor but also minimize the influences of temperature, light and erosion by the testing solutions on the characteristics of MOSFET since the MOSFET is not in direct contact with the samples [2]. Therefore, combining the EGFET and the μcRE will make the sensor suitable to continuously monitor changes of ion concentration.

2.2 Sensor Structure and Manufacturing

2.2.1 Structure of Electrode

The presented EGFET-based ion sensor is composed of a 3D-printed serpentine channel with an embedded Ag/AgCl electrode, a PE-based mini frit with a mean pore size of 20 μm, a test sample cell, a working electrode (WE), and a printed circuit board (PCB) with a readout electronic circuit. The schematic of the sensor is shown in Figure 2.1. A printed zigzag channel is embedded in a printed case with the dimensions of 22 mm (length) × 22 mm (width) × 5 mm (height). The printed circuit board consisting of a commercial MOSFET (STL42P6LLF6) and an operational amplifier (LM358DT) is attached to the bottom of the printed case to form the EGFET. A four-turn channel is chosen for the proposed μcRE, as a result of the trade-off between the long-term stability and fabrication simplicity, which will be discussed in 2.3.1.

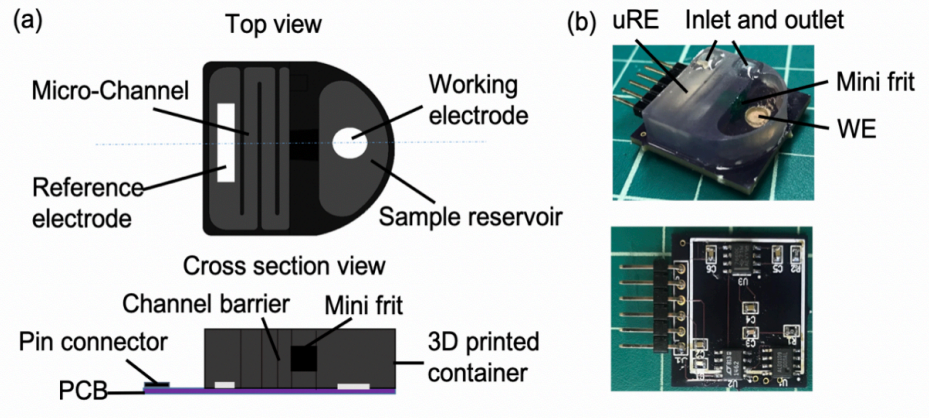

Figure 2.1 *(a) Schematic of the EGFET ion sensor integrating a RE with 3D printed zigzag micro-fluidic channel and (b) sensor photo with PCB on the backside.*

As a demonstration, the WE was functionalized with a nitrate ion-selective membrane. A potential difference between the WE and RE is converted to a current change using the MOSFET, processed by a home-made data logger, and then transmitted to a smartphone through Bluetooth, shown in Figure 2.2.

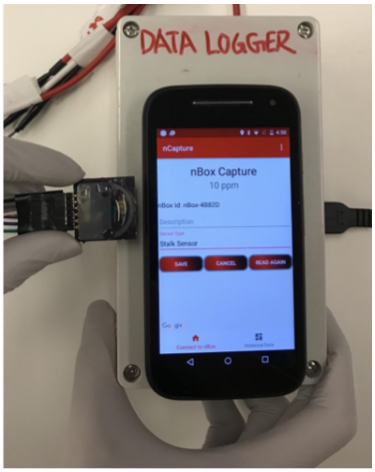

Figure 2.2 *Photo of the EGFET sensor and the home-made data logger.*

2.2.2 Materials and Manufacturing

Materials

Methyltriphenylphosphonium bromide, polyvinyl chloride (PVC), nitrocellulose, 2-nitrophenyl octyl ether, tetrahydrofuran, tridodecylmethylammonium nitrate, and PE frit were

purchased from Sigma Aldrich. Ag/AgCl ink (comprised finely dispersed chloridized silver flakes) was purchased from Fisher Scientific. Deionized water (DI) was obtained from a Millipore™ purification system and utilized for all experiments. Potassium nitrate (KNO_3) and KCl were obtained from Fisher Scientific. Gelatin was purchased from Walmart. All electronic components and epoxy (CircuitWorks, CW2500) were purchased from Digi-key.

Electrodes preparation

Ag/AgCl paste was screen-printed on the surface of the rectangle-shaped (10 mm length × 2 mm width) and round-shaped (3-mm-diameter) conducting pads on the PCB, and then was cured at 110 °C for 30 min. The thickness of the screen-printed Ag/AgCl electrode (290 μm [13]) was controlled by the thickness of the stencil used here. The 3D-printed case with microfluidic channel [14] was assembled with the PCB using epoxy. The mini frit was inserted into a lateral hole to separate the inner filling electrolyte electrode from the test solution.

The inner filling gelatin was prepared by dissolving 0.5 g gelatin powder into 2 ml volume of 1M KCl solution by water bath at 100 °C. Constant stirring until the gelation powder thoroughly dissolved into the KCl solution, then the mixture was immediately injected into the channel via an inlet. Care was taken to avoid trapping air bubbles inside the channel before the gelatin solidified. A small outlet was required for air to escape from the channel. Both the inlet and outlet were sealed by epoxy at last.

Here the channel was designed to be 900 μm wide and 20 mm long and filled with the inner KCl electrolyte solution. The increasing distance between the Ag/AgCl electrode and the analyte solution minimized the variations of chloride ion concentration around the Ag/AgCl electrode, while still maintaining the ionic conductivity. By this way, a long-lasting reference

potential could be achieved. The device is shown in Figure 2b, where the WE and RE were formed on the same side of the PCB, while the other side contains other electronic components.

The nitrate ion-selective membrane was prepared. The cocktail of the ion-selective membrane contained methyltriphenylphosphonium bromide (0.25 wt. %), nitrocellulose (moistened with 2-propanol (35%); 1.93 wt. %), 2-nitrophenyl octyl ether (16.25 wt. %), polyvinyl chloride (5.75 wt. %), tetrahydrofuran (74.3 wt. %), and tridodecylmethyl-ammonium nitrate (1.50 wt. %) [15]. This membrane used an ionophore-doped PVC and was drop-cast on the top of the Ag/AgCl electrode working as the WE. The WE was further pre-conditioned in a 2000 ppm $NO3^-$-N solution for 12 hours. This step was shown crucial to minimize the response of the WE to other non-targeted ions such as Cl^- and $NH4^+$ [16, 17].

2.2.3 Instrumentation

The electronic circuit on the PCB contains two main components, including a MOSFET (ALD110900SAL) and an operational amplifier (LT1462CS8) as shown in Figure 2.3a. Here, a potential difference between the working and reference electrodes was generated due to the concentration difference between the sample solution and the gel-state inner filling electrolyte solution. This generated potential was converted to a change in current through an external MOSFET circuit, and then was read and recorded by a home-made data logger.

The home-made data logger circuit consists of a power module, a readout circuit module, a microcontroller module, and a data transmission module. The flow chart of the circuit is shown in Figure 2.3b, where the orange, blue, and black arrows represent power transmission, data transmission, and general connections, respectively. The power module provides power for the whole sensor system. The readout circuit captures the voltage potential coming from the sensor electrodes, and then transmits the signal to the microcontroller for data

processing. The processed data can be either stored into a micro SD card or be wirelessly transmitted by the Bluetooth module.

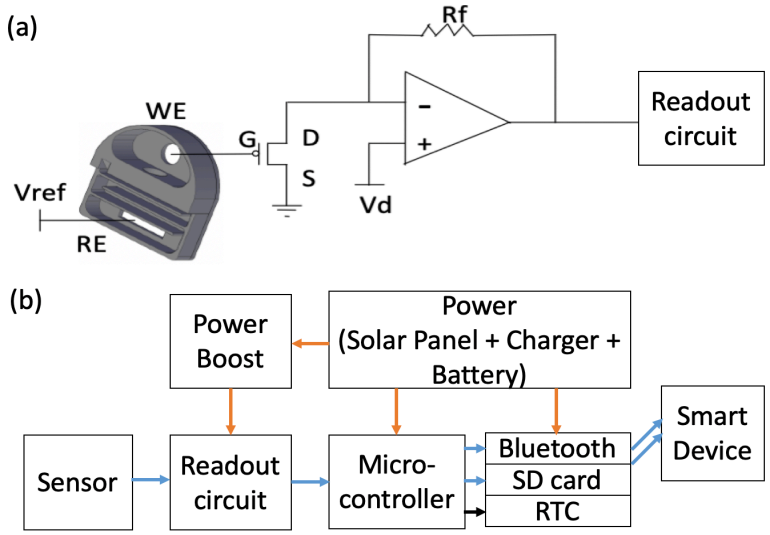

Figure 2.3 *(a) Schematic of the circuit diagram for the EGFET and (b) flow chart of the home-made datalogger used for data reading, recording and transmission.*

2.3 Results and Discussion

As a comparison, all the experiments were conducted for both non-channel (nc)- and µc-structured RE. The two REs are identical except for the inner structure inside the 3D printed case.

2.3.1 Simulation Results

A finite element analysis (FEA) method was used to simulate the variations of chloride ion concentration for nc and µc- structured electrolyte containers. The initial Cl^- concentration inside the gelatin was set to 1 M, and the temperature was set to 24 °C. The simulation was conducted for three different types of designs, including nc, with a two-turn and a four-turn µc- structured electrolyte containers. The simulation results in Figure 2.4 firstly show the Cl^- concentration inside the three containers at the initial (day 0) and the 30th day. Then a 30-day

continuous change of Cl^- concentration at the Ag/AgCl electrodes were obtained for the three types of containers.

For the nc-based RE, the Cl^- concentration near the RE started decreasing after a few hours, and after 15 days the Cl^- was run off; for the two-turn μc-based RE, the Cl^- concentration could remain constant for 1 day and then depleted to almost zero after 15 days; while for the four-turn μc-based RE, the Cl^- concentration remained constant for 3 days, and after 30 days the remaining Cl^- concentration was still about half of the initial concentration. Therefore, the longer distance between the RE element and the test solution, the longer constant time the Cl^- concentration near the RE resulting in a longer stable time of RE. However, more than four-turn serpentine channels were difficult to print out, because the solvent of the printed materials tended to be trapped inside the channels and thus could not be washed out even under a vacuum condition. Therefore, our channel design chose four turns.

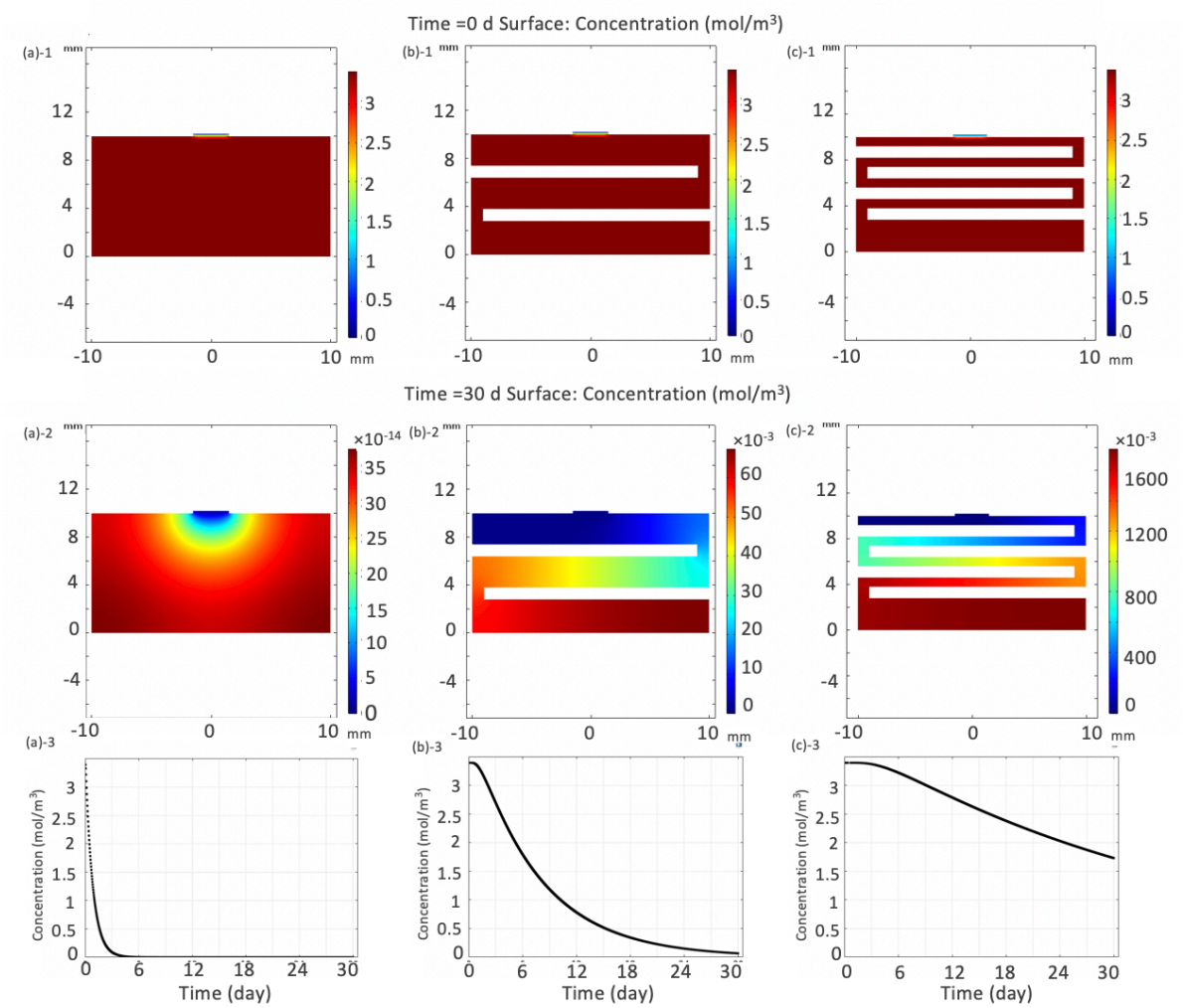

Figure 2.4 *Simulation results of the Cl^- concentration inside the nc (a), 2-turn µc (b) and 4-turn µc structured (c) RE containers. (a)-1, (b)-1 and (c)-1 are the initial concentration status (day 0); (a)-2, (b)-2 and (c)-2 are the 30th-day results, and (a)-3, (b)-3 and (c)-3 are the Cl^- concentration change at the RE point for 30 days.*

2.3.2 Chloride Susceptibility

To study the chloride ion susceptibility of the µcRE (also known as the sensitivity to Cl^- concentration in the analyte solution), the electrical potentials of the nc- and µc-based REs were measured individually against a commercial calomel double junction-based RE (HANNA Instruments; Model HI5414; containing 3.5 M KCl inner filling electrolyte). The experiments

were performed in a series of KCl solutions containing 10^{-6} M, 10^{-5} M, 10^{-4} M, 10^{-3} M, 10^{-2} M, 10^{-1} M and 1.0 M concentration of Cl^-. Before switching to the next test solution, both the nc- and µc-based REs were thoroughly rinsed in DI water and air dried to remove residual chloride solutions. The test time was 5 min for each test solution. All the measurements were conducted at 24 °C.

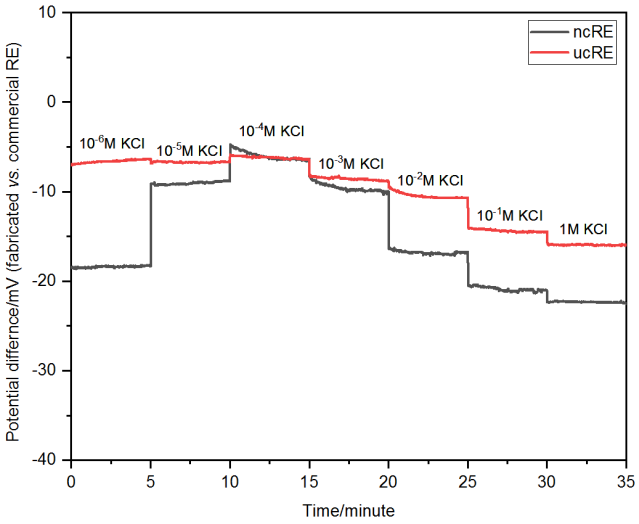

Figure 2.5 *Reference potential against the base potential provided by a commercial calomel double junction RE a function of time in different KCl solutions from 10^{-6} to 1M.*

From the results shown in Figure 2.5, the potential of the µcRE against the commercial calomel RE is practically independent of Cl^- concentration, and the absolute values of the slope is lower than 1 mV dec^{-1} from 1×10^{-6} M to 1 M KCl solutions. While for the ncRE, within the same KCl range, the absolute values of slope is about 4.2 mV dec^{-1}. Therefore, the µcRE exhibits a less susceptibility to the external Cl^- concentration, compared to the ncRE, which results from using the long serpentine channel that helps to decelerate the reduction of Cl^- concentration around the embedded Ag/AgCl.

2.3.3 Response Time

Response time (RT) of a RE is generally defined as the time interval required to obtain a stable electrical potential when the RE is moved from one to another solution having a different chloride ion concentration. RT can be affected by the electrode type, temperature, magnitude and direction of the concentration change, and hysteresis, etc. [18]. The RT of the ncRE and μcRE were individually tested by changing the chloride concentrations of the sample solutions in the following concentration pattern, high-low-high-low-high. For example, the concentrations of testing solutions for ncRE are successively 1 M, 10^{-5} M, 1 M, 10^{-6} M and 1 M, and the results are presented in Figure 2.6. The experimental temperature kept at 24 °C.

Figure 2.6a shows that for ncRE, the RT is about 50 minutes when the testing solution is changed from the high to low concentration and is about 5 minutes when the solution concentration is changed back to high. In contrast, for the μcRE shown in Figure 2.6b, the RT is around 20 minutes when the electrode is placed from the high to low concentration solutions and is about 3 minutes when the solution concentration is changed back to high. Therefore, the μcRE has much faster response compared with the ncRE when the electrodes are moved from the high to low concentration solutions, however the RT exhibits a similar value when the solution concentrations are changed from low to high. In general, the RT is controlled by the time taken for the REs to regain a stable liquid junction potential. Both the ncRE and μcRE use the same PE frit as the salt bridge, for which the liquid junction potential is established at the surface of the PE frit, therefore, they are expected to have similar RT.

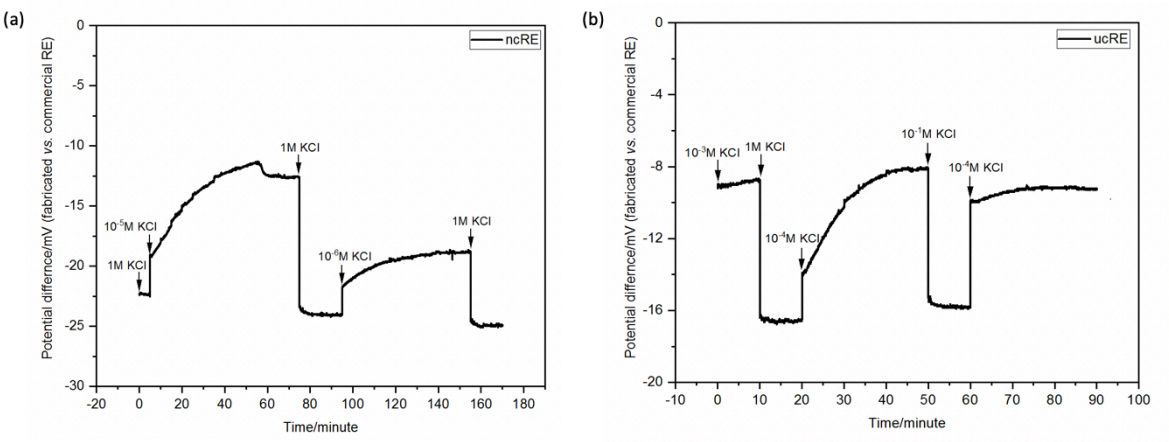

Figure 2.6 *Reference potential of (a) ncRE and (b) µcRE against the base potential provided by a commercial calomel double junction RE for response time test in different KCl solutions.*

2.3.4 Short-term Stability

The short-term stability test used the same setup with the chloride ion susceptibility test. But here, the sample solution was fixed at 10^{-3} M Cl^- concentration, and the measurement period was set longer to 2 hours. The results are presented in Figure 2.7.

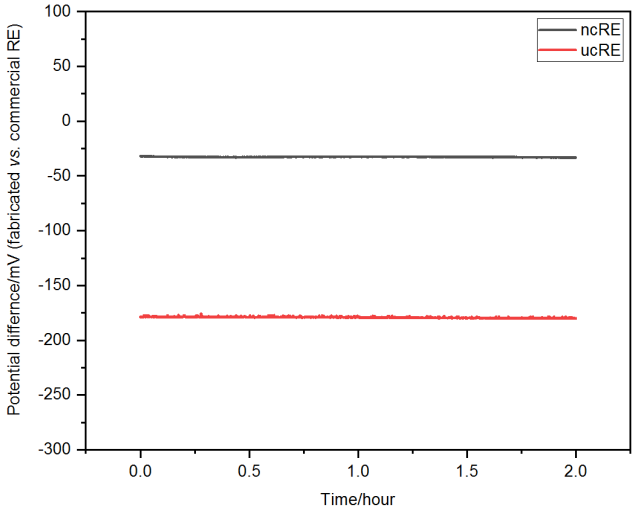

Figure 2.7 *Reference potential against the base potential provided by a commercial calomel double junction RE for short-term stability test in 10^{-3} M KCl solution for 2 hours.*

The results show that within the 2-hour period, both the µcRE and ncRE exhibited a good short-term stability with only 0.07 mV and 0.06 mV potential variation, respectively.

2.3.5 Long-term Stability

The long-term potential stability test was carried out in a capped beaker containing a 10^{-3} M KCl solution for 30 days. For the µcRE, the hydration time is about 12 hours, defined as the time required for the electrode to reach a stable potential when the new electrode is placed in a solution for the first time.

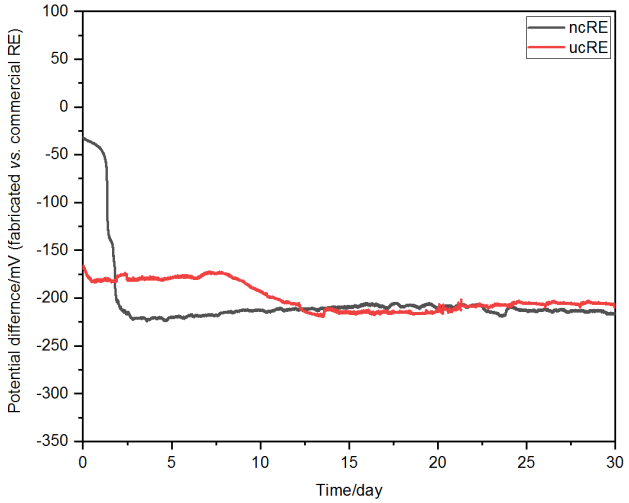

Figure 2.8 *Reference potential against the base potential provided by a commercial calomel double junction RE for long-term stability testin 10^{-3} M KCl solution for 30 days (data after 30 days are not presented in this figure).*

As shown in Figure 2.8 (red line), for the first 7.5 days (after the hydration), the potential of the µcRE remained stable with a 6 mV potential variation, and then, it started drifting with a -0.33 mV/hr drift rate for the next 5.5 days, and finally, the drifting rate reduced to 37 µV/hr for the rest days until the experiment was completed. In contrast, the ncRE started drifting at a -0.77 mV/hr rate from the initial point; then, after 1.25 days it drifted down with a high drift rate of -5.6 mV/hr for 1 day, and finally, it drifted for the rest 33 days with a drift

rate of 0.04 mV/hr. After 36 days (not shown here), the ncRE could not remain stable potential. Therefore, compared with the ncRE, the μcRE has a better long-term stability although both of them drifted with a certain drift rate; moreover, the μcRE has a longer lifetime, as agreed with the simulation results.

2.3.6 Temperature Effect on The Stability

It has been pointed out in the Introduction that not only the standard reduction potential of an electrode is influenced by the temperature, but also the Nernst equation is a function of temperature, both of which determines the slope of the sensitivity of an ISE. Moreover, both the liquid junction potential and solubility of the salts in the reference system vary with temperature.

To know the temperature effect on the stability and figure out the temperature range suitable for the μcRE, the sample container with a 0.1 M KCl solution was firstly put in a big beaker filled with DI water, and then the beaker was placed on a thermoelectric cooling (TEC) plate for varying the temperature. Figure 2.9 gives the experimental results.

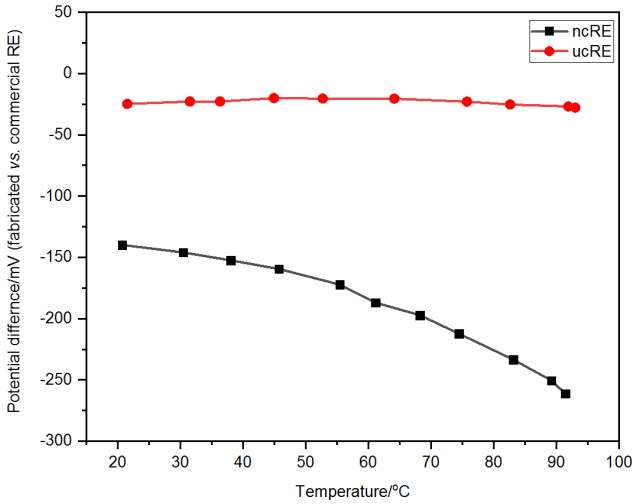

Figure 2.9 *Dependence of reference potential on temperature recorded in 0.1 M KCl solution.*

When the temperature increases, the leaching rate of chloride ion is accelerated to reduce the chloride ion concentration at the Ag/AgCl electrode, which, in turn, affects the reference potential. However, because of the increased longer diffusion length of the μcRE, the limited outflow of chloride ions from the channel into the external solution slows down the leaching rate of the chloride ion concentration at the μcRE, compared to the ncRE. Figure 2.9 shows that the μcRE has a 7.85 mV potential variation over the temperature range from 20 to 92 °C, while the ncRE reduces its potential by 121.26 mV. Thus, the μcRE is less affected by the temperature than the ncRE.

2.3.7 PH Effect on The Stability

Small potential changes at extreme high and low pH values can be interpreted as diffusion potential changes. Such diffusion potentials always appear at the interface between a reference electrolyte and a testing solution [19]. It should be noted that the measured diffusion potential is composed of the diffusion potentials at both the commercial RE and the μcRE (or ncRE), and that it is almost impossible to detect them separately. The pH effect on the stability was measured in a 0.1 M KCl solution by adding an appropriate quantity of HCl or NaOH to the KCl solution. The actual pH value was measured by a pH meter (pHTestr 10, Eutech Instruments).

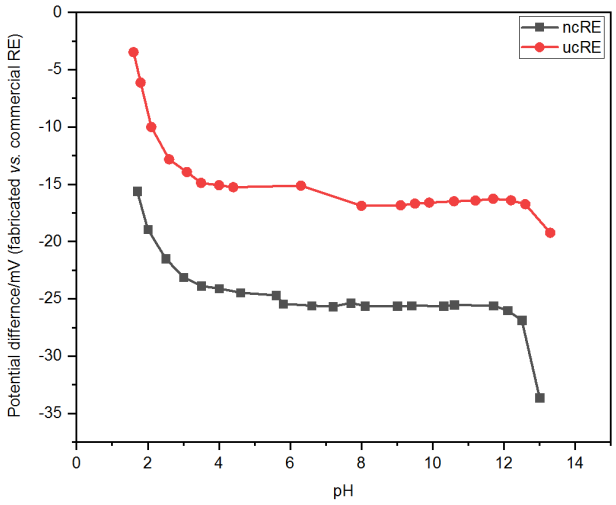

Figure 2.10 *Dependence of reference potential on pH (addition of HCl or NaOH) recorded in 0.1M KCl solution.*

The results in Figure 2.10 show that within the pH range from 2 to 12, the potential changes are less than 5 mV for both the µcRE and ncRE. A possible explanation is below: because both the µcRE and ncRE are liquid-state reference electrode using the same PE frit as the salt bridge, the pH should have the same effect on the diffusion potentials, as agreed with the experimental result. In addition, at the extreme high (>12) and low (< 3) pH conditions, the strong acidic or alkali environment will pose negative impacts on the material and mechanical properties of the structural materials (e.g., PE frit and gelatin), leading to a large potential deviation from the normal values.

2.3.8 Nitrate Detection

The prepared nitrate-selective membrane solution was drop cast on the top of the WE surface to realize the EGFET-based nitrate sensor. The curves shown in Figure 2.11a represent the potential as a function of nitrate concentration from 0 ppm to 2000 ppm in a logarithmic scale. The red curve represents the measured data, and the black curve indicates its linear fit. The fitting result shows the slope of the calibration curve for this EGFET sensor is -

202.16±5.55 mV/decade (or per decade across the measured concentration range) with a R-Squared value of 0.997.

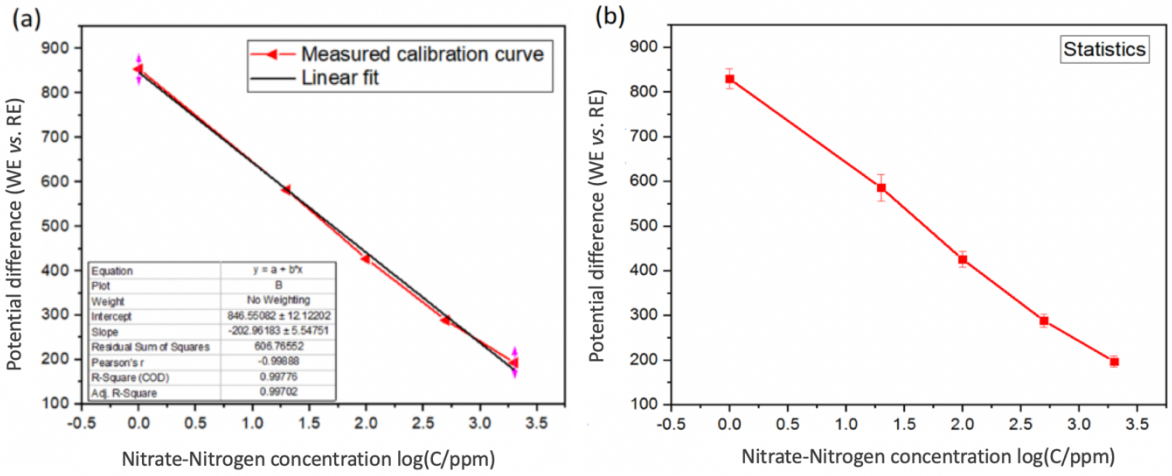

Figure 2.11 *(a) Output voltage of the sensor versus nitrate concentration. (b) Repeatability. The average voltage in every solution was calculated based on 3 rounds of testing.*

The repeatability experimental test was conducted for 3 runs. The first-run testing involves exposing the senor from 1 ppm, 20 ppm, 100 ppm 500 ppm to 2000 ppm concentration solutions, then the second-run is from 2000 ppm to 1 ppm, and the last-round is from 1 ppm to 2000 ppm again. The results in Figure 2.11b show that for all concentrations the potential variation of the sensor is within 50 mV.

2.4 Conclusion

A new RE with a serpentine microfluidic channel was developed. The performance of the RE was characterized in terms of chloride susceptibility, response time, short-term and long-term stability, pH and temperature influences on the potential stability. Low chloride, temperature and high long-term potential stability were observed for this µcRE.

An EGFET-based nitrate sensor was presented by integrating the μcRE. Owing to the easy fabrication, small footprint size, increased stability, and low cost, this sensor will be suitable for long-term field sensing applications such as continuous monitoring of nutrient concentration changes in water and soil [20, 21].

References

1. P. Salvatore, et al. "EGFET-Based Sensors for Bioanalytical Applications: A Review." *Sensors* 18.11 (2018): 4042.

2. Q. Li, et al. "Stable thin-film reference electrode on plastic substrate for all-solid-state ion-sensitive field-effect transistor sensing system." *IEEE Electron Device Letters* 38.10 (2017): 1469-1472.

3. C.P. Chen, et al. "Ultrasensitive in situ label-free DNA detection using a GaN nanowire-based extended-gate field-effect-transistor sensor." *Analytical chemistry* 83.6 (2011): 1938-1943.

4. E.M. Guerra, et al. "Extended gate field effect transistor using V2O5 xerogel sensing membrane by sol–gel method." *Solid State Sciences* 11.2 (2009): 456-460.

5. T. Sakata, et al. "Potential behavior of biochemically modified gold electrode for extended-gate field-effect transistor." *Japanese Journal of Applied Physics* 44.4S (2005): 2860.

6. D.C. Harris. Exploring chemical analysis. Macmillan, 2012.

7. I.Y. Huang, et al. "Fabrication and characterization of a new planar solid-state reference electrode for ISFET sensors." *Thin Solid Films* 406.1-2 (2002): 255-261.

8. Y.G. Vlasov. "New solid-state ion-selective electrodes—Sensors for chemical analysis of solutions. "*Fresenius' Zeitschrift für analytische Chemie* 335.1 (1989): 92-99.

9. T. Kim, et al. "A solid-state thin-film Ag/AgCl reference electrode coated with graphene oxide and its use in a pH sensor." *Sensors* 15.3 (2015): 6469-6482.

10. M. Shinwari, et al. "Microfabricated reference electrodes and their biosensing applications." *Sensors* 10.3 (2010): 1679-1715.

11. Ł. Tymecki, et al. "Screen-printed reference electrodes for potentiometric measurements." *Analytica Chimica Acta* 526.1 (2004): 3-11.

12. M.A.G. Zevenbergen, et al. "Solid state pH and chloride sensor with microfluidic reference electrode." *2016 IEEE International Electron Devices Meeting (IEDM). IEEE,* 2016.

13. A. Simoniset, et al. "Miniaturised reference electrodes for field-effect sensors compatible to silicon chip technology." *Electrochimica acta* 51.5 (2005): 930-937.

14. L. Dong, et al. Selective formation and removal of liquid microlenses at predetermined locations within microfluidics through pneumatic control. *Journal of Microelectromechanical Systems*, 17.2 (2008): 381-392.

15. J. Sutter, et al. "Solid-contact polymeric membrane electrodes with detection limits in the subnanomolar range." *Analytica Chimica Acta* 523.1 (2004): 53-59.

16. T. Guinovart, et al. "A reference electrode based on polyvinyl butyral (PVB) polymer for decentralized chemical measurements." *Analytica chimica acta* 821 (2014): 72-80.

17. S.S. Sridharamurthy, et al. "A microfluidic chemical/biological sensing system based on membrane dissolution and optical absorption." *Measurement Science and Technology* 18.1 (2006): 201.

18. http://www.nico2000.net/datasheets/glossary.html#platinum

19. Mroz, A. "Disposable reference electrode." *Analyst* 123.6 (1998): 1373-1376.

20. M.A. Ali, et al. "Microfluidic impedimetric sensor for soil nitrate detection using graphene oxide and conductive nanofibers enabled sensing interface." Sensors and Actuators B: Chemical, 239 (2017): 1289-1299.

21. M.A. Ali, et al. "In situ integration of graphene foam–titanium nitride based bio-scaffolds and microfluidic structures for soil nutrient sensors." *Lab on a Chip*, 17.2 (2018): 274-285.

CHAPTER 3. MINIATURIZED FRIT-FREE SILVER-SILVER CHLORIDE REFERENCE ELECTRODE WITH MICRO-CHANNEL

A manuscript to be submitted to Lab on a Chip

Xinran Wang, Yang Tian and Liang Dong

Abstract

This paper reports a novel silver-silver chloride (Ag/AgCl) reference electrode (RE) incorporating a microfabricated channel as a liquid junction, without using any glass or polymer based bulky frit. The presented RE consists of a polydimethylsiloxane (PDMS) reservoir (2 mm diameter and 2 mm height) for storing potassium chloride (KCl)-based liquid electrolyte, a microchannel (10 μm width, 50 μm height, and 1 mm length) placed beneath the reservoir to serve as a virtual frit, and a screen-printed Ag/AgCl electrode embedded inside the electrolyte reservoir. The reduced orifice of the microchannel decreases the rate of chloride ion loss from the Ag/AgCl electrode surface to the external environment, thus increasing the potential stability of the electrode. This frit-less RE exhibits a low temperature dependence with a good potential stability over a few days.

3.1 Introduction

Miniaturization has become an inevitable trend for ion-selective electrode (ISE)-based sensors, driven by a wider range of applications such as lab-on-a-chip electrochemical analysis, and clinical point-of-care revolution, etc. As one of the crucial components, lots of efforts have been devoted on the development of stable, reliable, and inexpensive REs because the commercial REs are not suitable for portable applications due to the large dimensions and high cost. The technological strategies include miniaturizing liquid-junction REs [1-3], introducing

solid-state planar electrode designs [4-12], and adopting microsystems technology [13, 14], etc. Despite of these efforts, the performance of the reported miniature REs is not comparable with the gold standard glass-body REs [15, 16].

It should be noted that the requirements for the REs vary with different applications, and the trade-offs exist between the performance and miniaturization of the REs. For example, for monitoring environmental traces, long-term potential stability is a more important feature than the footprint size of the reference, given a similar cost budget. However, in many disposable sensor applications, short-term or even one-time use stability, reproducible and low-cost mass production, and effective miniaturization are more concerned than the ability of long-term measurements. In addition, high-performance REs are required to be reversible and non-polarizable, meaning that the reference potential must be dominated by a reaction with a high exchange current density so as not to be affected by any current flow across the liquid/solid interface [17]. Therefore, it seems a proper technical strategy to intuitively and naturally scale down the dimensions of the commercial glass-body, liquid-junction Ag/AgCl electrodes due to their high accuracy and potential stability. However, sufficient size reduction for the frits of commercial electrodes is challenging, thus hindering the progress of the RE miniaturization.

In this work, a novel miniature liquid-junction Ag/AgCl RE is presented without using any physical polymer or glass-based frit.

3.2 Sensor Structure and Manufacturing

3.2.1 Structure Design of Electrode

This miniature liquid-junction Ag/AgCl RE has a simple structure, consisting of only a cylinder potassium chloride (KCl) reservoir (2 mm diameter × 3 mm height) and a straight

microchannel (1 mm length × 20 µm width × 5 µm height) serving as the salt bridge. The schematic and the photo of the electrode are shown in Figure 3.1.

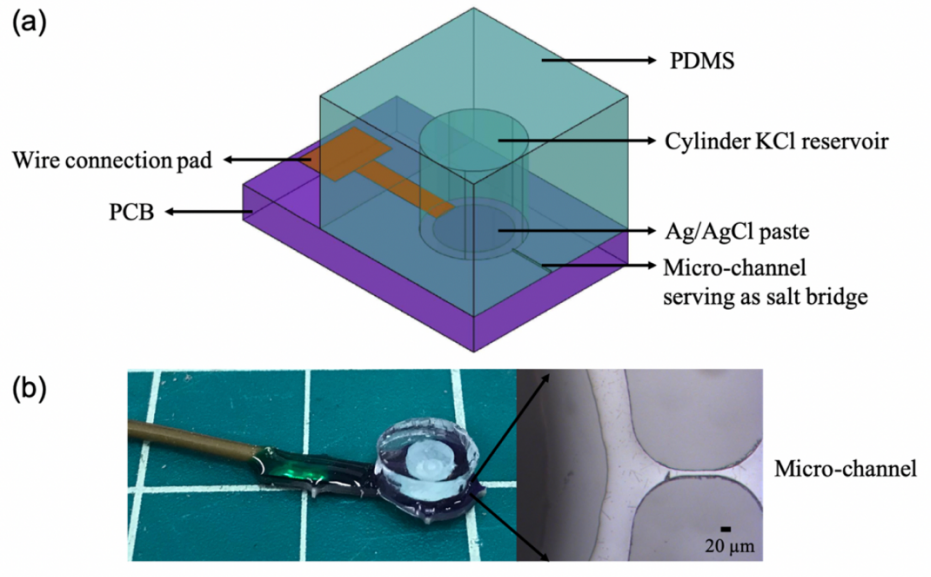

Figure 3.1 *(a) Schematic of the miniaturized RE's structure and (b) its physical photo.*

The dimensions of the microchannel in the RE are determined using a theoretical model that estimates the drift rate (DR) based solely on diffusion of chloride ions through the channel [18]. This DR model is described as

$$\mathrm{DR} = 2\mathrm{RTWH}/\mathrm{F}V_{res}(H + W + 2L) \quad (1)$$

where R is the gas constant, T is the temperature, W is the channel width, H is the channel height, F is the Faraday constant, V_{res} is the volume of the internal KCl reservoir, and L is the channel length. This model indicates that the DR is proportional to the channel width and height, while it is inversely proportional to the channel length. Therefore, the finer and longer of the channel, the lower of the DR value, resulting in the better stability of the RE. In our design, the smallest channel width and height was restricted by the SU-8 soft lithography technique in our lab, and the best feature size we can obtain is 20 µm width × 5 µm height. Considering the device dimension, a 1 mm channel length is chosen.

In addition, from equation 1 above, the DR is inversely proportional to the volume of the internal KCl reservoir V_{res}. Therefore, a tradeoff between the miniaturization and DR (stability) exists and restricts the diameter of the cylinder KCl reservoir. Here we chose a 2 mm diameter for the reservoir. In theory, the height of the internal KCl reservoir could be in the order of 10 meter. This is because the pressure drop on the liquid surface at the end of the channel or the orifice is determined by

$$\Delta P = \rho g h - 1.01 \times 10^5 - P_s \quad (2)$$

where ρ = 1.13 g/ml is the density of the 3M KCl solution, g is the gravity acceleration, h is the reservoir height, 1.01×10^5 Pa is the atmospheric pressure, and P_s is the pressure caused by the liquid surface tension. Because P_s is far less than the atmospheric pressure, equation (2) can be simplified to be

$$\Delta P = \rho g h - 1.01 \times 10^5 \quad (3)$$

As long as $\Delta P < 0$ (meaning that $h < 10$ m), the KCl solution will be confined inside the channel, however, the height of the reservoir will be determined to obtain a proper DR.

In the above design we assume the KCl reservoir is sealed perfectly, and the only outlet of the RE is the microchannel. However, from a practical perspective, it is worth knowing the maximum height allowed for the KCl reservoir if the reservoir is not perfectly sealed. In this case the pressure drop on the liquid surface at the end of the channel is

$$\Delta P = \rho g h - P_s \quad (4)$$

where P_s is describe by the Young-Laplace equation $P_s = \gamma(\frac{1}{R_1} - \frac{1}{R_2})$ [19-20], γ is the liquid surface free energy, and R_1 and R_2 are the radii of curvature in directions vertical and parallel, respectively, to the liquid stream. In our case, because the stream is straight R_2 is infinite. The Young-Laplace equation can thus be simplified to $P_s = \frac{\gamma}{R_1}$, where the value of R_1 is determined

by $R_1 = H/[2\sin(\theta_b - 90°)]$ and H is the channel height (here, 5 μm) and θ_b is the angle of curvature of a liquid confined by a virtual all inside the microchannel. Therefore, P_s can be described by

$$P_s = (\frac{2\gamma}{H})\sin(\theta_b - 90°) \quad (5)$$

Based on [21], for water inside a PDMS microchannel, the maximum pressure that a virtual wall in a straight stream can sustain occurs when $\theta_b = 105°$ and $\gamma = 72.8\ \frac{mN}{m}$. Thus, substituting equation (5) into equation (6), the maximum height of the KCl reservoir can be 0.75 m although a leakage existed in the reservoir. Therefore, the 2 mm height of the reservoir is safe.

3.2.2 Materials and Manufacturing

Materials

SU-8 2075 was purchased from MICRO·CHEM; a 3 M KCl solution saturated with AgCl and KCl were obtained from Sigma Aldrich; PDMS (Sylgard 184) was purchased from Dow Corning; Ag/AgCl ink (comprised finely dispersed chloridized silver flakes) was purchased from Fisher Scientific. Deionized (DI) water was obtained from a Millipore™ purification system and utilized for all experiments. The printed circuit board (PCB) was fabricated in OSHPark.

Electrode preparation

The cylinder KCl reservoir and microchannel were fabricated using a conventional soft lithography technique [22]. Briefly, to master a mold for the reservoir and microchannel, a silicon wafer was first coated with 5-μm-thick SU-8 photoresist. Then, a chrome photomask was used to create a round-shaped SU-8 pattern. A 3D-printed cylinder (2 mm diameter and 3 mm height) was glued on the SU-8 pattern, and then a prepolymer mixture of PDMS and its

curing agent with a weight ratio of 10:1 was poured onto the master mold, and then thermally cured on a hotplate at 90 °C for 1 hour. Subsequently, the hardened PDMS polymer was pealed from the mold. The purpose of the 3D-printed cylinder is to increase the volume of KCl reservoir, without which the height of the cylinder would be the same with the microchannel (only 5 μm thickness).

The PCB shown in Figure 3.1b has two base conducting pads of copper. The pad with rectangular shape is used to connect the RE to a home-made data logger and the other one with round shape (1.5 mm diameter) is used as the electron conducting layer for the RE. A 700 nm thin layer of silver is firstly coated on the top of the round-shaped copper pad by thermal evaporator with the help of a shadow mask to define the active electrode area. Then, Ag/AgCl paste is screen-printed on the top of the Ag pad and cured at 110 °C for 30 min. The thickness of Ag/AgCl paste (290 μm [23]) is controlled by the thickness of stencil. Subsequently, a thin layer of the prepolymer mixture of PDMS and its curing agent with a weight ratio of 10:1 is poured over the PCB leaving the opening for the round-shaped Ag/AgCl pad and the soldering pad. After the PDMS is thermally cured on a hotplate at 90 °C for 1 hour, the PCB is bonded to the PDMS cylinder KCl reservoir and microchannel by using oxygen plasma treatment.

The last step is to inject the 3M KCl solution with saturated AgCl into the KCl reservoir by a syringe through a punched hole on the top of the PDMS. The microchannel should be filled with the 3M KCl solution after the injection to make a good liquid junction. Lastly, the punched hole is sealed by a small drop of prepolymer mixture of PDMS and its curing agent. A schematic of the fabrication process is summarized in Figure 3.2.

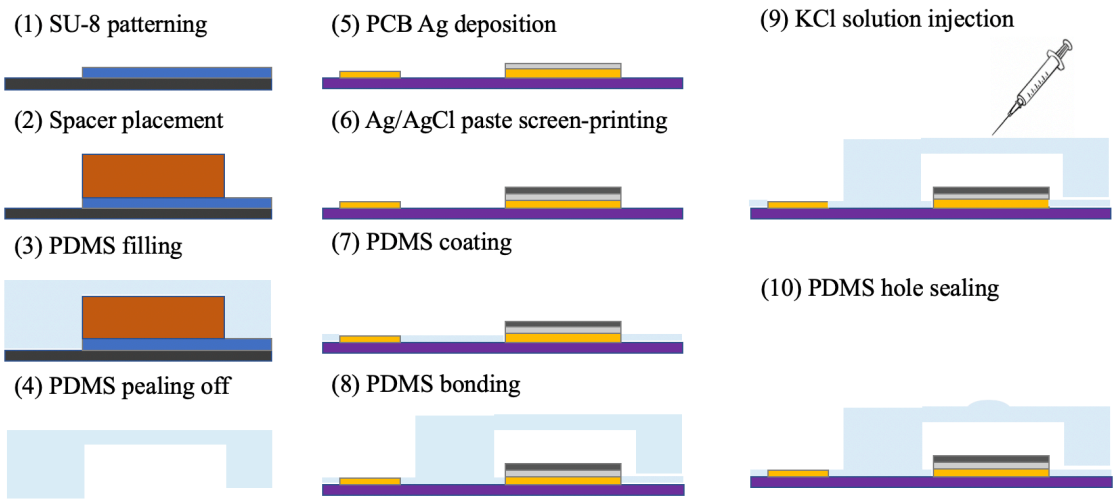

Figure 3.2 *A schematic of the fabrication process.*

Before use, the fabricated RE with the microchannel should be immersed into the 3 M KCl solution.

3.2.3 Instrumentation

The electrical potential of the fabricated RE is measured against a commercial calomel double junction RE (HANNA Instruments; Model HI5414) where 3.5 M KCl is used as the inner filling electrolyte and the measurement results are recorded using a home-made data logger (detailed information is included in Appendix A).

3.3 Results and Discussion

For comparisons, all the experiments are conducted for the Ag/AgCl electrode with the microchannel, and a bare Ag/AgCl one without a KCl reservoir. The electrode characterization is focused on determining the chloride susceptibility, response time, and stability, as well as the temperature and pH effect on the stability of the electrodes. The experimental setup is shown in Figure 3.3.

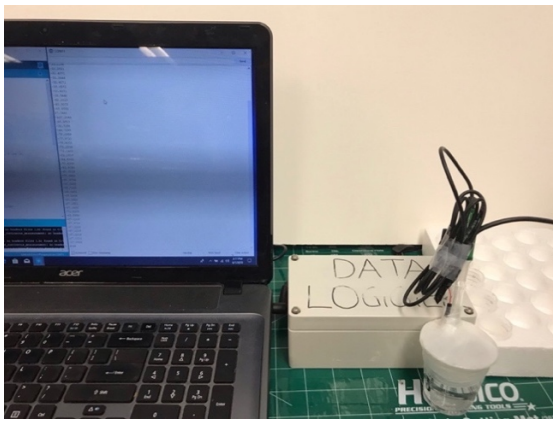

Figure 3.3 *Experimental setup used for characterization of the RE. The current showing setup is running for the short-term stability test.*

3.3.1 Chloride Susceptibility

A high-performance RE is expected to provide a stable potential under conditions of changing analyte solutions. The first set of experiments is performed in a series of KCl solutions containing 10^{-6} M, 10^{-5} M, 10^{-4} M, 10^{-3} M, 10^{-2} M, 10^{-1} M and 1.0 M concentrations of Cl^-. Before commencing a new test, the RE is thoroughly rinsed in DI water and air dried to remove residual chloride ions. The experimental time is set to 5 min for each test. And all the measurements are conducted at 24 °C.

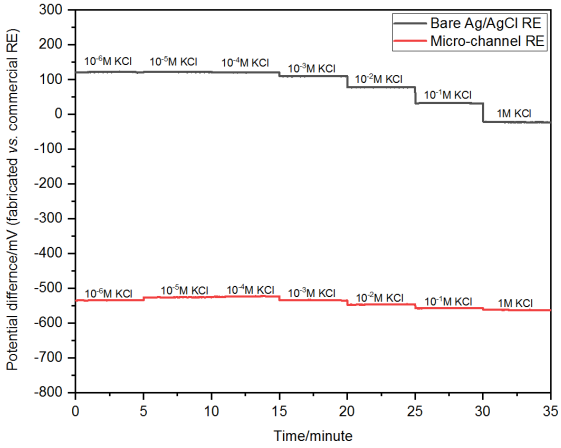

Figure 3.4 *Reference potential against the base potential provided by a commercial calomel double junction RE a function of time in different KCl solutions from 10^{-6} to 1 M.*

Figure 3.4 shows that the RE with the microchannel provides a reference potential that is almost independent of changes in Cl^- concentration of different external solutions. It exhibits the absolute values of the slope is less than 6 mV dec^{-1} in KCl solutions. For the bare Ag/AgCl electrode, the potential is also independent of Cl^- concentration when the concentration of KCl is very low but it exhibits a big Cl^- interference with the absolute values of the slope is about 20 mV dec^{-1}. Because without the KCl reservoir to remain a constant Cl^- concentration, the RE with bare Ag/AgCl paste is actually a Cl^- sensitive sensor as described by Nernst equation. Therefore, the RE with micro-channel has relatively lower Cl^- sensitivity.

3.3.2 Response Time

Generally, the response time (RT) of REs is defined as the time interval required to obtain a stable electrode potential when a RE is moved from one to another solution. RT is affected by the electrode type, temperature, magnitude and direction of the concentration change, and hysteresis, etc. [24]. The RT of the RE with the microchannel is tested by changing the chloride concentrations of the sample solutions in the following concentration pattern, high-low-high-low-high, successively 1 M, 10^{-3} M, 1 M, 10^{-4} M and 10^{-1} M. The experiment is conducted at 24 °C.

Figure 3.5a shows that the RT of the bare Ag/AgCl electrode is about 2 minutes when the RE is moved from the high to the low concentration KCl solutions, and is a few seconds when the RE is moved from the low back to the high concentration KCl solutions. While for the RE with the microchannel, the RT is about 5 minutes when the RE is moved from the high to the low concentration KCl solutions, and is less than 1 minute when the RE is moved from the low to the high concentration KCl solutions. As expected, the microchannel-based RE exhibits a relatively low response speed compared with the bare Ag/AgCl electrode, because the latter has direct contact with the KCl solutions. Nevertheless, the microchannel-based RE

is advantageous over other types of REs, such as the micro-fluidic RE, in terms of the response time.

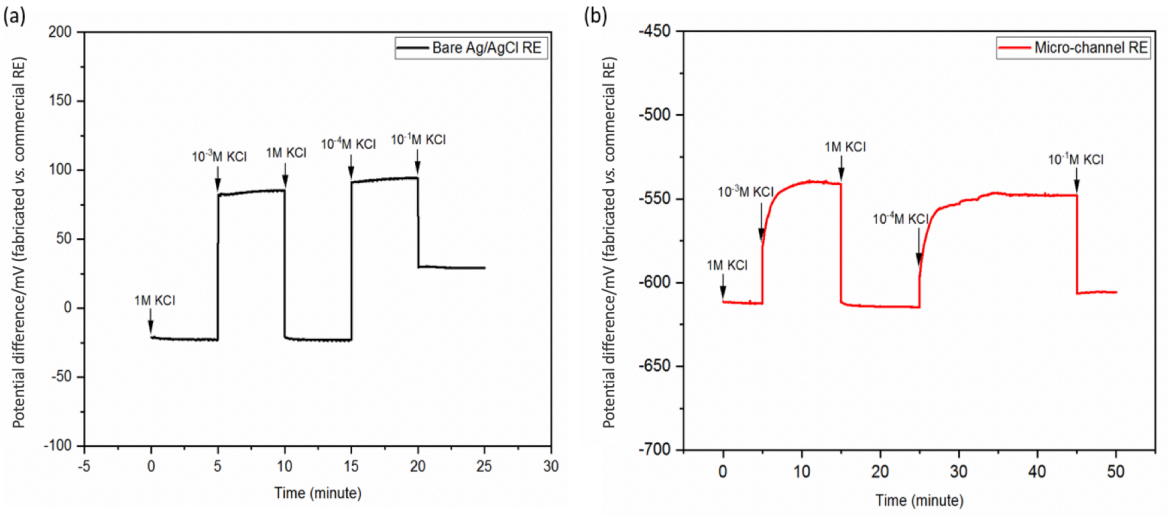

Figure 3.5 *Reference potential against the base potential provided by a commercial calomel double junction RE for response time test in KCl solutions.*

3.3.3 Potential Stability

For the stability test, the sample solution is fixed at 10^{-3} M Cl^- concentration, and the experimental period was set to 6 days. Based on equation (1), for the microchannel-based RE the estimated DR at 24 °C is 0.269 mV/h, while the measured DR is 0.52 mV/h (calculated based on the experimental data in Figure 3.6) for the first 5 days. However, after 5 days no stable potential could be obtained for the microchannel RE. The possible reasons for the failure may be 1) air bubbles generated by temperature change blocked the micro-channel; 2) the chloride ions were completely depleted or leached out. The difference between the theoretical and measured values may be caused by manufacturing errors. For example, the thickness of the SU-8 pattern may not be exact 5 µm affecting the DR estimation using equation

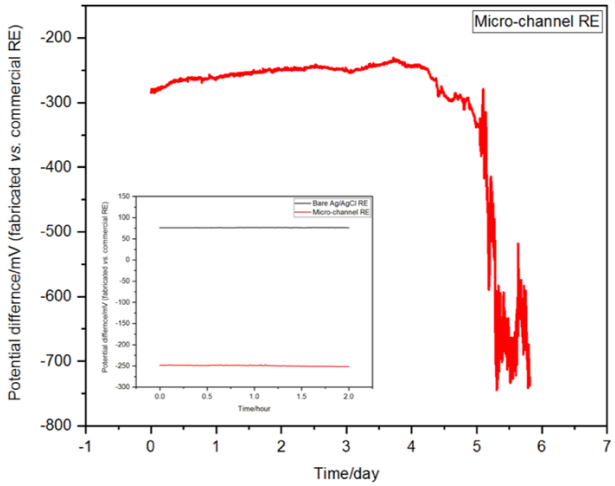

Figure 3.6 *Reference potential against the base potential provided by a commercial calomel double junction RE for stability test in 10^{-3} M KCl solution for 6 days.*

3.3.4 Temperature Effect on The Stability

Similarly, we study the temperature effect on the stability of the microchannel-based Ag/AgCl electrode. The sample container with 0.1 M KCl solution is firstly put inside a big beaker filled with DI water, and then the big beaker is placed on a thermoelectric cooling (TEC) plate to vary the solution temperature.

Figure 3.7 shows that the microchannel-based RE has a potential variation of less than 10 mV over the temperature range from 20 to 60 °C. Above 60 °C the potential deviates from the earlier potential by 40 mV. The bare Ag/AgCl electrode has a slightly low temperature dependence compared with the microchannel-based RE. For the microchannel-based RE, the leaching rate of the Cl^- inside the KCl reservoir increases with increasing temperature. The changing rate of the RE potential is proportional with the temperature, as described in equation (1). In contrast, the bare Ag/AgCl electrode does not have a KCl reservoir, thus there is no Cl^- leaking issue like the microchannel-based RE. However, the Cl^- concentration still depends on the temperature due to the solubility of AgCl in the KCl solution. Especially at high

temperatures, this solubility-induced issue may become obvious. Therefore, both the REs exhibit temperature-dependent behavior, and both have a wide working temperature range shown in Figure 3.7.

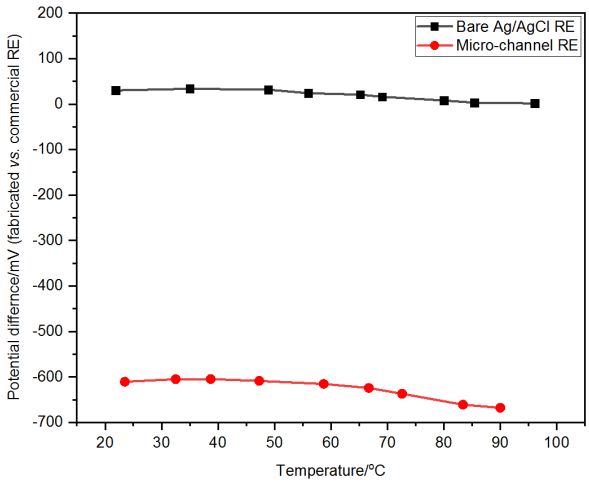

Figure 3.7 *Dependence of reference potential on temperature recorded in 0.1 M KCl solution.*

3.3.5 PH Effect on The Stability

A severe interferent for RE can result from the H^+/OH^- ions present in samples of different pH, affected, e.g., by the presence of dissolved CO_2 [25]. Figure 3.8 demonstrates the influence of changing pH, established by injection of concentrated HCl or NaOH to the 0.1 M KCl solution, on the potential stability of the microchannel-based RE. The real pH value is measured by a pH meter (pHTestr 10, Eutech Instruments).

Figure 3.8 shows that within the pH range from 1 to 11, the potential changes of both the REs are lower than 8 mV and exhibit a large deviation at high pH values. Because the microchannel-based RE is a liquid-state electrode using the microchannel as the salt bridge, the low pH will have a limited influence on the diffusion potentials; however, at high and low pH conditions, the strong acidic or alkali environment may change the chemical and

mechanical property of PDMS, thus, the potential of the electrode is seen deviating away from the normal values. The bare Ag/AgCl electrode has a similar pH response with the microchannel-based RE. Also, a low pH environment does not affect the electrode potential, but a strong acidic or alkali environment can erode the electrode resulting in a potential drift. Therefore, the testing results have given considerable encouragement to use this microchannel-based RE for the sensors that measure target species in the solutions with a wide pH range.

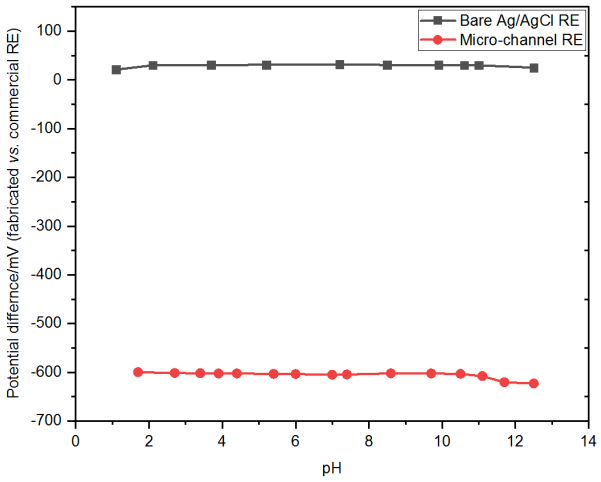

Figure 3.8 *Dependence of reference potential on pH (addition of HCl or NaOH) recorded in 0.1 M KCl solution.*

3.3.6 Nitrate Detection

A nitrate ion-selective electrode (ISE) reported in [26] is used here to validate the microchannel-based Ag/AgCl RE. The calibration and repeatability test are presented in Figure 3.9.

Figure 3.9a shows the potential as a function of nitrate concentration from 10 ppm to 5000 ppm in a logarithmic scale. From the parameters of the linear fitting line, the slope of the calibration curve of this nitrate sensor is -25.32±0.66 mV per decade with a R-Squared value of 0.996.

Figure 3.9b shows that the maximum variation of potential is 14.39 mV over the whole repeatability testing range. It should be noticed that in order to simulate the actual situation, the repeatability experiment is conducted for 3 rounds, and moreover for the first and third round, the concentrations of testing samples are from 10 ppm, 50 ppm, 100 ppm, 200 ppm, 500 ppm, 1000 ppm, 2500 ppm to 5000 ppm, but for the second round testing, the concentrations were from 5000 ppm, 2500 ppm, 1000 ppm, 500 ppm, 200 ppm, 100 ppm, 50 ppm to 10 ppm.

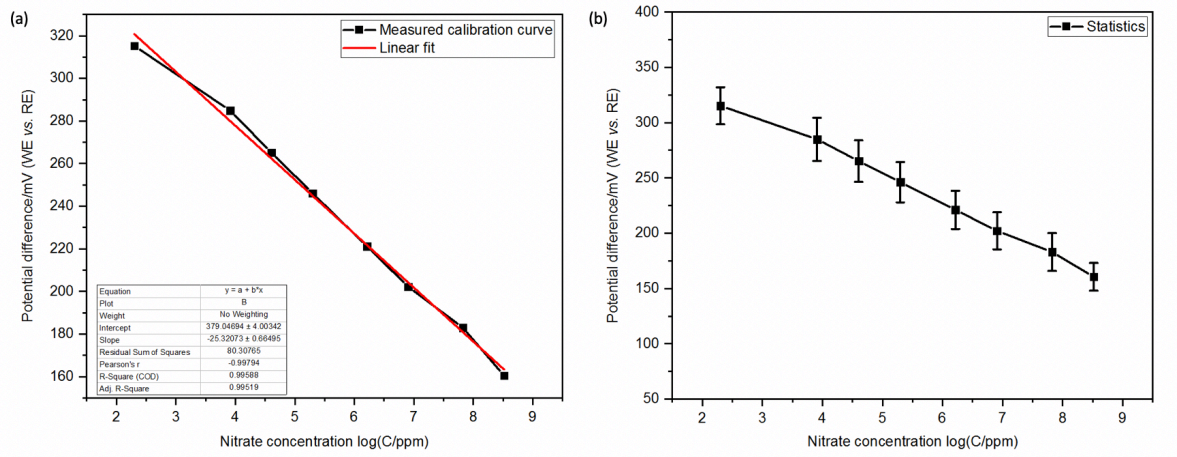

Figure 3.9 *(a) Output voltage of the ISE versus nitrate concentration. (b) Repeatability test. The average voltage in every solution was calculated based on 3 rounds of testing.*

3.4 Conclusion

A miniaturized Ag/AgCl reference electrode with a PDMS-based microchannel and KCl reservoir is developed. High stability, wide temperature and pH range, and small footprint size are demonstrated as the features of this microchannel-based electrode, compared to a counterpart bare Ag/AgCl electrode. The microchannel and KCl reservoir are formed by soft lithography, making it possible to realize low-cost mass production.

References

1. Suzuki, Hiroaki, et al. "Microfabricated liquid junction Ag/AgCl reference electrode and its application to a one-chip potentiometric sensor." *Analytical chemistr*y 71.22 (1999): 5069-5075.

2. Smith, Rosemary L., and Scott Collins. "Miniature liquid junction reference electrode and an integrated solid-state electrochemical sensor including the same." U.S. Patent No. 4,592,824. 3 Jun. 1986

3. Ciobanu, Madalina, et al. "Miniaturized reference electrodes based on Ag/AgiX internal reference elements. I. manufacturing and performance." *Electroanalysis: An International Journal Devoted to Fundamental and Practical Aspects of Electroanalysis* 14.14 (2002): 989-997.

4. Pedrotti, Jairo J., Lucio Angnes, and Ivano GR Gutz. "Miniaturized reference electrodes with microporous polymer junctions." *Electroanalysis* 8.7 (1996): 673-675.

5. Urban, G., et al. "Miniaturized thin-film biosensors using covalently immobilized glucose oxidase." *Biosensors and Bioelectronics* 6.7 (1991): 555-562.

6. Stanic, Z., and Stella Girousi. "Carbon paste electrodes in potentiometry: the state of the art and applications in modern electroanalysis (A review)." *Sens. Electroanal* 6 (2011): 89-128.

7. Shin, Jae Ho, et al. "Miniaturized solid-state reference electrode with self-diagnostic function." U.S. Patent No. 6,554,982. 29 Apr. 2003.

8. Ciosek, Patrycja, and Wojciech Wróblewski. "Miniaturized electronic tongue with an integrated reference microelectrode for the recognition of milk samples." *Talanta* 76.3 (2008): 548-556.

9. Kim, Sang Kyung, et al. "A miniaturized electrochemical system with a novel polyelectrolyte reference electrode and its application to thin layer electroanalysis." *Sensors and Actuators B: Chemical* 115.1 (2006): 212-219.

10. Mroz, A. "Disposable reference electrode." *Analyst* 123.6 (1998): 1373-1376.

11. Bilitewski, U., et al. "Miniaturized disposable biosensors." *Sensors and Actuators B: Chemical* 7.1-3 (1992): 351-355.

12. Ciobanu, Madalina, Jeremy P. Wilburn, and Daniel A. Lowy. "Miniaturized reference electrodes. II. use in corrosive, biological, and organic media." *Electroanalysis: An International Journal Devoted to Fundamental and Practical Aspects of Electroanalysis* 16.16 (2004): 1351-1358.

13. Kang, Sun, et al. "Micro reference electrode of implantable continous biosensor using iridium oxide, manufacturing method thereof, and implantable continuous biosensor." U.S. Patent Application No. 10/861,408.

14. Zhou, Jianhua, et al. "Fabrication of a microfluidic Ag/AgCl reference electrode and its application for portable and disposable electrochemical microchips." *Electrophoresis* 31.18 (2010): 3083-3089.

15. Hayashi, Ryuzo, Kariyone Akio, and Yoshio Hashizume. "Reference electrode and a measuring apparatus using the same." U.S. Patent No. 5,037,527. 6 Aug. 1991.

16. Guth, U., et al. "Solid-state reference electrodes for potentiometric sensors." *Journal of Solid State Electrochemistry* 13.1 (2009): 27-39.

17. Inzelt, György, Andrzej Lewenstam, and Fritz Scholz. Handbook of reference electrodes. Heidelberg:: Springer, 2013.

18. M.A.G. Zevenbergen, et al. "Solid state pH and chloride sensor with microfluidic reference electrode." 2016 IEEE International Electron Devices Meeting (IEDM). IEEE, 2016.

19. Zhao, Bin, Jeffrey S. Moore, and David J. Beebe. "Surface-directed liquid flow inside microchannels." Science 291.5506 (2001): 1023-1026.

20. Whitesides, George M., and Paul E. Laibinis. "Wet chemical approaches to the characterization of organic surfaces: self-assembled monolayers, wetting, and the physical-organic chemistry of the solid-liquid interface." *Langmuir 6.1* (1990): 87-96.

21. Mondal, Subrata, Monmee Phukan, and Animangsu Ghatak. "Estimation of solid–liquid interfacial tension using curved surface of a soft solid." *Proceedings of the National Academy of Sciences* 112.41 (2015): 12563-12568.

22. Weibel, Douglas B., Willow R. DiLuzio, and George M. Whitesides. "Microfabrication meets microbiology." *Nature Reviews Microbiology* 5.3 (2007): 209.

23. Thévenot, Daniel R., et al. "Electrochemical biosensors: recommended definitions and classification." *Analytical Letters*34.5 (2001): 635-659.

24. http://www.nico2000.net/datasheets/glossary.html#platinum

25. J. Sutter, et al. "Solid-contact polymeric membrane electrodes with detection limits in the subnanomolar range." Analytica Chimica Acta 523.1 (2004): 53-59.

26. Kisiel, Anna, et al. "All-solid-state reference electrodes with poly (n-butyl acrylate) based membranes." Electroanalysis: An International Journal Devoted to Fundamental and Practical Aspects of Electroanalysis 20.3 (2008): 318-323.

CHAPTER 4. REFILLABLE PLANAR SILVER-SILVER CHLORIDE REFERENCE ELECTRODE WITH DOUBLE JUNCTION

A paper to be submitted to Lab on a chip

Xinran Wang and Liang Dong

Abstract

A refillable planar double-junction reference electrode (RE) is developed to improve the potential stability of conventional silver-silver chloride (Ag/AgCl) electrode for long-term measurements. Screen-printing and 3D printing techniques are employed for mass production. The outer filling solution is made of a 0.1 M lithium acetate (CH_3COOLi) solution, while the internal filling electrolyte consists of gelatin with 1 M potassium chloride (KCl) and saturated AgCl. This planar double-junction RE consists of a 3D printed top with two chambers, a flexible printed circuit board (PCB) in the middle layer, and a 3D printed base substrate. Four pairs of mini magnets are embedded in the top and bottom layers to facilitate replacing the gel-state internal filling analyte when needed. The double junctions of this novel RE are laid out in the same plane through a microsystem approach, thus providing a compact size and easy integration with other components to form a miniature sensor system, which is advantageous over the vertical arrangement of two junctions in the commercial glass-body double-function RE with a bulky size. The developed RE exhibits a practical independence of changes in the external Cl^- concentration, and a high potential stability over a wide temperature and pH range. In addition, a short-term stability with 60 μV variation and a long-term stability with drift rate of 76 μV/hr are obtained for this RE. Lastly an almost perfect linearity with 0.999 R-Squared value is presented for the potentiometric measurement of nitrate using the presented RE.

4.1 Introduction

For direct potentiometric measurement, one of the main limitations is the potential drift during sequential measurements, which can be easily seen even if a series of standard solutions are repeatedly measured over a period. The major reason causing the potential drift is the varying liquid junction potential (LJP) of the reference electrodes (RE) [1]. Although the LJP does not drift a lot once stabilized in a solution at a constant temperature, it will change by several millivolts every time a RE is immersed in a new solution, or even re-immersed in the same one [2]. For most potentiometric applications, the potential drift is insignificant compared to other effects, such as ionic strength, interference, but for accurate measurements, steps must be taken to try to minimize this effect. In previous studies, a new type of liquid junction-free RE was devised by either employing solvent-processible polymer membranes which displayed a near-Nernstian response to pH change [3] or using plasticized poly(vinyl chloride) membrane containing the ion-exchanger tridodecyl-methylammonium chloride as RE [4-7]. A RE with a renewable free-diffusion liquid junction was also proposed for high-precision pH measurements and showed good reproducibility and stability [8]. In addition to the potential drift caused by the liquid junction, the presence of the liquid junction may also create the contamination to the sample solutions under test, due to the leakage of inner filling electrolyte through the porous plug or frit. For example, when measuring potassium or chloride ions when a potassium chloride (KCl) is used as the inner filling solution. To overcome the above problems to minimize the potential drift and contamination, double-junction REs have been developed [9-12].

Single-junction silver-silver chloride (Ag/AgCl) REs use a single chamber generally filled with a high concentration KCl solution saturated with silver chloride (AgCl) which directly contacts with the analyte solution through a single liquid junction by means of a porous

plug or fritted disc. In contrast, double-junction Ag/AgCl REs have two chambers with the first one called the internal reference system having a liquid junction with an intermediary salt bridge (the outer filling solution), then a second liquid junction to the external sample solution. The internal filling solution usually still is KCl solution, while the outer filling solution is chosen to avoid contamination of the solution to be tested with the target ion or any that would interfere with it, and to minimize the effects of the liquid junction potential. Therefore, lithium acetate (CH_3COOLi), KCl, potassium nitrate (KNO_3) are generally selected as the intermediary salt bridge due to their similar mobilities of ions, and usually CH_3COOLi is mostly used. There are several commercially available liquid-state double junction REs, such as HI5414 from HANNA Instruments, 4210N68 from Thermo Scientific Orion, etc. These commercial double-junction REs exhibit good performance in terms of stability, lifetime, response time, and reproducibility etc.; however, these glass-body aqueous REs are expensive ($150-300 /each), fragile, and bulky. Therefore, which resulting in difficult integration and massive deployment.

In this paper a refillable planar Ag/AgCl RE with double junctions is developed. A convenient and reliable manufacturing method is also developed, allowing for mass production with high reproducibility. The use of the mini magnets inside the sensor body makes it easy to replace the gel-state inner filling electrolyte when needed, while still offering sufficient sealing at the closed state.

4.2 Sensor Structure and Manufacturing

4.2.1 Structure of Electrode

The refillable Ag/AgCl RE (30 mm length × 18 mm width × 7 mm height) consists of three separate parts, including a 3D printed bottom, a 3D printed top, and a flexible PCB placed between the top and bottom cases. An assembled RE is shown in Figure 4.1a.

Figure 4.1b shows that four mini magnets (4 mm diameter × 2 mm depth) are embedded into the bottom case in where there is a 0.7 mm-deep groove to help assembling with the PCB and the top case. A small slot is also left for the PCB connector. The printed top case includes three cylinder chambers (3 mm diameter and 3 mm depth each) serving as the KCl, CH_3COOLi, and test sample reservoirs. Two small channels are inserted with two polyethylene (PE) frits that connect the three chambers through which different ions can pass through due to diffusion. Eights magnets are paired in the top and bottom layers. Six small holes are created to serve as the inlets and outlets for the electrolyte and test sample solutions. The flexible PCB has two copper pads (2 mm diameter) functioning as electron conductors; one of them is used as RE, and the other can be functionalized as an ion-selective electrode. And two rectangular copper pads are used to connect with the outer electrical circuit.

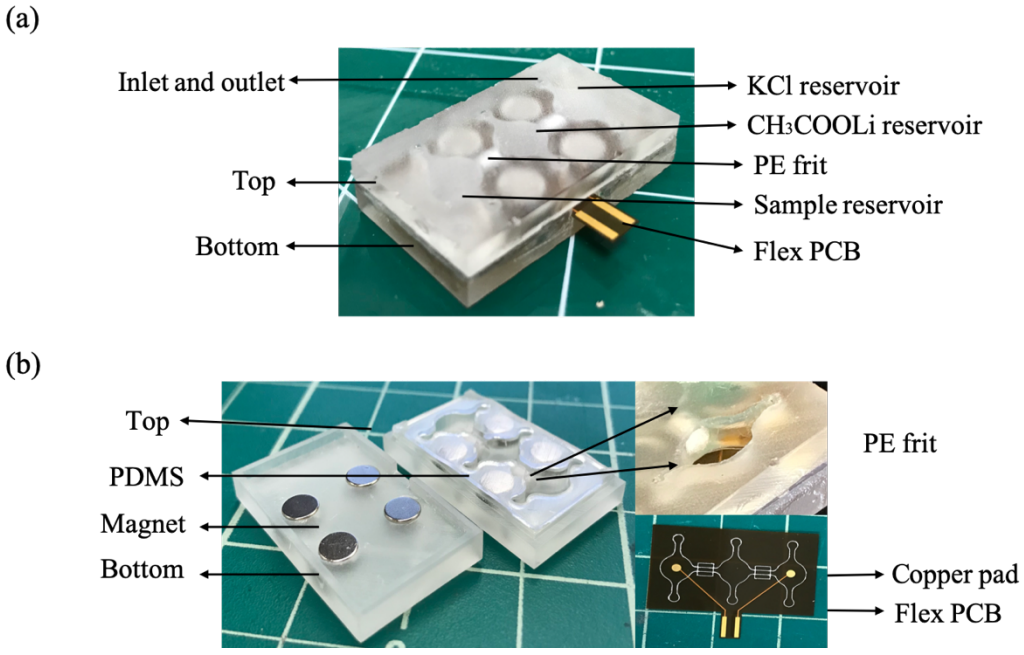

Figure 4.1 *(a) Photo of assembled device and (b) separate parts of the assembled device. From left to right, they are 3D printed bottom, top with a close-up figure for the PE frit and inner PCB.*

To obtain sufficient liquid isolation between the embedded chambers, a thin layer of polydimethylsiloxane (PDMS) is placed between the flexible PCB and the 3D printed top case prior to the assembling of the planar RE. No glue is used for assembling. The closing of the device relies on the four pairs of magnets. The RE can be easily opened and closed to replace the inner gel-state filling electrolyte or the flexible PCB containing sensing elements.

4.2.2 Materials and Manufacturing

Materials

KCl and CH_3COOLi powder were obtained from Sigma Aldrich; polydimethylsiloxane PDMS (Sylgard 184) was purchased from Dow Corning; Ag/AgCl ink (comprised finely dispersed chloridized silver flakes) was purchased from Fisher Scientific. Methyltriphenylphosphonium bromide, polyvinyl chloride, nitrocellulose, 2-nitrophenyl octyl ether, tetrahydrofuran, tridodecylmethylammonium nitrate and PE frits were purchased from Sigma Aldrich; Gelatin was purchased from Walmart; the PCB was fabricated in OSHPark. Deionized (DI) water was obtained from a Millipore^{TM} purification system and utilized for all experiments.

Device fabrication

A conventional 3D printer (FormLabs) is used to print all the parts. AutoCAD was used to design and draw the 3D structures. Then, the printed parts were immersed in isopropyl alcohol (IPA) for 10 minutes to wash away residual resin from the device surface and placed at room temperature until dry. The mini magnets were inserted into the holes on the 3D printed bottom and top cases as shown in Figure 4.1a and make sure the right direction of the magnets. Subsequently, two PE frits are inserted and fixed separately into the two lateral channels created in the top case.

A prepolymer mixture of PDMS and its curing agent with a weight ratio of 10:1 was poured onto the 3D printed mold and then thermally cured on a hotplate at 90 °C for 1 hour. Subsequently, the hardened PDMS polymer was pealed from the mold and placed on the top of the back side of the top case, as shown in Figure 4.1b.

A 700-nm thin layer of silver was firstly coated on the top of the round-shaped copper pads by evaporator with the help of a shadow mask to define the active electrode area. Then an Ag/AgCl paste was screen-printed on the top of the Ag pads and cured at 110 °C for 30 min. The thickness of Ag/AgCl paste (290 μm) was controlled by the thickness of stencil. For demonstration, a nitrate ion-selective membrane was prepared to functionalize the working electrode (WE). The cocktail contains methyltriphenylphosphonium bromide (0.25 wt. %), nitrocellulose (moistened with 2-propanol (35%); 1.93 wt. %), 2-nitrophenyl octyl ether (16.25 wt. %), polyvinyl chloride (5.75 wt. %), tetrahydrofuran (74.3 wt. %), and tridodecylmethylammonium nitrate (1.50 wt. %) [13]. This membrane used an ionophore-doped Polyvinyl chloride (PVC) and its solution was drop-cast on the top of the Ag/AgCl paste electrode to form the working electrode (WE). Before use, the WE was pre-conditioned in a 2000 ppm $NO3^-$-N solution for 12 hours. This step was shown crucial to minimize the response of the WE to other non-targeted ions such as Cl^- and $NH4^+$ [14]. Subsequently, the PCB was placed inside the groove of the 3D printed bottom case, and then the top case was placed on the top of the PCB. The magnets were then used to firmly close the whole device.

The inner filling electrolyte was prepared by dissolving 0.5 g gelatin powder into 2 ml 1 M KCl solution by a water bath method at 100 °C. Constant stirring until the gelation powder was totally dissolved into the KCl solution, then the mixture was immediately filled into the first chamber via an inlet. This process must be finished quickly and smoothly to reduce the

air bubble trapped inside the channel before the gelatin solidified. A small outlet was also required for air to flow out of the channel. Both the inlet and outlet were sealed by plugs made of PDMS at last.

The outer filling solution was prepared by dissolving 65.99 mg CH_3COOLi into 10 ml DI water to obtain 0.1 M CH_3COOLi solution. Then, the 0.1 M CH_3COOLi solution was filled into the middle chamber via an inlet. Same with the inner filling solution, air bubble should be removed, and both the inlet and outlet were sealed by the plugs made of PDMS at last. Sample solutions can flow through the third chamber containing the WE through the unsealed inlet and outlet for sensing.

4.2.3 Instrumentation

The potential of the planar RE with double junction was measured against a commercial calomel double junction RE (HANNA Instruments; Model HI5414) where 3.5 M KCl served as the inner filling electrolyte and the data was recorded using a home-made data logger (detailed information is included in Appendix A).

4.3 Results and Discussion

The experimental setup used for characterizing the presented double-junction RE is shown in Figure 4.2, where the commercial calomel glass-body RE and the planar RE were immersed in a big beaker filled with standard KCl testing solutions. When characterizing the performance of the RE, a big hole was opened on the top of the sample reservoir so that the standard testing solution could have a sufficient and direct contact with both of REs, in contrast, during the normal operation, no opening is needed because the sample solutions should flow through the sample reservoir via the inlet and outlet.

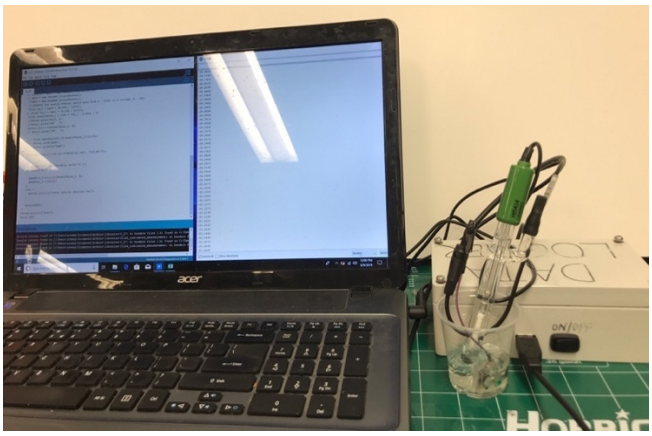

Figure 4.2 *Experimental setup used for charactering the performance of the proposed refillable planar RE, where the potential of the planar RE was measured against a commercial calomel double junction RE and is recorded by a home-made datalogger.*

4.3.1 Chloride Susceptibility

A RE should have a reproducible and stable potential that is not influenced by the composition and concentration of analyte solutions. Therefore, the first set of experiments was performed to study the chloride susceptibility of the RE using a series of KCl solutions that contain 10^{-6} M, 10^{-5} M, 10^{-4} M, 10^{-3} M, 10^{-2} M, 10^{-1} M and 1.0 M concentration of Cl^-. Before commencing a new test, the RE was thoroughly rinsed in DI water and air dried to remove any chances of residual chloride ions. The measurement time was set to 5 minutes for each test solution and all the measurements were conducted at 24 °C.

The potential differences between the planar double-junction RE and the commercial RE, when responding to the different Cl^- concentrations, is presented in Figure 4.3. As can be seen, the potential was hardly affected by the external Cl^- concentration, the absolute value of the slope is as low as 0.22 mV dec^{-1}. The Cl^- concentration insensitivity benefits from using the double-junction structure, in which the outer filling solution of CH_3COOLi helps to maintain a constant liquid junction potential, and meanwhile to reduce the outside interfering

ions' effect on the inner filling electrolyte. Given that the introduction of the intermediary liquid junction, it is likely that the proposed planar RE will offer a suitable RE for applications in which the Cl^- is a huge source of interference.

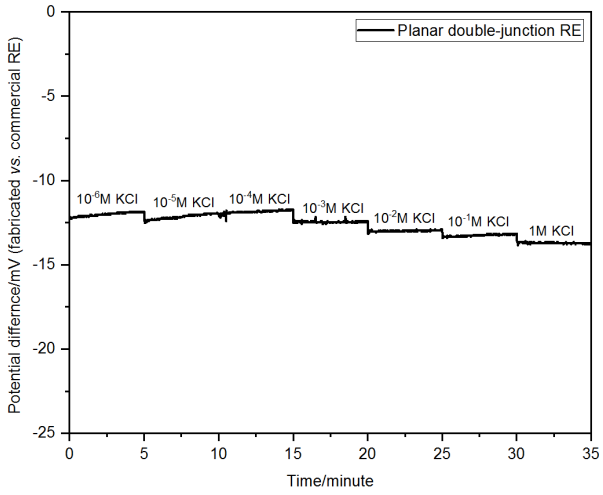

Figure 4.3 *Reference potential against the base potential provided by a commercial calomel double junction RE a function of time in different KCl solutions from 10^{-6} to 1 M.*

4.3.2 Response Time

The time interval, required to obtain a stable electrode potential when a RE is moved from one solution to a different solution, is defined as the response time (RT) of REs. Usually, the RT is affected by the direction of the concentration change and temperature. Therefore, in order to get the RT of the planar RE under different situations, the RE is tested by changing the chloride concentration of the solutions in the following concentration pattern, high-low-high-low-high. All the experiments here were conducted at 24 °C.

Figure 3.5 shows the experimental results, in which the RT is about 10 minutes when the planar RE was moved from high concentration to low concentration of KCl solutions and is less than 1 minute when the RE was moved from low concentration to high concentration of

KCl solutions. The high response speed of the planar RE maybe benefit from the high mobility of CH_3COO^- and Li^+.

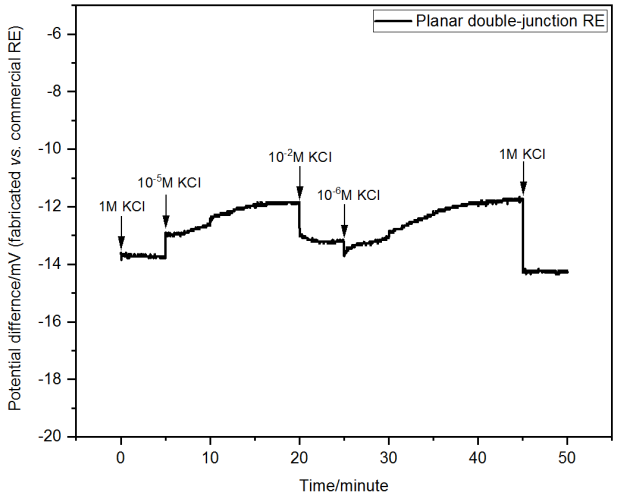

Figure 4.4 *Reference potential against the base potential provided by a commercial calomel double junction RE for response time test in KCl solutions.*

4.3.3 Short-term Stability

As one of the key features of RE, the short-term stability was studied by using the same setup used for the chloride ion susceptibility study. Here, the sample solution was fixed to 10^{-3} M Cl^- concentration, and the experimental period was set to 2 hours instead of 5 minutes. During the experiment, the RE was constantly immersed at constant temperature 24 °C. The experimental results are presented in Figure 4.5.

As can be seen in Figure 4.5, within a 2-hour time period, the planar RE with the double junctions exhibits a good short-term stability with only a small potential variation of 6 µV, which is comparable with the commercial glass-body REs. The high short-term stability was obtained due to the use of the double-junction structure that allows maintaining the chloride ion concentration constant in the inner filling chamber.

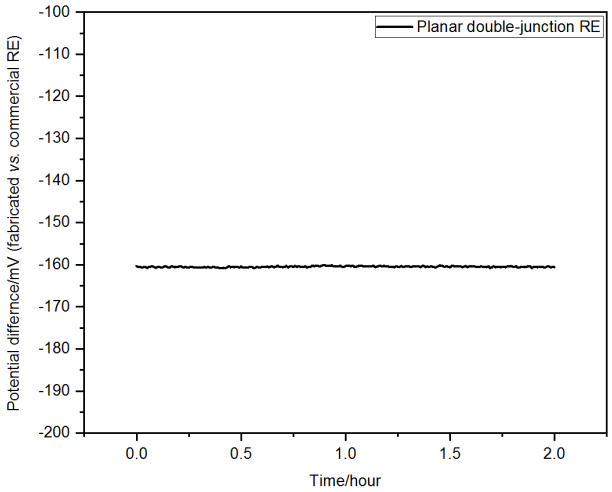

Figure 4.5 *Reference potential against the base potential provided by a commercial calomel double junction RE for short-term stability test in 10^{-3} M KCl solution for 2 hours.*

4.3.4 Long-term Stability

The long-term potential stability tests were carried out in a beaker containing 10^{-3} M KCl solution for 3 weeks and capped to minimize the solution evaporation. As shown in Figure 4.6, for the first 10 days, the potential of the planar RE with double junction remained stabilized, and then it started drifting with a -75 µV/hr drift rate.

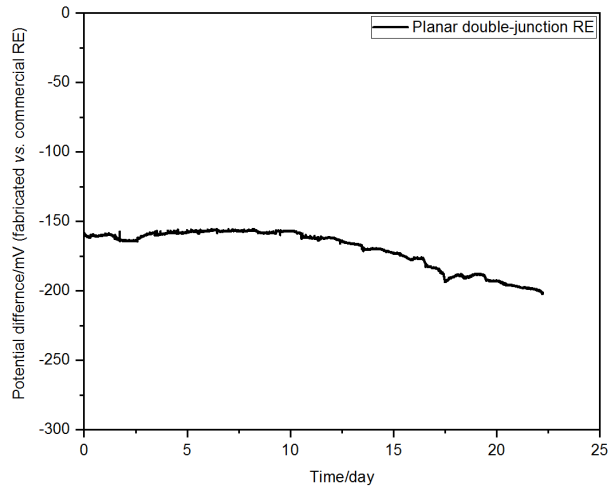

Figure 4.6 *Reference potential against the base potential provided by a commercial calomel double junction RE for long-term stability test in 10^{-3} M KCl solution for 3 weeks.*

After the planar RE was immersed into the testing solution, the chloride ions started to leach from the inner filling chamber into the outer filling chamber; however, because the KCl was dissolved into gelation, the leaching rate of the chloride ions was effectively reduced. Moreover, due to the outer filling lithium acetate, the inner filling KCl could not directly contact with the outside testing samples, which further helped to slow down the leakage rate of chloride ions. Thus, the concentration of Cl^- at the interface of Ag/AgCl could remain almost unchanged for a few days, resulting in a stable electrode potential (over 10 days according to the experimental results). Then, as time went by, the reference potential started to drift due to decreasing Cl^- concentration at the interface of Ag/AgCl because of the long-time Cl^- leaching. Therefore, this presented RE has an excellent long-term stability and suitable for applications where long-term measurement is needed.

4.3.5 Temperature Effect on The Stability

Temperature effect on the potential stability was studied by a water bath method, in which the sample container with 0.1 M KCl solution was firstly put inside a big beaker filled with DI water, and then the big beaker was placed on a thermoelectric cooling (TEC) plate to change the solution temperature.

In Figure 4.7, the planar double-junction RE shows a potential drift of -0.18 mV/°C in the temperature range from 20 to 90 °C, even at extremely high temperatures, the RE still can maintain good stability. This high temperature tolerance of the RE is attributed to using the gel-state inner filling electrolyte and the two-chamber structure. As early described, the gel-state electrolyte has a better temperature and pressure resistance compared with the liquid-state electrolyte. Although the gelatin melts in high temperature, the chloride ions are still soluble in the gelatin and the diffusion rate inside the gel becomes slower than it does in water.

Moreover, the two frits in the planar RE can effectively reduce the leakage of Cl^-, because the KCl is not in direct contact with the outside solutions. Therefore, this present planar RE is suitable for high temperature applications compared with the conventional REs with aqueous state inner filling solutions.

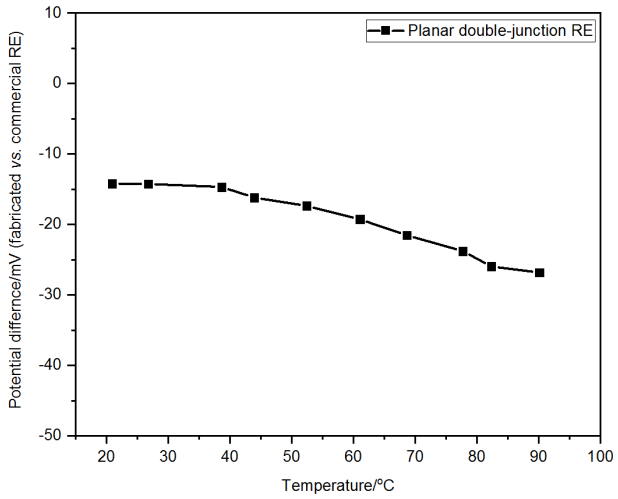

Figure 4.7 *Dependence of reference potential on temperature recorded in 0.1 M KCl solution.*

4.3.6 PH Effect on The Stability

The pH effect on the potential stability was measured in a 0.1 M KCl solution with the injection of concentrated HCl or NaOH to it. The real pH value was measured by a pH meter (pHTestr 10, Eutech Instruments). As shown in Figure 4.8, in the pH range from 3 to 12 the potential change was found to be lower than 0.08 mV/pH, and the potentials deviated far away only at extreme high and low pH values. This low pH sensitivity was obtained due to the outer filling electrolyte of CH_3COOLi. Because the CH_3COO^- and Li^+ do not have interactions with the H^+ and OH^-, the pH has a low effect on the diffusion potential. Therefore, this planar double-junction RE can be used in the samples across a wide pH range. However, in extremely high and low pH conditions, the sensor structure, mainly the PE frit and 3D printed case are

likely to be eroded, which may lead to a totally different diffusion potential, thus causing a dramatic potential drift as shown in Figure 4.8.

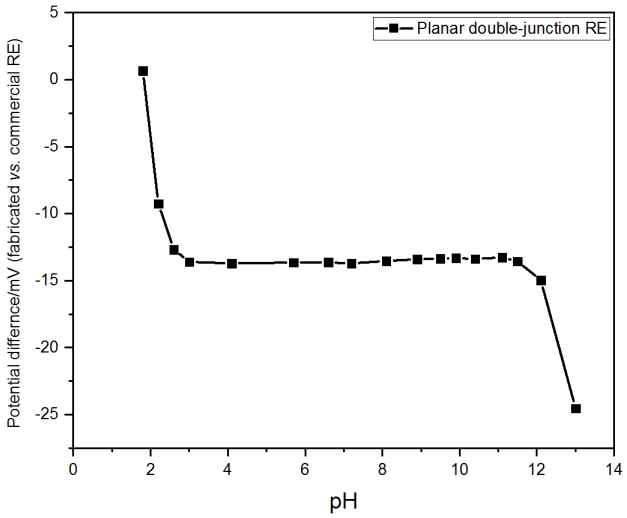

Figure 4.8 *Dependence of reference potential on pH (addition of HCl or NaOH) recorded in 0.1 M KCl solution.*

4.3.7 Nitrate Detection

A nitrate ion-selective electrode (ISE) reported in [15] was used to test the functionality of the planar double-junction RE. The curves shown in Figure 4.9a represent the potential as a function of nitrate concentration from 10 ppm to 5000 ppm in a logarithmic scale. The red curve represents the measured data, and the black curve indicates its linear fitting. From the parameters of the linear fit, the slope of the calibration curve of this nitrate sensor is -22.97±0.33 mV/decade with a R-Squared value of 0.999, which indicates a perfect linearity of the nitrate sensors based on the planar double-junction RE.

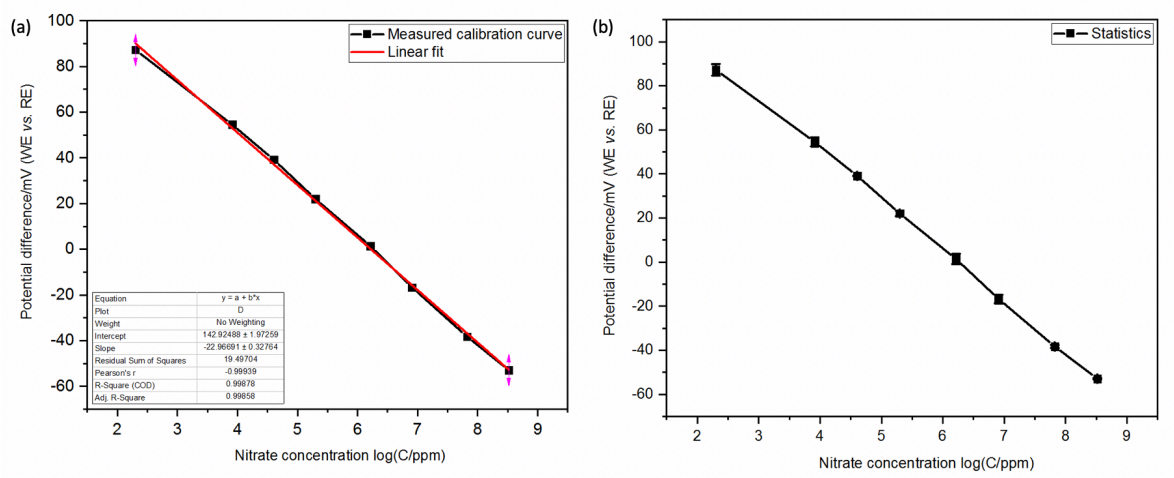

Figure 4.9 *(a) Output voltage of the ISE versus nitrate concentration. (b) Repeatability test. The average voltage in every solution was calculated based on 3 rounds of testing.*

To obtain the reproducibility of the nitrate sensor, 3 rounds of testing were conducted. In the first and third rounds, the concentrations of the testing solutions changed from 10 ppm, 50 ppm, 100 ppm, 200 ppm, 500 ppm, 1000 ppm, 2500 ppm to 5000 ppm, but for the second round testing, the concentrations were from 5000 ppm, 2500 ppm, 1000 ppm, 500 ppm, 200 ppm, 100 ppm, 50 ppm to 10 ppm. As shown in Figure 4.9b, the maximum standard deviation of potential is 5 mV over the whole testing range.

4.4 Conclusion

We report a refillable planar double-junction RE with excellent potential stability. The chloride susceptibility, response time, potential stability, temperature and pH effect on the potential stability of the planar RE were studied against a conventional glass-body calomel double-junction RE. The planar double-junction approach can improve the stability and insensitivity to the external Cl^- concentration changes, compared with the single-junction approach. In addition, the planar RE exhibits only a small potential variation over a wide pH

and temperature range. The double junctions of this RE are laid out in the same plane through an integration approach, providing a compact size and a high possibility to integrate with other components to form a miniature sensor system, which is advantageous over the vertically arranged two junctions in the commercial glass-body double-function RE that has a bulky size. Given that the introduction of the mini magnets, replacing the gel-state inner filling electrolyte becomes simple and easy. Therefore, due to the low cost, easy assembling process, and high performance, it is likely that the planar double-junction RE will offer a suitable RE solution for multiple applications, such as long-term environmental monitoring, smart agriculture, etc.

References

1. Inzelt, György, Andrzej Lewenstam, and Fritz Scholz. Handbook of reference electrodes. Heidelberg:: Springer, 2013.

2. Beginners Guide to ISE Measurement. Chapter 6: limitations and constraints on the application of ISE measurements, CCR-Nico2000 Ltd, 2016.

3. Lee, Hyuk Jin, et al. "Solvent-processible polymer membrane-based liquid junction-free reference electrode." *Analytical Chemistry* 70.16 (1998): 3377-3383.

4. Mi, Yanming, Sally Mathison, and Eric Bakker. "Polyion sensors as liquid junction-free reference electrodes." *Electrochemical and solid-state letters* 2.4 (1999): 198-200.

5. Yoon, Hyo Jung, et al. "Solid-state ion sensors with a liquid junction-free polymer membrane-based reference electrode for blood analysis." *Sensors and Actuators B: Chemical* 64.1-3 (2000): 8-14.

6. Cicmil, Dimitrije, et al. "Ionic Liquid-Based, Liquid-junction-free reference electrode." *Electroanalysis* 23.8 (2011): 1881-1890.

7. Bakker, Eric. "Hydrophobic membranes as liquid junction-free reference electrodes." *Electroanalysis: An International Journal Devoted to Fundamental and Practical Aspects of Electroanalysis* 11.10-11 (1999): 788-792.

8. Covington, A. K., P. D. Whalley, and W. Davison. "Improvements in the precision of pH measurements a laboratory reference electrode with renewable free-diffusion liquid junction." *Analytica chimica acta* 169 (1985): 221-229.

9. Kato, Kenneth J., and Dominick Frollini Jr. "Replaceable outer junction double junction reference electrode." U.S. Patent No. 4,390,406. 28 Jun. 1983.

10. Tymecki, Łukasz, Elżbieta Zwierkowska, and Robert Koncki. "Screen-printed reference electrodes for potentiometric measurements." *Analytica Chimica Acta* 526.1 (2004): 3-11.

11. Coetzee, J. F., and C. W. Gardner. "Teflon double-junction reference electrode for use in organic solvents." *Analytical Chemistry* 54.14 (1982): 2625-2626.

12. Arrance Sr, Frank C. "Double junction reference electrode." U.S. Patent No. 4,282,081. 4 Aug. 1981.

13. J. Sutter, et al. "Solid-contact polymeric membrane electrodes with detection limits in the subnanomolar range." *Analytica Chimica Acta* 523.1 (2004): 53-59.

14. T. Guinovart, et al. "A reference electrode based on polyvinyl butyral (PVB) polymer for decentralized chemical measurements." *Analytica chimica acta* 821 (2014): 72-80.

15. Kisiel, Anna, et al. "All-solid-state reference electrodes with poly (n-butyl acrylate) based membranes." Electroanalysis: An International Journal Devoted to Fundamental and Practical Aspects of Electroanalysis 20.3 (2008): 318-323.

CHAPTER 5. SANDWICHED ALL-SOLID-STATE SILVER-SILVER CHLORIDE REFERENCE ELECTRODE

A paper to be submitted to Sensors & Actuator: A. Physical

Xinran Wang, Md. Azahar Ali and Liang Dong

Abstract

This work presents a sandwiched all-solid-state silver-silver chloride (Ag/AgCl) reference electrode (S^3RE) fabricated on a silicon wafer. The S^3RE was formed by drop casting a mixture of polyvinyl butyral (PVB) and potassium chloride (KCl) on a screen-printed Ag/AgCl electrode, and another layer of aromatic polyurethane (PU) or Nafion coated on the top as the protection layer by an automated fluid dispensing robot. The presented S^3RE showed a performance comparable with the traditional liquid state reference electrodes in terms of stability, chloride susceptibility, and working temperature and pH range. This S^3RE can be made in micro-scale that is suitable for many applications concerning the size of the sensor.

5.1 Introduction

Development of reference electrodes (RE) with improved stability, reproducibility, and insensitivity to interfering species has become an attractive research topic in the area of electrochemical sensing. For decades, researchers have been seeking appropriate materials and structures to obtain high-performance REs. Since the concept of solid-state RE was proposed (i.e., replacing the inner filling solution in conventional REs with a solid contact), considerable efforts have been devoted to study proper materials suitable for serving as the solid contact between the electron-conducting substrate and the sample solutions. For a long time, the main focus is how to place a large quantity of potassium chloride (KCl) solution on the electrode in

limited space. For example, a solid KCl layer, prepared by directly melting KCl, was coated on the top of Ag/AgCl [1]. The RE with the solidified KCl electrolyte is suitable for applications in which the pH value varies a lot. But, its fabrication process requires high temperature, around 800 °C to melt KCl. Several other efforts have been attempted to use gel-like materials, such as agar, gelatin and (2-hydroxyethyl methacrylate) pHEMA, to work as a matrix to hold a high-concentration KCl (3 to 3.5M) [2, 3]. The high-concentration KCl can maintain a constant chloride ion level because the RE potential is considered proportional to the chloride ion concentration, same with the conventional RE [4, 5]. The employing of these types of materials as solid contacts indeed improve the performance of the RE; however, hydrogels with KCl can dry up if not stored under appropriate conditions. Some other porous materials have also been widely used as matrixes to hold KCl. For example, polyvinyl butyral (PVB) was used as a RE membrane cocktail and reported by Tomas in 2014 [6]. The fabricated RE presented a very good short and medium-term stability, however, due to the gradual leakage of Cl^-, its long-term stability was limited. In 2006, Maminska et al. developed a miniaturized all-solid-state RE based on polyvinyl chloride (PVC) membranes containing an ionic liquid [7]. Their fabricated RE exhibited a promising performance with a ± 5 mV short-term stability, and more than 2 months long-term stability. However, its lifetime is still not satisfactory compared with the conventional REs which have more than one-year lifetime. Therefore, in order to prevent the leakage of Cl^-, several additional materials were used as protective layers coated on the top surface. The most widely used materials include PVC, cellulose nitrate (CN), nafion (N) or their mixture. Anette Simonis et al. published a paper in 2005 characterizing different types of protective coating materials and concluded that with the

help of the protective coating, the leaching out of the chloride ions could be significantly reduced, and the stable time could be extended up to 51 days [2].

In spite of all the attentions paid on the material studies, some approaches relating to the structure development of RE have also been attractive, including reducing the contact area between the electrode and the analyte [8], providing a longer channel for the chloride ions movement [9], depositing KCl on both sides of Ag/AgCl layer [10], and using ion-sensitive field effect transistors (ISFETs) [11, 12].

Another key component determining the performance of a RE is the ion-to-electron layer. This layer is responsible for the electrode potential defined by the Nernst equation [13]. In solid-state REs, Ag/AgCl is used to form this layer due to its environmental compatibility. Generally speaking, there are two main methods to form this Ag/AgCl layer, including thin-film and thick-film technologies. In recent decades, thick-film technology has drawn increasing attention because of its robustness, ruggedness and low cost. A typical thick-film technology is screen printing. A review concerning the main challenges that screen-printed REs need to be overcome was published by M. Sophocleous et al. in 2017 [14]. In their review, they described the performance of different types of screen-printed REs and their applications.

Therefore, in this work we develop a sandwiched all-solid-state RE (S^3RE) with a mixture of polyvinyl butyral (PVB) and KCl as the ion-electron transductor and aromatic polyurethane (PU) as the protection layer. Investigations have been performed to characterize the S^3RE based on screen-printed Ag/AgCl in terms of Cl^- sensitivity, response time, stability, and temperature and pH effects. The S^3RE was shown to perform comparable to conventional REs for the potentiometric measurement.

5.2 Sensor Structure and Manufacturing

5.2.1 Structure of Electrode

The construction of the S^3RE is shown in Figure 5.1. The RE was screen-printed on a silicon wafer substrate consisting of three layers of functional materials, including an Ag/AgCl paste layer, a mixture of PVB and KCl membrane layer, and a PU protection layer (here Nafion is also possible in place of PU). Underneath the Ag/AgCl layer, a thin layer of silver (700 nm) was deposited for connecting to the external circuit.

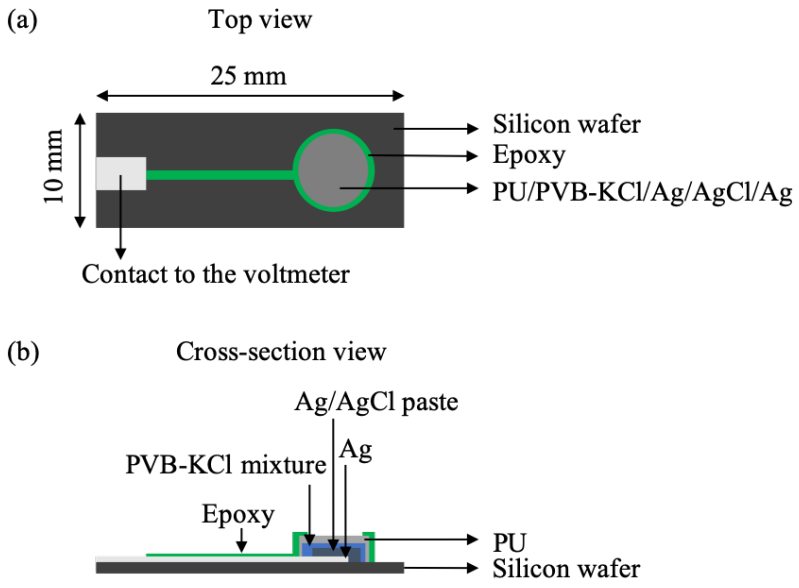

Figure 5.1 *(a) Top view and (b) cross-section view of the construction of the presented S^3RE.*

5.2.2 Materials and Manufacturing

Materials

Polyvinyl butyral (PVB), and Ag/AgCl ink (composed of finely dispersed chloritized silver flakes) were obtained from Fisher Scientific; 3M potassium chloride solution (KCl) saturated with AgCl , KCl, tetrahydrofuran (THF) and methanol were obtained from Sigma Aldrich; aromatic polyurethane (PU) was obtained from Lubrizol; epoxy (Circuitworks,

CW2500) was purchased from Digi-key; Deionized (DI) water with resistivity was obtained from a purification system from Millipore and utilized for all experiments.

Electrode preparation

The S^3RE was fabricated on a silicon wafer substrate using standard thick-film screen-printing technique and appropriate curing of several layers of functional materials. Figure 5.1b shows the schematic of the various layers that comprised the sensor structure. First, a 700-nm thin layer of silver was patterned by traditional soft lithography technique to define the active electrode area and contact area for connection. Then an Ag/AgCl paste was screen-printed on the top of the Ag pads (active electrode area) and was cured at 110 °C for 30 min. The thickness of Ag/AgCl paste (290 μm) was controlled by the thickness of stencil. Subsequently, the solid contact was made by drop casting a mixture of PVB and KCl, in which 80 mg PVB powder and 250 mg KCl crystal were dissolved into 1 mL methanol and was cured at room temperature for 2 hours. Then a PU layer was drop casted on the top of the PVB membrane. The PU was prepared by dissolving 1 g PU into 10 mL THF. All the drop casting work was accomplished by an automated fluid dispensing robot (Nordson EFD, RI). Finally, epoxy was printed on the top leaving the opening windows for the active electrode area and contact area. Epoxy was used to seal the edge of the PU layer in order to prevent the film from falling off and also protect the Ag connection wire. After the fabrication of the electrode, it was immersed into 3 M KCl solution for 3 days for preconditioning.

5.2.3 Instrumentation

The potential of the S^3RE was measured against a commercial calomel double junction RE (HANNA Instruments; Model HI5414), where 3.5 M KCl served as the inner filling electrolyte and the measurement results were recorded using a home-made data logger (detailed information is included in Appendix A).

5.3 Results and Discussion

5.3.1 Chloride Susceptibility

A high-quality RE should be stable under different analyte samples and the potential should remain constant in different Cl^- concentrations. A series of KCl solutions containing 0.01 M, 0.1 M, 0.5 M and 1.0 M concentration of Cl^- were firstly used to test the Cl^- effect on the proposed S^3RE. Before starting a new test, the RE was thoroughly rinsed in DI water and air dried to remove residual chloride ions. The experimental time was set to 5 min for each test. All the measurements were conducted at 24 °C. The potential differences between the commercial calomel double-junction RE and the S^3RE under different Cl^- concentrations were summarized in Figure 5.2.

For comparison, we tested two S^3REs based on the screen-printed Ag/AgCl electrode and the converted Ag/AgCl electrode by using $FeCl_3$. Additionally, for each fabrication method, we tested three electrodes: a bare Ag/AgCl electrode, an Ag/AgCl electrode coated with PVB layer, and an Ag/AgCl electrode coated with PVB and PU layers. As shown in both Figure 5.2a and Figure 5.2b, the Cl^- concentration has the smallest effect on the potential for the Ag/AgCl electrodes with both the PVB and PU layers, regardless of the fabrication methods for the Ag/AgCl layer. That is because without the PVB layer, the bare Ag/AgCl electrode is theoretically chloride ion sensitive, according to the Nernst equation. Therefore, the potential of the bare Ag/AgCl electrode RE showed the largest variation. For the electrode with the PU layer, because the chloride ion cannot easily penetrate this PU material, the leakage of the chloride ions is effectively reduced. Thus, the chloride ion concentration inside the PVB layer could remain constant, which helps to stabilize the reference potential. Also, by comparing the converted and the screen-printed Ag/AgCl electrodes, we can see both the electrodes show similar Cl^- susceptibility, and the slope is about 5 mV dec^{-1}. Thus, at the micro-scale, if the

thick-film technique is not easy to achieve, the converted Ag/AgCl can be used to serve as the functional element. Therefore, with the help of the PVB and PU layers, the solid-state RE can provide low chloride sensitivity comparable to the conventional liquid-state RE.

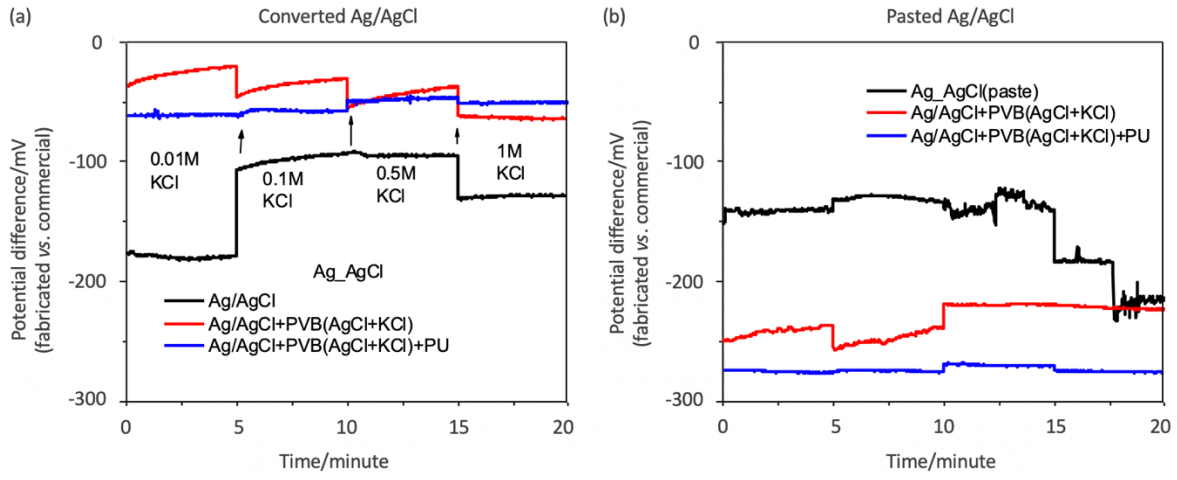

Figure 5.2 *Reference potential against the base potential provided by a commercial calomel double junction RE a function of time in different KCl solutions from 10^{-6} to 1 M.*

5.3.2 Response Time

The response time (RT) is an important character for REs. It can not only determine the response speed, but also affect the measurement accuracy because the potential data should be collected after the potential of RE becomes stable. In general, the RT of REs is defined as the time interval required to obtain a stable electrode potential when a RE is moved from one solution to another solution. RT is affected by the electrode type, temperature, magnitude and direction of the concentration change, and hysteresis, etc. [15]. Thus, the RT of the S^3RE was obtained by changing the chloride concentration of KCl solution in the following concentration pattern, high-low-high-low-high. All the experiments were conducted at 24 °C.

As seen in Figure 5.3, 3 minutes of RT was obtained when the S^3RE was moved from the high- to low-concentration KCl solutions. The RT was shown less than 1 minute when the

S^3RE was moved from the low to high concentration. The fast response of the S^3RE may benefit from using the semi-direct contact between the Ag/AgCl electrode and the testing solutions. Unlike other types of REs, the S^3RE does not have a long diffusion path. Therefore, the equilibrium could be quickly established in the same way as the bare Ag/AgCl electrode. Therefore, this S^3RE is suitable for applications in which fast response is preferred.

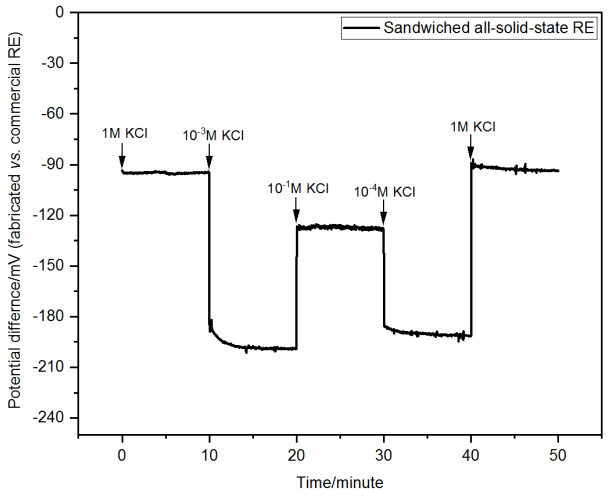

Figure 5.3 *Reference potential against the base potential provided by a commercial calomel double junction RE for response time test in KCl solutions.*

5.3.3 Pre-Conditioning Time on The Stability

In contrast to the liquid-state REs, the solid-state REs need to be immersed into a highly concentrated KCl solution for a period of time after the fabrication. This process is called pre-conditioning.

For a comparison, three measurements were conducted for the S^3RE, including without pre-conditioning, with 24-hour pre-conditioning, and with 72-hour pre-conditioning. As can be seen in Figure 5.4, after the pre-conditioning, the electrode potential stability increased. Also, with increasing pre-conditioning time, the electrode showed better stability. Therefore, the pre-conditioning is necessary for the solid-state REs. The possible reason for the stability

improvement may be because after a time period of immersion, the concentrated KCl solution helps to stabilize the junction potential at the interface between the PU layer and the testing solutions. However, since the development of the solid-state electrodes is still at the early stage, further study remains to be conducted to fully understand its working mechanism.

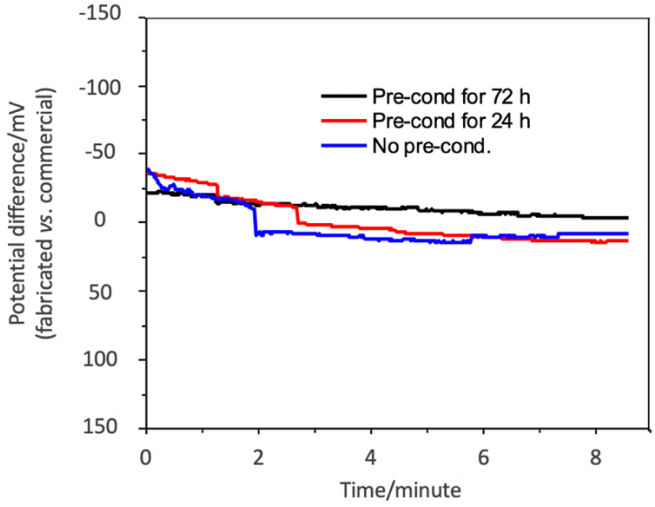

Figure 5.4 *Reference potential against the base potential provided by a commercial calomel double junction RE for short-term stability test in 10^{-3}M KCl solution for 2 hours.*

5.3.4 Long-term Stability

The long-term potential stability test was carried out in a beaker containing 10^{-3} M KCl solution for 3 weeks and capped to minimize the solution evaporation. As shown in Figure 5.5, the potential of the S^3RE was found to drift at a 104 μV/hr drift rate.

Due to the PU protection layer, the leakage of the chloride ions was effectively reduced. The PU layer helped to remain the concentration of chloride ions constant at the electrode. As a result, the potential drift rate largely reduced compared with the REs without the protection layer. The high long-term stability of the S^3RE is comparable with the conventional liquid-sate REs reported in the other literatures.

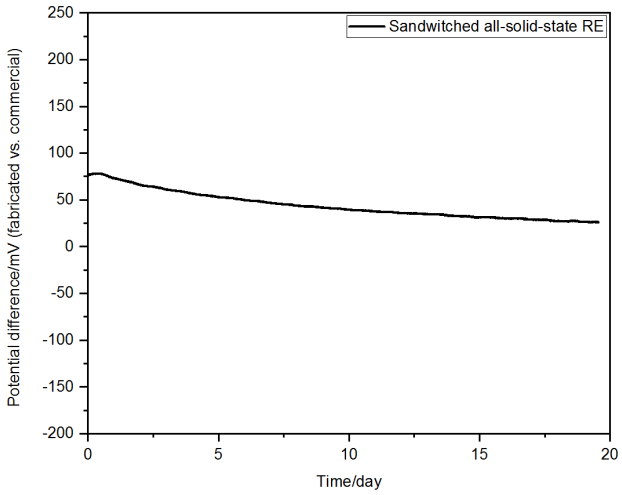

Figure 5.5 *Reference potential against the base potential provided by a commercial calomel double junction RE for long-term stability test in 10^{-3} M KCl solution for 3 weeks.*

5.3.5 Temperature Effect on The Stability

Temperature effect on the potential stability was studied by using a water bath method, in which the sample container with 0.1 M KCl solution was firstly put inside a big beaker filled with DI water, and then the big beaker was placed on a thermoelectric cooling (TEC) plate to change the solution temperature.

As shown in Figure 5.6, the S^3RE shows a small potential change of -0.5 mV/°C over a wide temperature range from 20 to 90 °C. No large deviation of potential was observed even under extreme high temperatures. The high temperature stability was achieved probably due to the use of all solid-state materials in this S^3RE. Note that in liquid-state REs, the solubility of AgCl strongly dependent on temperature.

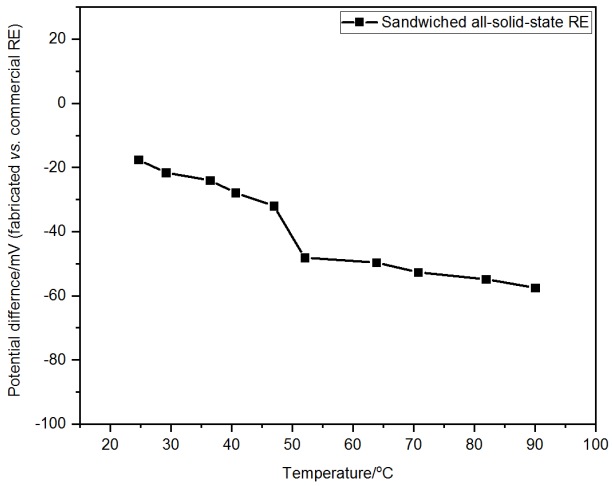

Figure 5.6 *Dependence of reference potential on temperature recorded in 0.1 M KCl solution.*

5.3.6 PH Effect on The Stability

A severe interferent for polymer based solid-state RE can result from the H^+/OH^- ions present in samples of different pH, affected, e.g., by the presence of dissolved CO_2. [16] Figure 5.7 presents influence of changing pH, established by injection of concentrated HCl or NaOH to the 0.1M KCl solution. The real pH value was measured by a pH meter (pHTestr 10, Eutech Instruments).

As shown in Figure 4.8, the potential changes are about 25 mV within the pH range from 3 to 11, and the potentials deviated far away at extreme high pH values. Thus, this S^3RE can be used in the samples across a wide pH range with high stability; however, compared with liquid-state REs, for example the micro-channel RE described in the previous chapter, the pH has a larger effect on the S^3RE potential. This is because the H^+ and OH^- have a large effect on the polarity of the PU layer, which are likely to change the diffusion potential of the S^3RE. In addition, strong acidic and alkali will also change the property of PU, thus leading to a big

potential drift. In many applications the environmental pH will be around the natural condition, therefore, the S^{3}RE is safe to be used in these applications.

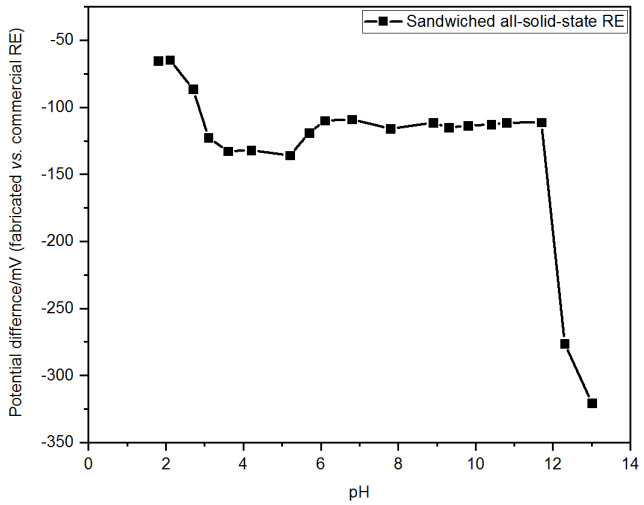

Figure 5.7 *Dependence of reference potential on pH (addition of HCl or NaOH) recorded in 0.1 M KCl solution.*

5.3.7 Nitrate Detection

As a demonstration, we built a nitrate ion sensor that integrates a nitrate ion-selective electrode (ISE) [17] and the S^{3}RE. The calibration graph and repeatability test are presented in Figure 5.8.

The potential output as a function of nitrate concentration from 10 ppm to 5000 ppm in a logarithmic scale is shown in Figure 5.9a. As shown in the parameter table of the linear fitting, the slope of the calibration curve of this nitrate sensor is -23.43±0.33 mV/decade with an R-Squared value of 0.999. The high R-Squared value indicates a good linearity of the nitrate sensors based on the S^{3}RE, ensuring high accuracy.

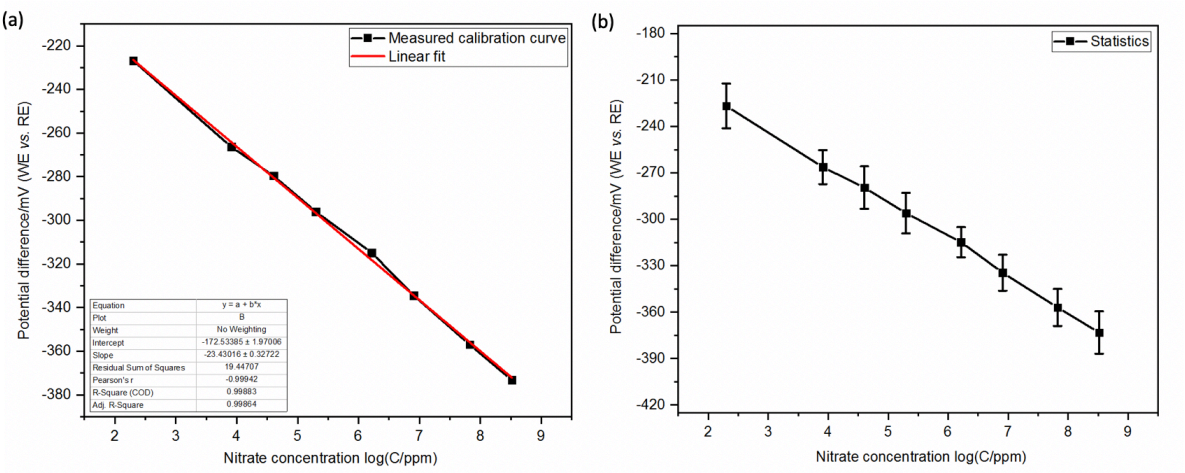

Figure 5.8 *(a) Output voltage of the ISE versus nitrate concentration. (b) Repeatability test. The average voltage in every solution was calculated based on 3 rounds of testing.*

For the reproducibility test shown in Figure 5.9b, the maximum potential variation is 13.69 mV over the whole repeatability testing range from 10 ppm to 5000 ppm. Such potential variation is lower than the serpentine microfluidic-channel based RE described in Chapter 2, but higher than the planar double-junction RE described in Chapter 3. Therefore, there is a lot of room to improve the repeatability of the S^3RE.

5.4 Conclusion

In this paper, we report a sandwiched all-solid-state silver-silver chloride reference electrode (S^3RE). The chloride susceptibility, response time, potential stability, temperature and pH effect on the potential stability of the S^3RE were studied against a conventional glass-body calomel double-junction RE. The protection layer of aromatic polyurethane (PU) or Nafion (as seen in the next Chapter) improved the long-term stability and insensitivity to Cl^- concentration changes in the testing solutions when compared with the REs with the bare PVB layer. In addition, the S^3RE exhibits only a small potential variation over a wide temperature

range. Further study remains to fully understand the mechanism for the S^3RE. Given the usage of an automated fluid dispensing robot, the S^3RE can be made with high throughput; therefore, the S^3RE has provided a new application field for potentiometric measurement.

References

1. Vonau, W., et al. "An all-solid-state reference electrode." Sensors and Actuators B: Chemical 144.2 (2010): 368-373.

2. Simonis, Anette, et al. "Miniaturised reference electrodes for field-effect sensors compatible to silicon chip technology." Electrochimica acta 51.5 (2005): 930-937.

3. Ganjali, Mohammad Reza, et al. "A novel Holmium (III) membrane sensor based on N-(1-thien-2-ylmethylene)-1, 3-benzothiazol-2-amine." Analytical letters 39.6 (2006): 1075-1086.

4. Giddings, J. Calvin. Dynamics of chromatography: principles and theory. CRC Press, 2017.

5. Ives, David JG, George J. Janz, and C. V. King. "Reference electrodes: theory and practice." Journal of The Electrochemical Society 108.11 (1961): 246C-247C.

6. Guinovart, Tomàs, et al. "A reference electrode based on polyvinyl butyral (PVB) polymer for decentralized chemical measurements." Analytica chimica acta 821 (2014): 72-80.

7. Mamińska, Renata, Artur Dybko, and Wojciech Wróblewski. "All-solid-state miniaturised planar reference electrodes based on ionic liquids." Sensors and Actuators B: Chemical 115.1 (2006): 552-557.

8. Tymecki, Łukasz, Elżbieta Zwierkowska, and Robert Koncki. "Screen-printed reference electrodes for potentiometric measurements." Analytica Chimica Acta 526.1 (2004): 3-11.

9. Zevenbergen, M. A. G., et al. "Solid state pH and chloride sensor with microfluidic reference electrode." 2016 IEEE International Electron Devices Meeting (IEDM). IEEE, 2016.

10. Guth, U., et al. "Solid-state reference electrodes for potentiometric sensors." Journal of Solid State Electrochemistry 13.1 (2009): 27-39.

11. Comte, Pierre A., and Jiří Janata. "A field effect transistor as a solid-state reference electrode." Analytica Chimica Acta 101.2 (1978): 247-252.

12. Wang, Joseph, and Lucio Angnes. "Miniaturized glucose sensors based on electrochemical codeposition of rhodium and glucose oxidase onto carbon-fA.ber electrodes." Analytical Chemistry 64.4 (1992): 456-459.

13. Inzelt, György, Andrzej Lewenstam, and Fritz Scholz. Handbook of reference electrodes. Heidelberg:: Springer, 2013.

14. Sophocleous, Marios, and John K. Atkinson. "A review of screen-printed silver/silver chloride (Ag/AgCl) reference electrodes potentially suitable for environmental potentiometric sensors." Sensors and Actuators A: Physical 267 (2017): 106-120.

15. http://www.nico2000.net/datasheets/glossary.html#platinum

16. J. Sutter, et al. "Solid-contact polymeric membrane electrodes with detection limits in the subnanomolar range." Analytica Chimica Acta 523.1 (2004): 53-59.

17. Kisiel, Anna, et al. "All-solid-state reference electrodes with poly (n-butyl acrylate) based membranes." *Electroanalysis: An International Journal Devoted to Fundamental and Practical Aspects of Electroanalysis* 20.3 (2008): 318-323.

CHAPTER 6. APPLICATION I: CONTINUOUS MONITORING OF SOIL NITRATE USING A MINIATURE SENSOR WITH POLY(3-OCTYL-THIOPHENE) AND MOLYBDENUM NANOCOMPOSITE

A paper submitted to ACS Applied Materials & Interfaces (in press)

Md. Azahar Ali, [1,$] Xinran Wang,[1,$] Yuncong Chen,[1] Yueyi Jiao,[1] Navreet K. Mahal,[2] Moru Satyanarayana,[1] Michael J. Castellano,[2] James C. Schnable,[3] Patrick S. Schnable,[2] and Liang Dong[1]

[1]Department of Electrical and Computer Engineering, Iowa State University, Ames, IA, USA

[2]Department of Agronomy, Iowa State University, Ames, IA, USA

[3]Department of Agronomy and Horticulture, University of Nebraska-Lincoln, Lincoln, NE, USA

[$]Co-first authors (equal contribution to the work)

Abstract

There is an unmet need for improved fertilizer management in agriculture. Continuous monitoring of soil nitrate would address this need. This paper reports an all-solid-state miniature potentiometric soil sensor that works in direct contact with soils to monitor nitrate-nitrogen (NO_3^--N) in soil solution with parts-per-million (ppm) resolution. A working electrode is formed from a novel nanocomposite of poly(3-octyl-thiophene) and molybdenum disulfide (POT–MoS_2) coated on a patterned Au electrode and covered with a nitrate-selective membrane using a robotic dispenser. The POT–MoS_2 layer acts as an ion-to-electron transducing layer with high hydrophobicity and redox properties. The modification of the POT chain with MoS_2 increases both conductivity and anion exchange, while minimizing the formation of a thin water layer at the interface between the Au electrode and the ion-selective membrane, which is notorious for solid-state potentiometric ion sensors. Therefore, the use of

POT–MoS_2 results in an improved sensitivity and selectivity of the working electrode. The reference electrode comprises a screen-printed silver/silver chloride (Ag/AgCl) electrode covered by a protonated Nafion layer to prevent chloride (Cl^-) leaching in long-term measurements. This sensor was calibrated using both standard and extracted soil solutions, exhibiting a dynamic range that includes all concentrations relevant for agricultural applications (1–1500 ppm NO_3^--N). With the POT–MoS_2 nanocomposite, the sensor offers a sensitivity of 64 mV/decade for nitrate detection, compared to 48 and 38 mV/decade for POT and MoS_2 alone, respectively. The sensor was embedded into soil slurries where it accurately monitored nitrate for a duration of 27 days.

6.1 Introduction

Low-cost, high-performance nutrient sensors that continuously monitor soil conditions for precision agriculture [1, 2], plant phenotyping [3], and environmental quality [2] are in high demand. Soil is the primary source of nutrients for plant growth [4-7]. Biologically available soil nitrogen (N) is one of the key limiting factors in plant growth, and crop productivity relies heavily on the application of supplemental N in the form of fertilizer. Yet the proper amount of N fertilizer input can vary within fields by >100% per year due to variation in the soil N supply that is mostly caused by inter-annual weather variability. Insufficient N fertilizer input reduces crop production and excessive N input harms the environment. Farmer income suffers from both.

Continuous monitoring of N dynamics in agricultural fields would help maximize control over fertilizer management. Several laboratory-based soil N measurement methods are widely used, such as gas chromatography-mass spectrometry (GC-MS), ultraviolet-visible (UV-VIS) spectrophotometry, ion chromatography (IC), chemiluminescence [8-12]. Although

these methods are highly sensitive and selective and exhibit superior performance, they are known to have instrumentational complexity and need laborious and time-consuming tasks. Colorimetric determination of nitrate relies on reduction of nitrate by vanadium (III) combined with detection by the Griess reaction, and needs extraction of nitrate ions from soil samples using high-concentration (e.g., 2M) KCl solution, which limits its practical operation in fields [7]. With an increasing demand for on-site nitrate monitoring, mobile vehicle-based nitrate sensors [13] have been reported but still require significant labor and are relatively expensive. Satellite remote sensing [14] provides an indirect measure of plant N dynamics and does not currently provide high accuracy or spatial resolution. The development of field-deployable soil nitrate sensors is an attractive solution to better manage N fertilizer. Noteworthy in-field nitrate sensing methods include electrochemical sensors [5, 6, 15] ion-selective electrodes (ISEs) [16, 17], and microfluidic electrophoresis [18]. But these miniature sensor methods need further development or remain challenging mainly due to the suboptimal sensitivity, relatively high signal drift, and material instability [19].

Ion-selective membrane (ISM)-based sensors are considered a promising approach to detect soil nutrients. Many ISEs are manufactured by simply coating thin metal wires with ISMs. However, redox-active charged species are difficult to transfer to metal wires, leading to a capacitive interface with the wire [20]. Conversely, non-metal wire-based ISEs often require an inner filling between the ISM and a conductive metal layer substrate [21-25]; their main drawbacks, however, include easy contamination of the filling solution with interfering ions, gradual evaporation of solutions, variations in both osmolality and ionic strength, membrane delamination, poor adhesion, and difficulty in device miniaturization [23, 26].

Although ISEs that do not use inner filling solutions are an attractive option, a thin water layer that often forms at the interface between the conducting metal layer and the ISM has created a major challenge to the development of these sensors. Usually, this thin water layer presents an interfacial barrier to fast electron transfer and negatively impacts selectivity of the sensor to specific ions because different ions are trapped inside it [27, 28]. Therefore, significant attempts have been made to replace the inner filling solutions with solid-contact materials as ion-to-electron transducing layers, with the objective of realizing an all-solid-state miniature ion sensor [29-33]. Many solid-contact candidate materials have been investigated, including hydrogel [34], carbon nanotubes (CNTs) [35-36], graphene [32], polymer-carbon composites [37], metallic nanostructures [38], macro-porous carbon [39], and conjugated conducting polymers such as polyaniline [19], poly(3,4-ethylenedioxythiophene) (PEDOT) [40], and poly(3-octylthiophene-2,5-diyl) (POT) [27, 41-42]. Of these, PEDOT has a strong ability to oxidize to PEDOT+, and thus has been extensively used as a solid-contact material30 to attract lipophilic ions from the ISM to the conducting metal layer to establish potential equilibrium. As another promising candidate, electropolymerized [41-42] drop-casted [43], and Langmuir–Blodgett [44] POT are redox sensitive, and can be oxidized reversibly in anion solutes with a low ohmic voltage drop; in addition, the high hydrophobicity of POT restricts the formation of a water layer between the POT and the ISM. Recently, the incorporation of 7,7,8,8-tetracyanoquinodimethane (TCNQ) into a POT matrix contributed to reducing the potential drift by more than one order of magnitude due to the introduction of a TCNQ/TCNQ− redox couple [45]. Despite its high redox property [41] POT has a relatively low conductivity (approximately 10-6 S/cm) [28] and is also sensitive to light [36], which negatively impacts the efficiency of charge transport through the POT to the conducting metal substrates.

Here, we report a miniature solid-state potentiometric sensor for the continuous monitoring of soil nitrate. The sensor uses a nanocomposite of POT and transition metal dichalcogenides of molybdenum disulfide (MoS_2) nanosheets [46] as a solid-contact ion-to-electron transducing layer. MoS_2 nanosheets provide large surface area, high conductivity [47], insensitivity to light and pH, and absence of any side-reactions. The working electrode (WE) was built on top of a copper pad of printed circuit board (PCB) covered by a thin, patterned gold (Au) layer, a molybdenum disulfide (POT–MoS_2) nanocomposite-based solid-contact layer, and a nitrate-specific ISM. The incorporation of MoS_2 into POT not only increases the redox properties of POT [48], but also maintains high hydrophobicity to minimize the formation of a thin water layer between the ISM and the Au layers. The use of POT–MoS_2 remedies the issue of the trapped water layer, thus contributing to increased charge transfer and ion selectivity of the WE [49-51]. The reference electrode (RE) of this nitrate sensor includes a silver/silver chloride (Ag/AgCl) electrode covered by a proton-exchange membrane to reduce redox reaction-induced chloride leaching from the RE, thus minimizing the drift of the reference potential. The sensor features an all-solid-state design that incorporates the POT–MoS_2 nanocomposite for improved device performance. The sensor can also be directly embedded in soil slurries for continuous measurement of nitrate dynamics for approximately four weeks. Furthermore, all the sensor materials (except for the screen-printed Ag/AgCl and evaporated Au) are deposited and patterned using a high-resolution dispensing robot with good control over the uniformity of material thickness.

6.2 Methods and Experimental Section

6.2.1 Materials

Methyltriphenylphosphonium bromide, polyvinyl chloride, Nafion, nitrocellulose, 2-nitrophenyl octyl ether, tetrahydrofuran, and tridodecylmethylammonium nitrate were purchased from Sigma Aldrich, MO. Polyvinyl butyral (PVB), regioregular POT, and Ag/AgCl ink (composed of finely dispersed chloritized silver flakes) were obtained from Fisher Scientific, MA. Ultrafine powders of MoS_2 nanosheets were obtained from Graphene Supermarket, NY. Deionized water with a resistivity of 18.2 MΩ cm was obtained using a purification system from Millipore, MA. Potassium nitrate (KNO_3), calcium sulfate ($CaSO_4$), sodium chloride (NaCl), sodium bicarbonate ($NaHCO_3$), and sodium phosphate monobasic (NaH_2PO_4) were also obtained from Fisher Scientific, MA. The PCB was manufactured by OHSPARK, OR.

The NO_3^- ISM cocktail contained methyltriphenylphosphonium bromide (0.25 wt. %), nitrocellulose (moistened with 2-propanol (35%); 1.93 wt. %), 2-nitrophenyl octyl ether (16.25 wt. %), polyvinyl chloride (5.75 wt. %), tetrahydrofuran (THF; 74.3 wt. %) and tridodecylmethylammonium nitrate (1.50 wt. %). This solution was sealed and stored at -20 °C [52].

6.2.2 Nanocomposite of POT–MoS_2

The weight ratio of POT to MoS_2 was varied from 1:1 to 1:10 to study the influence of material composition on the redox properties of different POT–MoS_2 nanocomposites. In each case, the concentration of POT solution was fixed at 2.6 mg/mL. For example, in order to prepare a POT–MoS_2 sample with a 1:4 weight ratio of POT to MoS_2, 2.6 mg POT powders were dissolved in 1 mL THF solvent. 10.4 mg MoS_2 was added to the POT solution and

sonicated for 4 h. Due to the attraction between the opposite charges of MoS_2 and POT, a homogeneous solution of POT–MoS_2 nanocomposite was formed.

6.2.3 Electronic Circuitry

A homemade data logger with embedded readout circuitry was used to detect and record potential variations between the WE and RE. The voltage potential provided by the sensor was first isolated from other parts of the readout circuit using two buffer amplifiers. Then, the output signal from the buffer amplifiers was fed to a differential amplifier to obtain a single output voltage, which could be further enhanced five-fold by using an inverting amplifier. Further, a voltage lifter circuit was introduced to obtain both negative and positive data from the sensor using a microcontroller. A two-order filter with 1 Hz cut-off frequency was then used to reduce the noise signal at the output. Finally, an Adafruit Feather 32u4 microcontroller was used to realize analog-to-digital signal conversion.

6.2.4 Device Fabrication

The sensor had two 5-mm-diameter, round-shaped electrodes formed on the PCB that served as the WE and RE. The rectangular pads on the PCB allowed for connecting the WE and RE to an external data logger. The base material of the WE and RE was copper. With the help of a shadow mask, a 5.2-mm-diameter and 100-nm-thick Au layer was deposited on top of one of the base electrodes using electron-beam evaporation. The same approach was used to form a 5.2-mm-diameter and 500-nm-thick Ag layer on top of the other base electrode. Figure 6.1 (a) shows a wafer-scale PCB containing arrays of RE and WE. To form the POT–MoS_2 nanocomposite and nitrate-selective ISM layers, a high-precision, automated fluid dispensing robot (Nordson EFD, RI) was used to dispense the prepared POT–MoS_2 and ISM solutions, respectively, on top of the Au surface (Figure 6.1c). During this process, the POT–MoS_2 solution was first dispensed out of a syringe (size 10 cc) under an air pressure of 2 psi,

followed by thermal treatment on a hotplate at 65 ºC for 1 h. After the ISM solution was dispensed, the WE was dried at room temperature for 10 h. The same material coating technique was applied to make other WEs using POT or MoS_2 alone as the solid-contact ion-to-electron transducing layer for comparison with the proposed WE with the POT–MoS_2 nanocomposite. To form the RE of the sensor, the round-shaped Ag electrode was further screen-printed with Ag/AgCl paste using a stencil mask placed on top of the PCB. The 200-µm-thick Ag/AgCl paste was dried at 110 ºC for 2 h. To prevent the leaching of chloride ions as a result of the redox reaction of Ag/AgCl during long-term measurement [53], a 15-nm-thick perfluorinated polymer layer, or Nafion was coated on the surface of Ag/AgCl using the above-mentioned fluid dispensing robot, and was then dried at 90 ºC for 1 h. In addition, the Nafion layer could also block anions entering the RE from the surrounding environment. Lastly, a 1.2-mm-thick waterproof insulating epoxy (Circuitworks, CW2500) was used to cover the PCB except for the regions of the WE, RE, and contact pads. This insulation layer impedes water penetration from the sidewalls of the coated materials when the sensor is embedded in soil slurries. The sensor was preconditioned by dipping it into 1500 ppm NO^-_3-N solution for 24 h. Figure 1c shows the fabricated solid-state nitrate sensor.

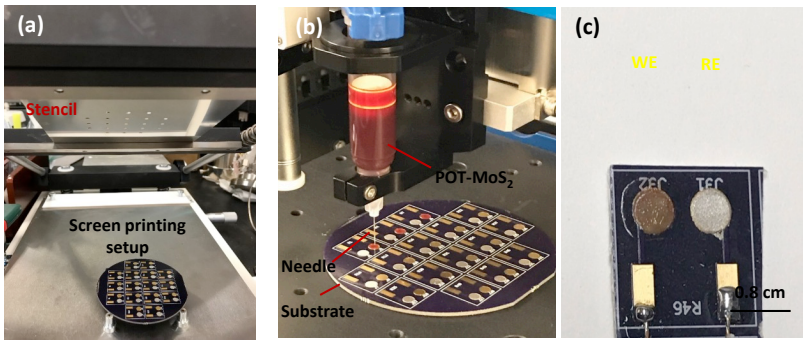

Figure 6.1. *Step-wise representation of the fabrication of all-solid-state soil nitrate sensor. (a) Photograph taken during printing Ag/AgCl paste on circular-shaped silver (Ag) electrodes*

using a stencil printer. (b) Photograph taken during materials dispensing (POT–MoS_2 in THF solvent) on circular-shaped Au electrodes using a programmable high-precision. (c) Photograph of the device.

6.2.5 Working Principle

As the ion-to-electron transducing layer, the POT–MoS_2 nanocomposite layer undergoes a redox reaction during sensing. The mechanism of anion (or cation) exchanging through POT is demonstrated in the previously reported literature [27], Si *et al.,* demonstrated a cyclic voltammetric experiment for anion (lipophilic) exchanging process in POT electrode-based ion selective membrane [27]. Kim *et al.,* also explained the anion-exchanging in POT film coated with ISM using ion-transfer stripping voltammetry [42]. Figure 6.2 shows the oxidation and reduction associated with the sensing mechanism. The mechanism for extracting electrochemically mediated anions (NO_3^-) into the ISM involves three phases [27], including (1) oxidizing the POT–MoS_2 (or P) to $(POT–MoS)^+$ (or P^+); (2) triggering the extraction of NO_3^- from the test sample; (3) re-distributing lipophilic anions (R^-) from the ISM to the POT–MoS_2 layer. The corresponding redox reaction accompanied by NO_3^- transfer at the ISM is given by:

$$P^+_{(p)} + e^- + R^-(p) + NO_3^-{}_{(m)} \leftrightharpoons P_{(p)} + R^-_{(m)} + NO_3^-{}_{(aq)} \quad 6.1$$

where m, p, and aq represent the ISM phase, POT–MoS_2 nanocomposite phase, and aqueous phase, respectively, and $P_{(p)}$ and $P^+_{(p)}$ represent a few monomeric units of the POT chain in the neutral insulating state and the oxidized state with polaronic sites, respectively. Owing to the oxidation process (Figure 6.2a), the POT–MoS_2 extracts the sample anions $NO_3^-{}_{(aq)}$ into the ISM and forces the redistribution of lipophilic anions (R^-) into the POT–MoS_2 layer. In the reduction process (Figure 6.2b), the $(POT–MoS_2)^+$ becomes neutral POT–MoS_2, releasing the lipophilic

anions R^- (p) into the ISM, which in turn leads to a release of $NO_{3^-(aq)}$ from the outer membrane ($NO_{3^-(m)}$) into the test solution. Therefore, by combining the redox and ion-exchange processes at the WE, an equilibrium is established at the aqueous-nanocomposite-ISM interfaces, leading to charge separation at each interface, thus generating a phase-boundary potential [12]. This phase-boundary potential E_1 is given by $E_1 = \frac{RT}{zF} \times \ln a_I$, where, the R, T, z, F, and a_I represent the gas constant, temperature, charge of target ion, Faraday constant, and the primary ion activity without interfering ions. On the other hand, the RE of the sensor also undergoes a redox reaction, providing a constant potential (E_0) [54]. The Nafion layer coated on the surface of the Ag/AgCl not only minimizes leaching of the chloride ion from Ag/AgCl, but also blocks other anions in the external environment from entering the RE. As the anions or cations move from high to low regions of concentration, a potential difference is produced during ion exchange. Therefore, the potential (E) is dependent on the logarithm of the ion activity and is described by the Nernst Equation [55]:

$$E = E_0 + E_1 = E_0 + \frac{RT}{zF} \ln a_I(I) \qquad 6.2$$

To determine the ion selectivity of the sensor, according to Nicolskii-Eisenman formalism [56], the logarithm term in Eq. (6.2) can be replaced by a sum of selectivity-weighted activities given by:

$$E = E_0 + \frac{RT}{nF} \ln(a_I(IJ) + K_{IJ}^p a_J(IJ)^{Z_I/Z_J}) \qquad 6.3$$

where K_{IJ}^p is the selectivity coefficient, $a_I(IJ)$ and $a_J(IJ)$ are the activities of I and J, respectively, in the test solution, and Z_I and Z_J are the charges of the primary and interfering ions, respectively.

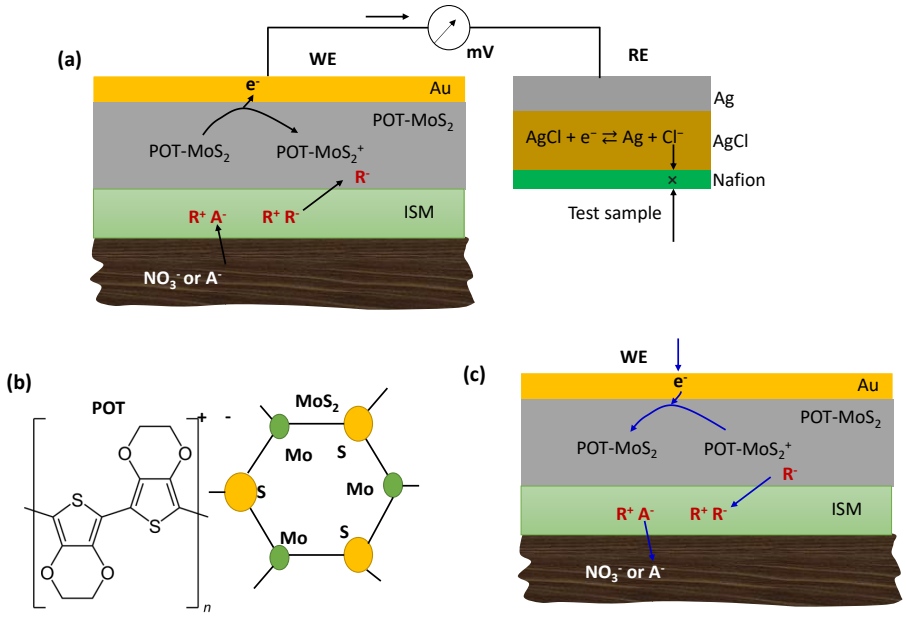

Figure 6.2. *Schematic of the working principle of the soil sensor. (a) The oxidation process for the working electrode (ISM/POT–MoS_2/Au) in the presence of soil solution NO_3^- ions. R^+ and R^- represent anion and cation exchangers at the organic membrane, and M^+ and A^- are hydrophilic ions in soil water. POT–MoS_2 and POT–MoS_2^+ indicate neutral and oxidized POT–MoS_2 units. Oxidation/reduction is shown for the Ag/AgCl reference electrode. (b) Molecular structure of POT and MoS_2 for composite formation in this sensor. (c) Mechanism of the reduction process for the WE (ISM/POT–MoS_2/Au).*

6.3 Results and Discussion

6.3.1 Surface Morphology and Water Repellent Properties

Figure 6.3 shows the scanning electron microscopic (SEM) images for different ion-to-electron transducing layers formed on the Au surface, including MoS_2, POT, and POT–MoS_2 nanocomposite. The MoS_2 layer is seen as a mixture of MoS_2 sheets of different sizes (Figure 6.3a). The POT film exhibits continuous distribution and microtexture (Figure 6.3b). In the POT–MoS_2 nanocomposite, MoS_2 sheets are embedded with POT due to the electrostatic interactions between them (Figure 6.3c, d). In addition, Figure 6.3e–g shows the measured water contact angles of the MoS_2 (θ = 68°), POT (θ = 86°), and POT–MoS_2 (θ = 107°)

surfaces. With MoS_2, the nanocomposite remains hydrophobic, which may contribute to minimize the formation of a thin water layer between the ISM and Au layers.

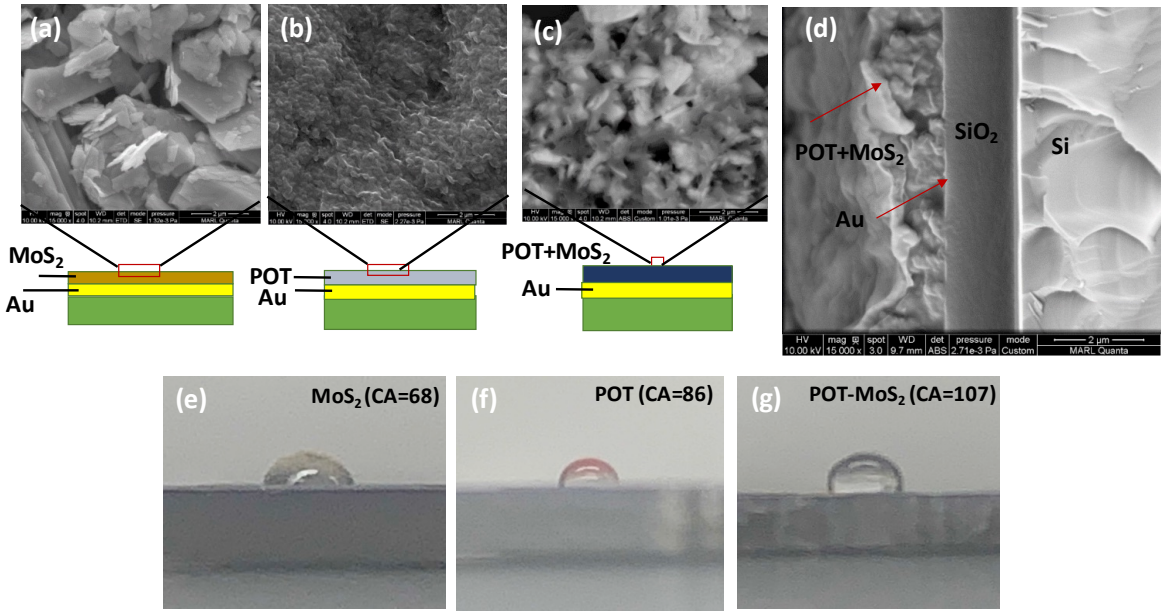

Figure 6.3. *Scanning electron micrographs for MoS_2 sheets (a), POT (b), and POT–MoS_2 materials (c) with schematic representation of various layers. (d) Cross-sectional view of SEM image for POT–MoS_2 composite on Au. Contact angle (CA or Θ) studies for investigation of the hydrophobicity of the working electrode materials. A syringe was used to drop 3 µL volume of deionized water on the Au/PCB substrate coated with different working electrode materials, including MoS_2 (e), POT (f), and POT–MoS_2 (g). Images were analyzed using image J plugin software.*

6.3.2 X-Ray Photoelectron Spectroscopic (XPS) Analysis

XPS was conducted to confirm the chemical structures of MoS_2, POT–MoS_2, and ISM/POT–MoS_2. Figures 6.4a–c show the carbon 1s spectra of the MoS_2, POT–MoS_2, and ISM/POT–MoS_2 layers coated on the Au surface. After deconvolution into characteristic peaks, the C 1s peaks of MoS_2 are found at 284.9, 285.9, and 289.5 eV, indicating the presence of C–C, C–OH, and O–C=O groups, respectively [57]. The presence of carbon may be due to the impurity of the MoS_2 sheets. The incorporation of MoS_2 into the POT matrix leads to a

shift in the peak location from 284.9 eV to 285.3 eV with a full-width half maximum of 2.5 eV (Figure 6.4b), perhaps due to the POT hydrocarbons. A peak at 285.8 eV can be ascribed to the C–S bond, indicating the formation of strong chemical bonding at the interface between MoS_2 and POT. After the ISM was coated on the POT–MoS_2 layer, the peak for the C–C bond was found to be at 284.3 eV (Figure 6.4c). Another peak at 286.1 eV was obtained on the surface of ISM due to the C–O group present in the ISM.

Figure 6.4d shows the MoS_2 layer with two S 2p core-level peaks of MoS_2 at the binding energies of 165.5 eV and 164.9 eV, corresponding to the S $2p_{1/2}$ and S $2p_{3/2}$ orbitals of divalent sulfide ions (S^{2-}). In Figure 6.4e, two S 2p peaks appear at 162.7 eV and 163.9 eV due to the formation of S*–Mo and C–S*–C groups, respectively, [58] indicating incorporation of POT into MoS_2, and another peak found at 169.2 eV is associated with the S in sulfone. Furthermore, the S peaks were observed to shift towards higher energies of 1.6 eV and 1.2 eV due to the ISM coating on POT–MoS_2 film (Figure 6.4f).

In the Mo 3d spectrum of MoS_2, a peak at 227.2 eV corresponds to S 2s with a chemical state of S^2, while other peaks at 229.9 eV, 233.1 eV, and 236.4 eV are ascribed to $Mo^{4+}3d_{5/2}$, Mo^{4+} $3d_{3/2}$, and Mo^{6+} $3d_{3/2}$, respectively (Figure 6.4g). For the POT–MoS_2 (Figure 6.4h), two additional peaks appear at 233.1 eV and 231 eV because of Mo^{6+} $3d_{5/2}$ and Mo^{5+} 3d, respectively. In the N 1s spectrum of ISM/POT–MoS_2 (Figure 6.4i), the peaks seen at 402.7 eV and 408.4 eV correspond to -NH_2 and nitrooxy (-N-NO_2) groups due to the presence of nitrocellulose in the ISM. Therefore, the formation of a composite between POT and MoS_2 due to the appearance of chemical C-S bond is confirmed. Further, the presence of -NH_2 and nitrooxy (-N-NO_2) groups at ISM/POT–MoS_2 indicates the ISM coating on the surface of the POT–MoS_2 matrix.

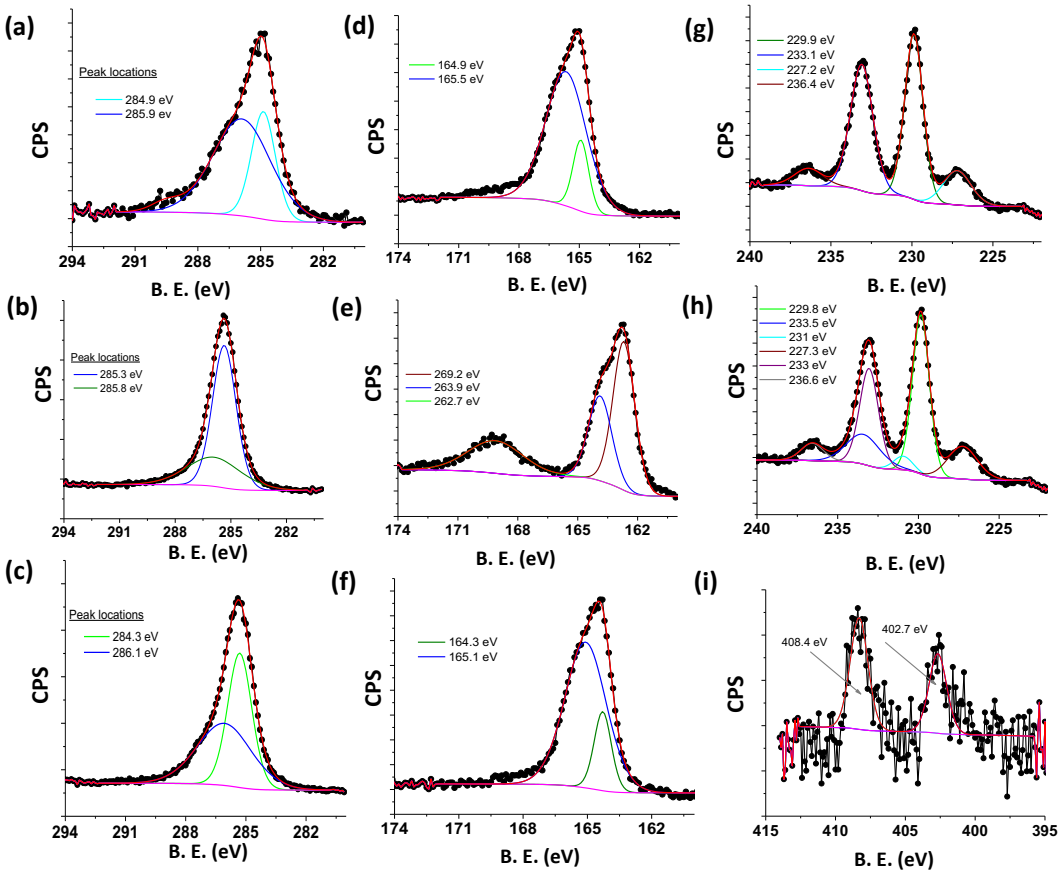

Figure 6.4. *XPS analysis for the working electrodes using MoS_2, POT–MoS_2, and ISM/POT–MoS_2 materials. XPS spectra of the carbon 1s region of MoS_2 (a), POT–MoS_2 (b), and ISM/POT–MoS_2 (c). Sulphur (S 2p) peaks for the MoS_2 (d), POT–MoS_2 (e) and ISM/POT–MoS_2 (f) electrodes. XPS peaks for molybdenum (Mo) 3d found for the MoS_2 (g) film and POT–MoS_2 (h) film. XPS spectra for the nitrogen 1s peaks region of ISM/POT–MoS_2 film.*

6.3.3 Electrochemical Characterizations

Cyclic voltammetry (CV) was conducted at room temperate to investigate the redox properties of the MoS_2, POT, POT–MoS_2, and ISM/POT–MoS_2 layers coated on the Au electrodes (Figure 6.5a), and the POT to MoS_2 ratio of the composite was set to 1:4. The cyclic voltammograms for the MoS_2-, POT-, and POT–MoS_2-based electrodes exhibited clear reversible oxidation and reduction reactions for the $[Fe(CN)_6]^{3-/4-}$ redox probes. The oxidation

current for the POT–MoS_2-based electrode was higher (115 μA) than that for the MoS_2-based electrode (90 μA) and that for the POT-based electrode (65 μA), because the incorporation of high-conductivity MoS_2 facilitates an improved electron transfer from the POT–MoS_2 to the Au current conductor. Also, the values of peak-to-peak potential difference (ΔE) for the POT- and POT–MoS_2-based electrodes were found to be 0.127 V and 0.38 V, respectively. After modification with the ISM, the POT–MoS_2-based electrode exhibited reduced oxidation and reduction peaks for the $[Fe(CN)_6]^{3-/4-}$ redox probes, perhaps due to sluggish ion exchanges, or a high selectivity of ISM that rejected $[Fe(CN)_6]^{3-/4-}$ ions (inset of Figure 6.5a).

To optimize the weight ratio of POT to MoS_2 in composite formation, CV measurements were taken for composites at varying weight ratios with the objective of obtaining the composite that offered the largest value of ΔE. Figure 6.5b shows that as the weight ratio of POT to MoS_2 changes from 1:1 to 1:10, the obtained ΔE increases at lower weight ratios, reaches a maximum ΔE = 0.345 V at a 1:4 weight ratio, and then deceases at higher weight ratios. Further, Figure 6.5c shows that the oxidation current decreases with increasing POT–to-MoS_2 weight ratios from 1:1 to 1:3, due to a reduction in the free POT in the POT–MoS_2 matrix. At a weight ratio between 1:4 and 1:6, the oxidation current is observed to be relatively stable at a low value, due to the full bond formation. With further increase in the MoS_2 component, the free MoS_2 in the matrix prompts the oxidation current due to the inherent electroactivity of MoS_2 (Figure 6.5c). Therefore, for the potentiometric measurement, the optimum POT-to-MoS_2 weight ratio was chosen to be 1:4.

Figure 6.5d presents the redox activity studies of the POT–MoS_2 based electrode (POT-to-MoS_2 weight ratio: 1:4). The POT-MoS_2 based electrode shows well-redox behavior for the oxidation and reduction of ferro/ferricyanide redox species. The difference between the

oxidation and reduction potentials is found to increase with an increase in scan rate. The peak current is proportional to the square root of the scan rate (inset of Figure 6.5d), indicating a diffusion-controlled process on this redox sensitive material.

For open circuit potential (OCP) measurement, the MoS_2, POT, and POT–MoS_2 layers were coated with nitrate-specific ISM. Figure 6.5e shows the output voltage signals of the fabricated sensors in response to 1000 ppm NO_3^--N. The magnitude of the potential for the POT–MoS_2-based electrode exhibits a maximum value of 325 mV, higher than the counterpart electrodes using POT (255 mV) and MoS_2 (66 mV). As is evident in the CV studies (Figure 6.5a), compared to the POT alone, the POT–MoS_2 nanocomposite offers a better redox property, such as good electro-active mediator to allow selective interaction with NO_3^- ions in the surrounding solutions, (Figure 6.3a–b), thus providing an increased OCP.

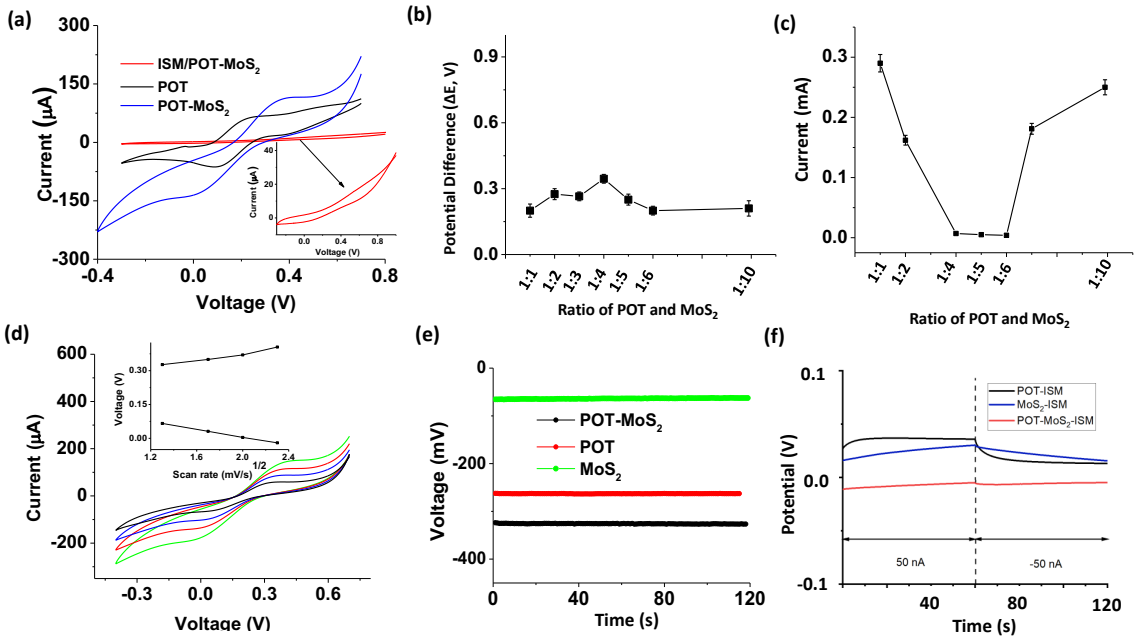

Figure 6.5 *(a) Cyclic voltammogram (CV) for different electrodes (a) MoS2, POT, POT–MoS2 and ISM/POT–MoS2. These experiments were conducted using phosphate-buffered saline (PBS) solution mixed with a ferro/ferricyanide ([Fe(CN)6]3-/4-) of concentration 2 mM. Inset shows zoom CV curve of ISM/POT–MoS2. (b) Potential differences (ΔE) obtained from CV*

curves were plotted against the ratio of POT–MoS2-based electrodes. In the composite formation, the ratio of POT-to-MoS2 was varied from 1:1 to 1:10 by weight percentage. (c) Oxidation current obtained from CV curves vs. ratio of POT to MOS2 (1:1 to 1:10), and (d) CV graphs for the optimized electrode based on POT–MoS2 (at ratio 1:4) in the presence of [Fe(CN)6]3-/4-. (e) Voltage measurements (open circuit potential) for three electrodes, such as MoS2-, POT-, and POT–MoS2-based sensors, after coating with nitrate-ion selective membrane in the presence of 1000 ppm NO3--N. (f) Chronopotentiometry measurements for three nitrate sensors using POT, MoS2 and POT-MoS2 as ion-to-electron transducing layers. Constant 50 nA anodic and cathodic currents were applied uninterruptedly for 60 s each and the respective potential responses over time were recorded.

The potential stability of the electrodes and the electrical capacitance of the solid contact were evaluated using chronopotentiometry[19] (Figure 6.6f). The characteristic chronopotentiometric curves present the change in potential over time measured in a 500 ppm NO_3^--N solution. The obtained results are shown in Figure 6.6. The potential drift of electrode was calculated as $\Delta E/\Delta t$. The $\Delta E/\Delta t$ values for the POT, MoS_2 and POT-MoS_2 based nitrate-selective electrodes were found to be 115.4 μVs^{-1}, 213.3 μVs^{-1}, and 95 μVs^{-1}, respectively. Similarly, the low-frequency capacitances C of the POT, MoS_2, and POT-MoS_2 based electrodes were estimated to be 433 μF, 234 μF, and 526 μF, respectively, according to the equation $\Delta E/\Delta t = I/C$. These results indicate that the POT-MoS_2 based electrode has a larger capacitance and a lower potential drift compared to the electrode using POT or MoS_2 (see Table B.1).

6.4 Quantification of Nitrate-Nitrogen

6.4.1 Calibration

Nitrate detection by the sensors using MoS_2, POT, and POT–MoS_2 as the solid-contact ion-to-electron transfer layer materials was investigated. Figure 6.6a shows the calibration

curves, i.e., the OCP values of the sensors as a function of nitrate concentration ranging from 1 to 1500 ppm (NO_3^--N). The slope of the voltage response versus logarithm concentration for the POT–MoS_2-based sensor is 64 mV/decade (10-1500 ppm), which is higher than the POT (approximately 48 mV/decade, 10-1500 ppm) and the MoS_2 (approximately 38 mV/decade, 10-1500 ppm). The high electro-activity and redox property of the POT–MoS_2 layer is believed to contribute to improved sensitivity in nitrate detection. In addition, the high hydrophobicity of the POT–MoS_2 layer could minimize water accumulation between the ISM and the Au current collector, lowering the barrier of charge transfer to the Au layer and thus improving the sensor sensitivity. Although the MoS_2-based sensor also provides a wide dynamic range up to 1000 ppm (NO_3^--N); the output voltage was found to be unstable (particularly during the detection of high nitrate concentrations), possibly due to poor adhesion of the MoS_2 layer to the ISM layer, leading to membrane delamination. Following the method described in Buck *et al.* [59], we calculated the limit of detection (LOD) as 0.84 ppm, 1.3 ppm and 1.4 ppm for the three sensors using MoS_2, POT and POT-MoS_2, respectively, according to the obtained calibration plots in Figure 6.6a. Table 1 compares nitrate monitoring using different nanostructured materials. The laboratory-based nitrate measurement methods based on Griess assay, UV-VIS spectrophotometry, GC-MS and chemiluminescence for nitrate monitoring in different medium showed higher performance in terms of their limit of detection compared to the POT-MoS_2 based sensor. However, our sensor can conduct long-term measurements, exhibit a wider detection range, and have considerable performances suitable for field applications [8-12]. In addition, our sensor uses an integrated solid-state RE, thus offering the possibility of miniaturization and mass production, while the above-mentioned counterpart

sensors require commercial large-sized REs. The sensor is used in direct and long-term contact with soil particles across a range of wetness for nitrate quantification.

Table 6.1 Comparison for NO_3^--N monitoring using different nanomaterials

Electrode materials or Transducers	Methods	Test range (ppm)	Detection limit (ppm)	Sensitivity (mV/dec)	Test period and environment	Ref.
CNTs	OCP	0.14×10^{-3}-14.02	0.0014	58.9	NA	60
Polypyrrole	OCP	0.14-1400.6	0.42	53.9	7 d in water	61
Graphene	OCP	0.14-1400.6	0.3	54.8 ± 2.5	Not tested	62
Polypyrrole	OCP	1.4-56.1	1.68	51.6	Not tested	63
POT	OCP	0.14-1400.6	NA	53	~90 d in water	64
Poly(aniline)	OCP	0.14-1400.6	NA	51.5	~90 d in water	64
PEDOT	OCP	0.011-63.34	0.25	NA	NA	65
Ionic liquid	OCP	0.044- 442.8	0.012	60.1	NA	66
Graphene–tetrathiafulvalene	OCP	0.004-442.8	~0.004	59.14	NA	67
Carbon black	OCP	0.044- 442.8	0.1	60	NA	68
Tetrathiafulvalene	OCP	0.044- 442.8	0.01	58.8	NA	69
Spectroscopic	VCl_3/Griess	0.02–5	0.016	NA	NA	8
Optical	Greiss	0–9.3	0.027	NA	Sea water	9
Optical	UV	0.3-3.1	0.007	NA	Waste water	10
Optical	Chemiluminescence	0.001-0.9	0.001	NA	Atmospheric	11
Gas chromatography	Nitration	0.062-6.2	0.1	NA	~3d in	12
POT–MoS_2	OCP	1-1500	1.3	64	25 d in soil	This work

6.4.2 Selectivity, Repeatability, and Stability Studies

Figure 6.6b shows the selectivity of the sensors using the MoS_2, POT, and POT–MoS_2 as the ion-to-electron transducing layers in the presence of interfering anions such as chloride (Cl^-), phosphate (PO_4^{3-}), bicarbonate (HCO_3^-), sulfate (SO_4^{2-}) and nitrite (NO_2^-). The selectivity coefficient, K_{IJ}^p, described in Eq. 6.4, is a numerical measure of how adequately the sensor is able to discriminate against the interfering ions.

$$K_{IJ}^p = \frac{a_I}{a_J^{z_I/z_J}} \tag{6.4}$$

where a_I, a_J, Z_I, and Z_J are the activity of primary ions, activity of interfering ions, charge of the primary ions, and charge of the interfering ions, respectively. According to IUPAC recommendations, a matched potential method, including the separate solution method (SSM), is practical and unique for estimating K_{IJ}^p , which does not depend on the Nicolskii–Eisenman equation [70-71]. In the SSM method, the potential of the sensor is adjusted by introducing two different concentration solutions separately, wherein one contains the ion I with activity a_I (no J), and the other one contains the ion J with the same activity a_J (no I) to attain the same measured potential. To calculate the value of K_{IJ}^p, the a_I was calculated from the extrapolated calibration graph where the potential of the interfering ion concentration (a_J) is equal. The result demonstrates that the POT–MoS_2 based sensor shows less susceptibility to PO_4^{3-} and SO_4^{2-} than the sensor using POT or MoS_2 alone as the transducing layer, perhaps due to the improved hydrophobicity of the POT–MoS_2 layer, while the influence of HCO_3^- and Cl^- on the output potential is comparable between all the sensors. For NO_2^-, the sensors based on POT or MoS_2 showed more negative selectivity coefficients compared to the POT-MoS_2 based sensor.

Figure 6.6c shows the stability of fabricated Nafion-modified Ag/AgCl RE with respect to commercial RE by varying the KCl concentration from 0.01 M to 3 M KCl. Without the

Nafion coating, the Ag/AgCl electrode shows a stable OCP with 0.01 M and 0.05 M of KCl concentration, however, with a higher concentration of KCl, such as 1 and 3 M, the electrode shows a significant potential change. This change of potential is due to the considerable electrochemical reaction in the AgCl layer, which may leach Cl^- ions from the AgCl layer, resulting in unstable OCP. With increasing KCl concentration, the Nafion-modified Ag/AgCl electrode does not show a change in the OCP. The pronated Nafion layer on the Ag/AgCl surface acts as a protective layer that does not allow Cl^- ions to leach out and rejects Cl^- from outside the Nafion. Figure 6.6d shows the long-term stability (approximately 32 d) of the fabricated solid-state Ag/AgCl electrode with and without a Nafion layer in the presence of 0.01 M of KCl. With no Nafion coating on the Ag/AgCl surface, the OCP was not constant in long-term measurements due to Cl^- leaching. However, blocking the Ag/AgCl surface with Nafion resulted in an almost constant OCP for 32 d with minimum drift. This indicates that Nafion-coated Ag/AgCl is not externally influenced by Cl^- ions and is more stable for long-term measurement.

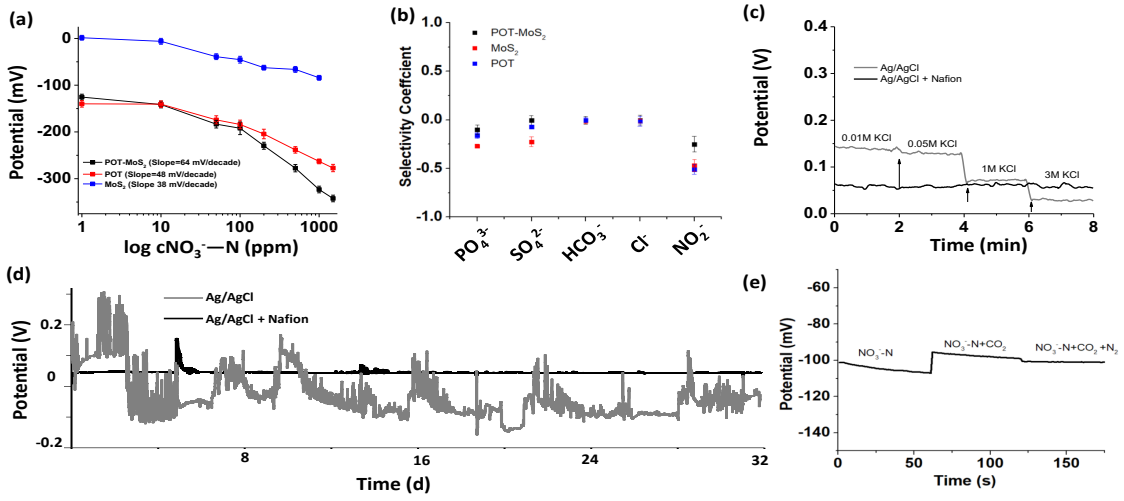

Figure 6.6 *(a) Sensor responses in millivolts (mV) made by MoS2, POT, and POT–MoS2 electrodes modified with ISM. A stock solution of 1500 ppm of nitrate-nitrogen was made in*

DI water and diluted from 1500 ppm to 1 ppm. Sensor measurements were conducted for 2 min at each concentration. Corresponding average voltages for all the sensors (MoS2, POT, and POT–MoS2) were plotted against the logarithm of nitrate-nitrogen in ppm. Error bars were calculated using three consecutive measurements for each concentration. (b) For the selectivity studies, the NO3--N concentration was set to 100 ppm, and the hydrophilic interfering ions were set to 400 ppm. The selectivity coefficients were calculated for MoS2, POT, and POT–MOS2-based ISM sensors using the separate solution method (SSM). (c) The stability of the fabricated RE (Ag/AgCl) with and without Nafion coating was tested separately by varying the concentration of KCl from 0.01 M to 3 M. For the stability test, the OCP of the fabricated RE was measured with respect to a leak-less miniature Ag/AgCl RE having an internal electrolyte of 3.4 M KCl (obtained from EDAQ, ET072-1). (d) Long-term stability measurement of the Ag/AgCl electrodes with and without Nafion coating: plot of the OCP of the electrodes vs. time in the presence of 0.01 M KCl solution. (e) Interference studies of the POT-MoS2 based sensor in presence of CO2 and N2 gases purging into a nitrate solution. After the nitrate measurement, the sensor was tested in a closed chamber where CO2 and N2 gases continuously flowed for 15 minutes before the measurement.

To investigate the repeatability of the sensor, we repeatedly measured the OCP as the sensor was transferred between 1 ppm and 1300 ppm NO_3^--N (Figure B.3). For 12 repeated measurements, the sensor was dipped with high nitrate-nitrogen (1300 ppm) for 2 min, and the OCP was recorded. Then, the sensor was immediately dipped in low concentration nitrate-nitrogen (1 ppm), and then washed with DI water for another 2 min, and the OCP was recorded. The sensor responded within less than 5s when switching from high to low concentration, or vice versa. With a high concentration of NO_3^--N (1300 ppm), the percentage of relative standard deviation for the output voltage was calculated as ±3.0%, while with a low concentration, the sensor showed a deviation of ±5.0 % over six repeated measurements. This result indicates high repeatability of the test.

For the interference study in presence of CO_2, the POT-MoS_2 based sensor was tested in a closed chamber with a controlled CO_2 environment (Figure 6.6e). Before the measurement the CO_2 gas (saturated) was injected into a nitrate solution for 15 minutes to ensure satirized dissolved CO_2 in the solution. The test result shows that the introduction of CO_2 into the solution led to a ±5% relative deviation from the initial signal of the sensor. This may be caused by a pH change induced by the dissolved CO_2 in the solution. Also, we found that the introduction of N_2 into the solution had almost no influence on the sensor readout. Nevertheless, the sensor exhibited a good potential stability in the CO_2 environment.

We studied reproducibility of the POT-MoS_2 based nitrate electrode (Figure B.1). The concentration of NO_3^--N was set to 100 ppm in DI water and the measurement was performed for 2 min for each POT-MoS_2 electrode. The results show that the variation in potential among these electrodes is negligibly small, as evident by its low relative standard deviation (RSD = ~3.5%) due to the uniform coating of the electrode materials (i.e., POT-MoS_2 ad ISM) using a high-resolution robotic dispensing machine.

We carried out potential stability measurement for the POT-MoS_2 based nitrate sensor over ~10 days (Figure B.2). The electrode was pre-conditioned in a 1500 ppm NO_3^--N solution for 3 days. The result of the continuous measurement shows the potential at day 10 (~ -184 mV) remained almost unchanged from the initial potential (~-186 mV). Therefore, the pre-conditioned electrode was found relatively stable.

6.4.3 Nitrate Measurement in Extracted Soil Water

To demonstrate nitrate measurement in extracted soil water, soil water was extracted from three locations at the Iowa State BioCentury Research Farm (Ames, IA) using a suction lysimeter. The suction head of the lysimeter was inserted at a depth of 25 cm from the soil

surface. As the POT–MoS_2 based sensor was dipped into different test solutions, the sensor responded by providing different voltage signals (Figure 6.7a). The inset of Figure 6.7a shows the converted nitrate concentration using the calibration curve of the sensor (Figure 6.6a). For comparison, a commercial sensor (LAQUA HORIBA nitrate sensor) was used to measure the same sample solutions. Our sensor and the commercial sensor showed comparable reading.

6.4.4 Short-Term Nitrate Measurement in Soil Column

To demonstrate short-term nitrate measurement in a soil column, two identical POT–MoS_2 based sensors were fixed on the walls of two column beakers filled with soil slurries (Figure 6.7c). The column beakers were 6 cm in diameter and 10 cm in height and loaded with soils to a height of 9 cm from the bottom of the beaker. Several 3-mm-diameter holes were created at the bottom of beaker to flush out the water. Each sensor was located 7 cm from the bottom, as shown in Figure 6.7b. The soil used here was collected from the soil surface at the research farm mentioned above. During the demonstration, the soil in one beaker was flushed with alternating solutions of 0 and 50 ppm NO_3^--N at different time points, each time lasting 2 min, while the soil in the other beaker was flushed with 0 and 100 ppm NO_3^--N. Figure 7d shows the voltage outputs of the two sensors installed in the two beakers. When the soil was flushed with DI water (0 ppm), the output voltage of the sensor reached a baseline voltage of approximately -110 mV. When the soil was treated with 50 ppm or 100 ppm nitrate solution, the sensor 1 and sensor 2 outputs went down to approximately -123 mV or approximately -150 mV, respectively. Figure 6.7e shows the nitrate concentrations converted from the voltage outputs of the sensors. It should be noted that the converted concentrations are evidently lower than the known input nitrate concentrations. The nitrate solution was flushed out of the soil slurries immediately after introducing the solution, and the pre-wetted soil particles already

had water content that may have diluted the external original concentration of nitrate in the testing soil slurries, resulting in reduced ppm levels compared with the original input concentration of nitrate. Alternatively, when we introduced the external nitrate concentration into the soil, as nitrate has a low charge density compared to other common pre-existing anions in soil solution and they always occupy the few positively charges sites, in turn, the nitrate ions may have failed to bind with soil particles within a short period of time or denitrification of nitrate ions, thus both sensors showed reduced ppm nitrate levels. However, the sensor response returned to the baseline ppm level immediately as we flushed with DI water.

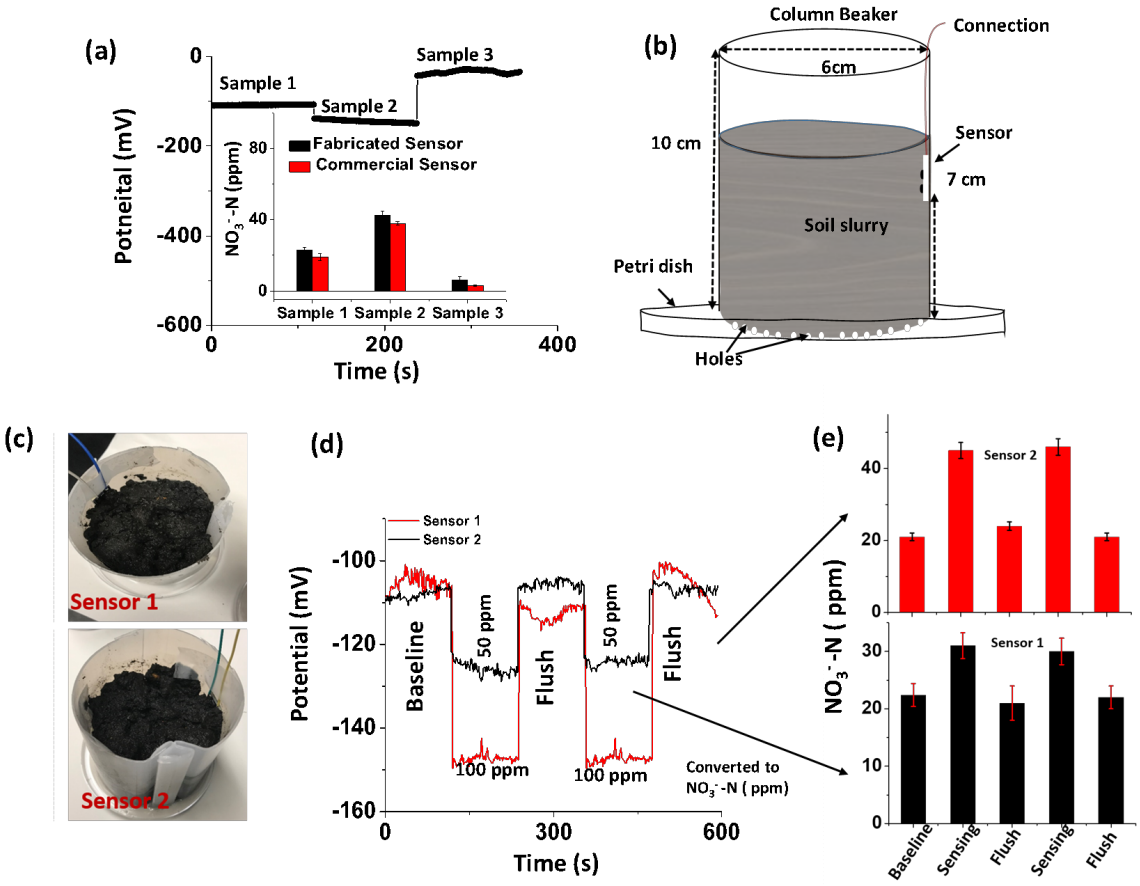

Figure 6.7 *(a) Sensor responses (commercial and fabricated) for real soil extracted solutions collected directly from Ames, Iowa with a suction lysimeter. (b) Schematic presentation of soil-column setup for nitrate-nitrogen measurement. (c) Photographs of soil-column beakers with*

soil slurries wherein the sensors were hung on the wall of the column. (d) Short-term soil nitrate-nitrogen sensing in the soil column, where the baseline was set in the presence of DI water (baseline), and the column was flushed with DI water after the soil was treated with 100 and 50 ppm of NO3--N, and (e) Plot for corresponding sensor readings.

6.4.5 Long-Term Nitrate Measurement in Soil Column

For long-term measurement, two identical sensors (sensor 1 and sensor 2) were deployed directly into soil slurries in column beakers over approximately 4 weeks with different rates of nitrate concentration (50 and 100 ppm NO_3^--N), and OCP was measured continuously (Figure 6.8a–b). For this measurement, the beaker dimensions were the same, and the sensors were fixed at the same location as for the short-term measurement. However, unlike the previous design of the beakers for short-term measurement, there were no holes at the bottom of the beakers to promote denitrification of nitrate ions in the soil slurries before evaporation.

The long-term monitoring of nitrate in soil slurries using sensor 1 and sensor 2 is shown in Figure 6.8c and Figure 6.8d–e, respectively. For sensor 1, when the soil beaker was treated with DI water, the NO_3^--N level was found to be approximately 14–23 ppm (Figure 6.8c, marked with box) which is a similar result to that observed in the short-term measurement. Due to the slow diffusion of pre-occurring nitrate ions from the soil slurry into the water, the nitrate level slowly increased after water was poured until it reached a maximum concentration. Further, the sensor showed a slow decrease in NO_3^--N concentration to the range of 2–5 ppm due to denitrification at room temperature (25 ºC). In this parched soil condition, the nitrate ppm was found to be almost constant. Upon further repeating the experiment two times, the sensor showed similar results.

Interestingly, when the 50 ppm of NO_3^--N was poured into the soil beaker, sensor 1 began to show a slow increase in NO_3^--N, and reached a maximum value of 53 ppm NO_3^--N. With the addition of external nitrate into the soil, the sensor took approximately 3 hours to reach a maximum nitrate level, indicating slow diffusion of nitrate ions into the soil. This is because when soil particles at the sensor interface are completely wet, nitrate ions may diffuse slowly from the external nitrate solution (as we filled the beaker) due to the concentration gradient. The NO_3^--N concentration was further decreased to a low value of 2–5 ppm when the soil particles became parched due to water evaporation, which restricted the mobility of the nitrate ions. Sensor 1 showed an almost similar performance of NO_3^--N, while the sensor was further flushed with 50 ppm NO_3^--N concentration another three times. When more water containing NO_3^--N (see the last two repeated measurements, Figure 6.8c) was poured, the sensor showed a longer nitrate response at 50 ppm, as the evaporation of water from the soil takes time.

Similarly, for sensor 2, the sensor performance was investigated in the presence of DI water and 100 ppm of NO_3^--N concentration for 2 weeks (Figure 6.8d), and the sensor was kept in parched soil conditions for another 2 weeks (Figure 6.8e). With DI water filling, the sensor exhibited a concentration of approximately 20–25 ppm of NO_3^--N due to the pre-existing nitrate ions in the soil. Further, the soil water content dried slowly, and the soil became parched under this condition. The sensor showed a similar NO_3^--N response as was observed in the case of sensor 1. When the soil slurry was flushed with 100 ppm NO_3^--N solution, the output of the sensor reached a maximum value of NO_3^--N (approximately 104 ppm), after which the sensor response began to decay to less than 10 ppm of NO_3^--N due to water evaporation. Further, sensor 2 was kept in the same soil without the addition of water for approximately 2 weeks,

and the concentration variability was investigated (Figure 6.8e). The soil become parched without the addition of water and NO_3^--N solution. Under this condition, however, the sensor still exhibited a low ppm of nitrate (approximately 10–2 ppm). Interestingly, the sensor response decreased from approximately 10 ppm to 3 ppm over a long period of time (13 d), but the sensor response was found to be irregular, perhaps because of the changing room temperature or humidity level. The sensor deployed into soil slurries can monitor nitrate-nitrogen accurately monitored for at least a duration of 27 days.

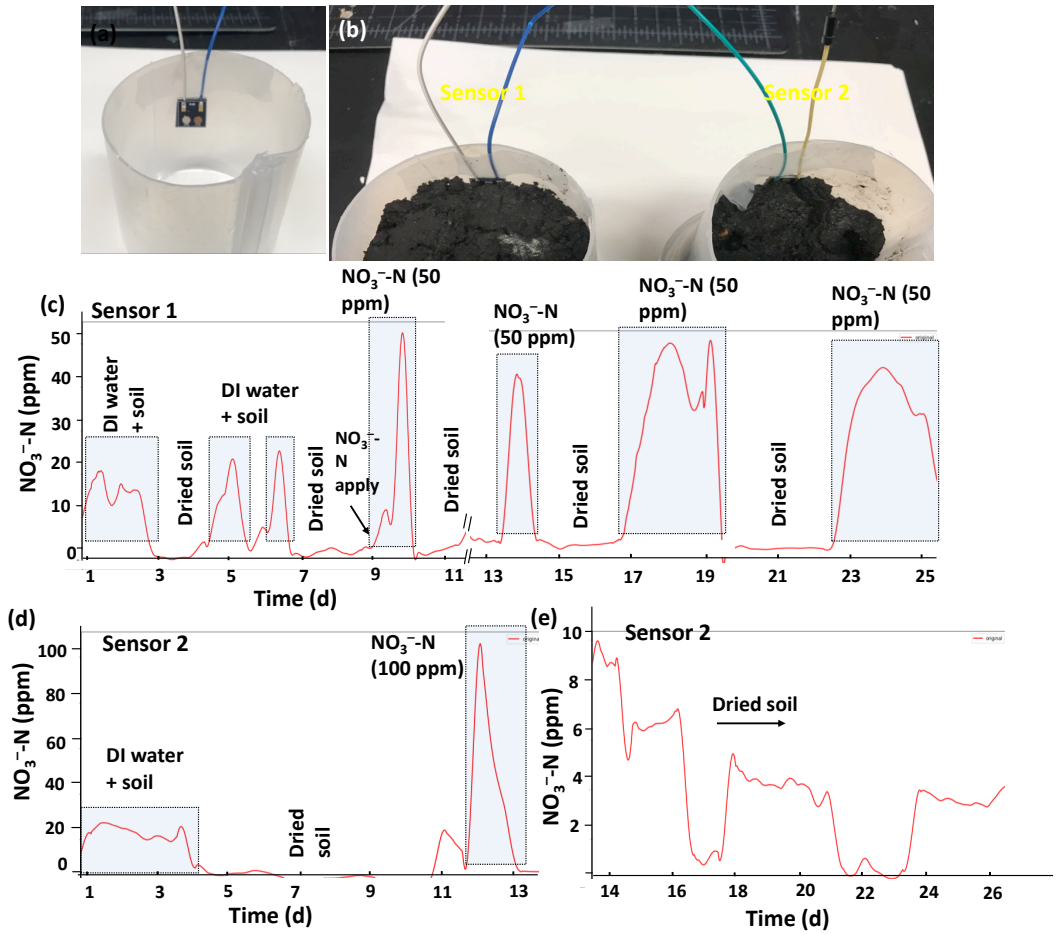

Figure 6.8 *Long-term measurement (approximately 4 weeks) using two different individual sensors (made with POT–MoS2 material), wherein sensor 1 and sensor 2 were deployed in beakers containing soil slurries. Photographs of column beakers without soil slurries (a), and with soil slurries and sensor 1 and sensor 2 (b). For sensor 1 (c), the soil beaker was filled with DI water and then left to dry, and the soil slurry was again treated with water multiple*

times and then parched. Finally, DI water mixed with nitrate-nitrogen (50 ppm) was poured into the soil slurry in the column beaker with sensor 1 and left to dry. The process was repeated multiple times (for approximately 4 weeks) for sensor 1. For sensor 2, the soil slurry was initially filled with DI water, parched, and flushed with 100 ppm nitrate-nitrogen (d). After drying, sensor 2 was kept in the parched condition for about 2 weeks (e).

6.5 Conclusion

In this manuscript, a novel all-solid-state miniature sensor designed for long-term use in continuous monitoring of soil nitrate was presented. The sensor was fabricated on a PCB using patterned WE and RE. To characterize the sensor materials, solid-state components using MoS_2, POT, and POT–MoS_2 were directly coated on the patterned PCB and functionalized with an ISM using a high precision robotic-armed auto-dispenser machine. The electro-activity properties of POT–MoS_2 composite were found to be excellent, and the material was used as an ion-to-electron transducing layer for nitrate detection in the sensor. The POT–MoS_2 composite material produced superior sensor performance in terms of selectivity and sensitivity compared with MoS_2 and POT, and the reported nitrate sensors shown in Table 1. This may be the result of the high hydrophobicity and high redox properties of the POT–MoS_2 layer. The solid-state sensor is selective to nitrate ions even when other anions are present at significant concentrations and offers long-term stability. This sensor can be deployed into the soil for long-term nitrate monitoring (about 4 weeks). In the future, by replacing the ion selective membrane, the sensor could be adapted to detect other soil nutrients, including potassium, phosphate, and sulfate. These other nutrients are also essential to plant growth and agricultural productivity. Continuous measurements of these nutrients thus have significant potential applications in plant biology, plant breeding, environmental science, and production agriculture.

References

1. Lipper, L.; Thornton. P.; Campbell, B. M.; Baedeker, T.; Braimoh, A.; Bwalya, M.; Caron, P.; Cattaneo, A.; Garrity, D.; Henry, K.; Hottle, R. Climate-smart agriculture for food security. *Nat Clim Chang*. 2014, 4, 1068.

2. Walter, A.; Finger, R.; Huber, R.; Buchmann, N. Opinion: Smart Farming is Key to Developing Sustainable Agriculture. *Proc. Natl. Acad. Sci*. 2017, 114, 6148-50.

3. White, J. W.; Andrade-Sanchez, P.; Gore, M. A.; Bronson, K. F.; Coffelt, T. A.; Conley, M. M.; Feldmann, K. A.; French, A. N.; Heun, J. T.; Hunsaker, D. J.; Jenks, M. A. Field-based Phenomics for Plant Genetics Research. *Field Crop. Res*. 2012, 133, 101-12.

4. Adamchuk, V. I.; Hummel, J. W.; Morgan, M. T.; Upadhyaya, S. K. On-The-Go Soil Sensors for Precision Agriculture. *Comput. Electron. Agr*. 2004, 44, 71-91.

5. Ali, M. A.; Jiang, H.; Mahal, N.K.; Weber, R.J.; Kumar, R.; Castellano, M.J.; Dong, L. Microfluidic Impedimetric Sensor for Soil Nitrate Detection using Graphene Oxide and Conductive Nanofibers Enabled Sensing Interface. *Sensors and Actuators B: Chemical* 2017, 239, 1289-1299.

6. Ali, M. A.; Mondal, K.; Wang, Y.; Jiang, H.; Mahal, N. K.; Castellano, M. J.; Sharma, A.; Dong, L. In Situ Integration of Graphene Foam–Titanium Nitride based Bio-Scaffolds and Microfluidic Structures for Soil Nutrient Sensors. *Lab Chip* 2017, 17, 274-85.

7. Dalal, R. C.; Henry, R. J. Simultaneous Determination of Moisture, Organic Carbon, and Total Nitrogen by Near Infrared Reflectance Spectrophotometry. *S. S. S. A.* 1986, 50, 120-3.

8. Hood-Nowotny, R.; Umana, N. H.; Inselbacher, E.; Oswald-Lachouani, P.; Wanek, W. Alternative methods for measuring inorganic, organic, and total dissolved nitrogen in soil. Soil *Sci. Soc. Am. J*. 2010, 74, 1018-27.

9. Daniel, A.; Birot, D.; Lehaitre, M.; Poncin, J. Characterization and reduction of interferences in flow-injection analysis for the in situ determination of nitrate and nitrite in sea water. *Anal. Chim. Acta* 1995, 308, 413-24.

10. Schroeder, D. C.; The analysis of nitrate in environmental samples by reversed-phase HPLC. J. *Chromatogr. Sci*. 1987, 25, 405-8.

11. Yoshizumi, K.; Aoki, K.; Matsuoka, T.; Asakura, S. Determination of nitrate by a flow system with a chemiluminescent nitrogen oxide (NOx) analyzer. *Anal. Chem*. 1985, 57, 737-40.

12. Englmaier, P. Nitrate analysis by gas-liquid chromatography using the nitration of 2, 4-dimethylphenol in sulphuric acid. *J. Chromatogr. A* 1983, 270, 243-51.

13. Zhang, C.; Kovacs, J. M. The Application of Small Unmanned Aerial Systems for Precision Agriculture: A Review. *Precis. Agric*. 2012, 13, 693-712.

14. Mills, H. A.; Jones, Jr J. B. Nutrient Deficiencies and Toxicities in Plants: Nitrogen. J. Plant Nutr. *Soil. Sci*. 1979, 1, 101-22.
15. Ali, Md. A.; Hong, W.; Oren, S.; Wang, Q.; Wang, Y.; Jiang, H.; Dong, L. Tunable Bioelectrodes with Wrinkled-Ridged Graphene Oxide Surfaces for Electrochemical Nitrate Sensors. *RSC Adv*. 2016, 6, 67184-67195.

16. Schazmann, B.; Diamond, D. Improved Nitrate Sensing using Ion Selective Electrodes based on Urea–Calixarene Ionophores. *New J. Chem*. 2007, 31, 587-92.

17. Jiang, H.; Ali, Md. A.; Jiao, Y.; Yang, B.; Dong, L. In-situ, Real-time Monitoring of Nutrient Uptake on Plant Chip Integrated with Nutrient Sensor. *In Proceedings of the 2017 19th International Conference on Solid-State Sensors, Actuators and Microsystems (TRANSDUCERS), Kaohsiung, Taiwan*. 2017, pp 289–292 (IEEE).

18. Xu, Z.; Wang, X.; Weber, R. J.; Kumar, R.; Dong, L. Nutrient Sensing using Chip Scale Electrophoresis and In situ Soil Solution Extraction. *IEEE Sens. J.* 2017, 17, 4330-9.

19. Bobacka, J. Potential Stability of All-Solid-State Ion-Selective Electrodes using Conducting Polymers as Ion-to-Electron Transducers. *Anal. Chem.* 1999, 71, 4932.

20. Cattrall, R. W.; Freiser, H. Coated Wire Ion-Selective Electrodes. *Anal. Chem*. 1971, 43, 1905–1906.

21. Bobacka, J.; Ivaska, A.; Lewenstam, A. Potentiometric Ion Sensors. *Chem. Rev*. 2008, 108, 329-51.

22. Silvester, D. S. Recent Advances in the Use of Ionic Liquids for Electrochemical Sensing. *Analyst* 2011, 136, 4871-82.

23. Hu, J.; Andreas, S.; Philippe, B. Rational Design of All-Solid-State Ion-Selective Electrodes and Reference Electrodes. *Trends Anal. Chem*. 2016, 76, 102-114.

24. Cadogan, A.; Gao, Z.; Lewenstam, A.; Ivaska, A. Diamond, D. All-Solid-State Sodium-Selective Electrode based on a Calixarene Ionophore in a Poly (Vinyl Chloride) Membrane with a Polypyrrole Solid Contact. *Anal. Chem*. 1992, 64, 2496-501.

25. McQuade, D. T.; Pullen, A. E.; Swager, T. M. Conjugated Polymer-based Chemical Sensors. *Chem. Rev*. 2000, 100, 2537-74.

26. Lindner, E.; Gyurcsányi, R. E. Quality Control Criteria for Solid-Contact, Solvent Polymeric Membrane Ion-Selective Electrodes. J. *Solid State Electrochem*. 2009, 13, 51-68.

27. Si, P.; Bakker, E. Thin Layer Electrochemical Extraction of Non-Redoxactive Cations with an Anion-Exchanging Conducting Polymer Overlaid with a Selective Membrane. *Chem. Comm.* 2009, 5260-2.

28. Vázquez, M.; Bobacka, J.; Ivaska, A. Potentiometric Sensors for Ag+ based on Poly (3-Octylthiophene)(POT). *J. Solid State Electrochem*. 2005, 9, 865-73.

29. Gao, W.; Emaminejad, S.; Nyein, H. Y.; Challa, S.; Chen, K.; Peck, A.; Fahad, H. M.; Ota, H.; Shiraki, H.; Kiriya, D.; Lien, D. H. Fully Integrated Wearable Sensor Arrays for Multiplexed in situ Perspiration Analysis. *Nature* 2016, 529, 509-514.

30. Bobacka, J. Potential Stability of All-Solid-State Ion-Selective Electrodes using Conducting Polymers as Ion-to-Electron Transducers. *Anal. Chem*. 1999, 71, 4932-7.

31. Fibbioli, M.; Morf, W. E.; Badertscher, M.; de Rooij N. F.; Pretsch, E. Potential Drifts of Solid-Contacted Ion-Selective Electrodes due to Zero-Current Ion Fluxes Through the Sensor Membrane. *Electroanalysis* 2000, 12, 1286-92.

32. Ping, J.; Wang, Y.; Wu, J.; Ying, Y. Development of an All-Solid-State Potassium Ion-Selective Electrode using Graphene as the Solid-Contact Transducer. *Electrochem. Commun*. 2011, 13, 1529-32.

33. Anastasova-Ivanova, S.; Mattinen, U.; Radu, A.; Bobacka, J.; Lewenstam, A.; Migdalski, J.; Danielewski, M.; Diamond, D. Development of Miniature All-Solid-State Potentiometric Sensing System. *Sens. Actuators B Chem*. 2010, 146, 199-205.

34. Dam, V. A.; Zevenbergen, M. A.; Van Schaijk, R. Toward Wearable Patch for Sweat Analysis. *Sens. Actuators B Chem*. 2016, 236, 834-8.

35. Athavale, R.; Dinkel, C.; Wehrli, B.; Bakker, E.; Crespo, G. A.; Brand, A. Robust Solid-Contact Ion Selective Slectrodes for High-Resolution in situ Measurements in Fresh Water Systems. Environ. *Sci. Technol. Lett.* 2017, 4, 286-91.

36. Yuan, D.; Anthis, A. H.; Ghahraman, A. M.; Pankratova, N.; Cuartero, M.; Crespo, G. A.; Bakker, E. All-Solid-State Potentiometric Sensors with a Multiwalled Carbon Nanotube Inner Transducing Layer for Anion Detection in Environmental Samples. *Anal. Chem.* 2015, 87, 8640-5.

37. Zhu, J.; Li, X.; Qin, Y.; Zhang, Y. Single-Piece Solid-Sontact Ion-Selective Electrodes with Polymer–Carbon Nanotube Composites. *Sens. Actuators B Chem*. 2010, 148, 166-72.

38. Criscuolo, F.; Taurino, I.; Stradolini, F.; Carrara, S.; De Micheli, G. Highly-Stable Li+ Ion-Selective Electrodes based on Noble Metal Nanostructured Layers as Solid-Contacts. *Anal. Chim. Acta* 2018, 1027, 22-32.

39. Lai, C. Z.; Fierke, M. A.; Stein, A.; Bühlmann, P. Ion-Selective Electrodes with Three-Dimensionally Ordered Macroporous Carbon as the Solid Contact. *Anal. Chem*. 2007, 79, 4621-6.

40. Bobacka, J. Conducting Polymer-based Solid-State Ion-Selective Electrodes. *Electroanalysis* 2006, 18, 7-18.

41. Guo, J.; Amemiya, S. Voltammetric Heparin-Selective Electrode based on Thin Liquid Membrane with Conducting Polymer-Modified Solid Support. *Anal. Chem.* 2006, 78, 6893-902.

42. Kim, Y.; Amemiya, S. Stripping Analysis of Nanomolar Perchlorate in Drinking Water with a Voltammetric Ion-Selective Electrode based on Thin-Layer Liquid Membrane. *Anal. Chem*. 2008, 80, 6056-65.

43. Veder, J. P.; De Marco, R.; Clarke, G.; Chester, R.; Nelson, A.; Prince, K.; Pretsch, E.; Bakker, E.; Elimination of Undesirable Water Layers in Solid-Contact Polymeric Ion-Selective Electrodes. *Anal. Chem*. 2008, 80, 6731-40.

44. Silva, E. A.; Oliveira, V. J.; Braunger, M. L.; Constantino, C. J.; Olivati, C. D. Poly (3-Octylthiophene)/Stearic Acid Langmuir and Langmuir-Blodgett Films: Preparation and Characterization. *Mat. Res*. 2014, 17, 1442-8.

45. Jarvis, J. M.; Guzinski, M.; Pendley, B. D.; Lindner, E.; Poly(3-Octylthiophene) as Solid Contact for Ion-Selective Electrodes: Contradictions and Possibilities. *J. Solid State Electrochem*. 2016, 20, 3033–3041.

46. Yang, L.; Wang, S.; Mao, J.; Deng, J.; Gao, Q.; Tang, Y.; Schmidt, O. G. Hierarchical MoS2/Polyaniline Nanowires with Excellent Electrochemical Performance for Lithium-Ion Batteries. *Adv. Mater*. 2013, 25, 1180-4.

47. El Beqqali, O.; Zorkani, I.; Rogemond, F.; Chermette, H.; Chaabane, R. B.; Gamoudi, M.; Guillaud, G. Electrical Properties of Molybdenum Disulfide MoS2. Experimental Study and Density Functional Calculation Results. *Synth. Met*. 1997, 90, 165-72.

48. Wu, S.; Zeng, Z.; He, Q.; Wang, Z.; Wang, S. J.; Du, Y.; Yin, Z.; Sun, X.; Chen, W.; Zhang, H. Electrochemically Reduced Single-Layer MoS2 Nanosheets: Characterization, Properties, and Sensing Applications. *Small* 2012, 8, 2264-70.

49. Barua, S.; Dutta, H. S.; Gogoi, S.; Devi, R.; Khan, R. Nanostructured MoS2-Based Advanced Biosensors: A Review. *ACS Appl. Bio Mater*. 2018, 1, 2-5.

50. Yang, T.; Meng, L.; Chen, H.; Luo, S.; Li, W.; Jiao, K. Synthesis of Thin-Layered Molybdenum Disulfide-based Polyaniline Nanointerfaces for Enhanced Direct Electrochemical DNA Detection. *Adv. Mater. Interfaces* 2016, 3, 1500700.

51. Wang, J.; Wu, Z.; Yin, H.; Li, W.; Jiang, Y. Poly (3, 4-ethylenedioxythiophene)/MoS2 Nanocomposites with Enhanced Electrochemical Capacitance Performance. *RSC Adv. 2014, 4, 56926-32.*

52. Jang, A.; Zou, Z.; Lee, K. K.; Ahn, C. H.; Bishop, P. L. Potentiometric and Voltammetric Polymer Lab Chip Sensors for Determination of Nitrate, pH and Cd (II) in Water. *Talanta* 2010, 83, 1-8.
53. Nolan, M. A.; Tan, S. H.; Kounaves, S. P. Fabrication and Characterization of a Solid State Reference Electrode for Electroanalysis of Natural Waters with Ultramicroelectrodes. *Anal. Chem*. 1997, 69, 1244-7.

54. Bates, R. G. Macaskill, J. B. Standard Potential of the Silver-Silver Chloride Electrode. Pure Appl. *Chem.* 1978, 50, 1701-6.

55. Bakker, E.; Pretsch, E. Potentiometric Sensors for Trace-Level Analysis. *Trends Anal. Chem.* 2005, 24, 199-207.

56. Bakker, E. Selectivity of Carrier-based Ion-Selective Electrodes: is the Problem Solved? *Trends Anal. Chem*. 1997, 16, 252-60.

57. Baker, M. A.; Gilmore, R.; Lenardi, C.; Gissler, W. XPS Investigation of Preferential Sputtering of S from MoS2 and Determination of MoSx Stoichiometry from Mo and S peak Positions. *Appl. Surf. Sci*. 1999, 150, 255-62.

58. Wang, F.; Mori, K.; Oishi, Y. Electrochemical Polymerization of 6-(N-allyl-1, 1, 2, 2-Tetrahydroperfluorodecyl) Amino-1, 3, 5-Triazine-2, 4-Dithiol Monosodium on Aluminum. *Polym. J.* 2006, 38, 484.

59. Buck, R. P.; Lindner, E. Recommendations for Nomenclature of Ionselective Electrodes (IUPAC Recommendations 1994). *Pure Appl. Chem*. 1994, 66, 2527-36.

60. Cuartero, M.; Crespo, G. A.; Bakker, E. Tandem Electrochemical Desalination–Potentiometric Nitrate Sensing for Seawater Analysis. *Anal. Chem*. 2015, 87, 8084-9.

61. Bendikov, T. A.; Kim, J.; Harmon, T. C. Development and Environmental Application of a Nitrate Selective Microsensor based on Doped Polypyrrole Films. Sens. *Actuators B Chem*. 2005, 106, 512-7.

62. Garland, N. T.; McLamore, E. S.; Cavallaro, N. D.; Mendivelso-Perez, D.; Smith, E. A.; Jing, D.; Claussen, J. C. Flexible Laser-Induced Graphene for Nitrogen Sensing in Soil. *ACS Appl. Mater. Interfaces* 2018, 10, 39124-33.

63. Chaneam, S.; Taweetong, W.; Kaewyai, K.; Thienwong, P.; Takaew, A.; Chaisuksant, R. Fabrication of a Nitrate Selective Electrode for Determination of Nitrate in Fertilizers by using Flow Injection Analysis System. *Procedia Chem*. 2016, 20, 73-5.

64. Khripoun, G. A.; Volkova, E. A.; Liseenkov, A. V.; Mikhelson, K. N. Nitrate-Selective Solid Contact Electrodes with Poly (3-Octylthiophene) and Poly (aniline) as Ion-to-Electron Transducers Buffered with Electron-Ion-Exchanging Resin. *Electroanalysis* 2006, 18, 1322-8.

65. Rudd, S.; Dalton, M.; Buss, P.; Treijs, A.; Portmann, M.; Ktoris, N.; Evans, D. Selective Uptake and Sensing of Nitrate in Poly (3, 4-ethylenedioxythiophene). *Sci. Rep*. 2017, 29, 16581.

66. Wardak, C. Solid Contact Nitrate Ion-Selective Electrode Based on Ionic Liquid with Stable and Reproducible Potential. *Electroanalysis* 2014, 26, 864-72.

67. Pięk, M.; Piech, R.; Paczosa-Bator, B. All-solid-state nitrate selective electrode with graphene/tetrathiafulvalene nanocomposite as high redox and double layer capacitance solid contact. *Electrochim. Acta* 2016, 210, 407-14.

68. Paczosa-Bator, B. Effects of type of nanosized carbon black on the performance of an all-solid-state potentiometric electrode for nitrate. *Microchim. Acta* 2014, 181, 1093-9.

69. Pięk, M.; Piech, R.; Paczosa-Bator, B. Improved nitrate sensing using solid contact ion selective electrodes based on TTF and its radical salt. *J. Electrochem. Soc*. 2015, 162, B257-63.

70. Umezawa, Y.; Bühlmann, P.; Umezawa, K.; Tohda, K.; Amemiya, S. Potentiometric Selectivity Coefficients of Ion-Selective Electrodes. Part I. Inorganic cations (technical report). *Pure Appl. Chem*. 2000, 72, 1851-2082.

71. Nägele, M.; Bakker, E.; Pretsch, E. General Description of the Simultaneous Response of Potentiometric Ionophore-based Sensors to Ions of Different Charge. *Anal. Chem*. 1999, 71, 1041-1048.

CHAPTER 7. CONCLUSION

We have developed four silver/silver chloride reference electrodes with different structures and characteristics to address the challenges of reference electrodes that hinder the fast development of modern potentiometry, including the stability, miniaturization, cost efficiency, and immunity from interferences. The development of these four reference electrodes will benefit the electrochemical analysis in multiple applications, such as the environmental trace analysis, potentiometric biosensing, food safety supervision, and fertilizer management in agriculture, etc.

First, a reference electrode (RE) based on a serpentine microfluidic channel was developed. Owing to the channel structure, good long-term stability was achieved, and in comparation with the traditional glass body Ag/AgCl REs, the dimensions of the present RE were also largely reduced. In addition, gelatin mixed with 1 M KCl was filled inside the channel to work as the inner filling electrolyte to obtain a wide working temperature range. Moreover, we demonstrated that by integrating the present RE with a MOSFET and a nitrate sensitive ion-selective electrode (ISE) to form an extended gate filed effect transistor, it is possible to obtain a highly sensitive nitrate sensor with a high slope of -202.96±5.55. Further research and development remain to be done to improve the response time of the present RE for applications in which instant reading is required. This RE with serpentine microfluidic channel is expected to lead to the establishment of a powerful and cost-efficient platform for long-term measurement, such as pollution monitoring in river.

Second, we developed a miniaturized Ag/AgCl RE with a straight micro-channel serving as the salt bridge to allow ions to diffuse between the inner and outer electrolytes. Owing to the micro-channel, not only the porous frit or disk used in conventional liquid-state

Ag/AgCl REs was eliminated, but also it helped to reduce the manufacturing cost. Moreover, traditional soft lithography technique was employed for the fabrication process to realize an economical and reproducible mass production. Although the long-term stability of the present RE is not comparable with the traditional Ag/AgCl REs, the feature design of the miniaturized RE allows an easy integration of it with other ISEs to form portable devices, which are suitable for one-time or short-term measurements due to its short response time and small footprint size.

Third, we developed a refillable planar double-junction Ag/AgCl RE with gelatin mixed with 1M potassium chloride (KCl) as the internal filling electrolyte and 0.1 M lithium acetate (CH_3COOLi) as the intermediate filling solution. We demonstrated that by using double-salt bridge approach, it is possible to reduce the sensitivity of the RE's stability to chloride ion, temperature and pH. Additionally, high response speed and good stability were also achieved for this present double-junction RE. A nitrate sensor based on the present RE was built to prove that the planar double-junction RE has the performance comparable with the traditional REs. Even though the present RE has higher fabrication cost compared with single junction REs, the device can be refurnished by replacing the inner and outer filling electrolytes thanks to the four pairs of mini magnets, which made the present planar double-junction RE become a detachable device. To our knowledge, this is the first effort to realizing a planar refillable RE for its inner and outer electrolytes. This presented RE will offer a suitable RE for precise ion detection applications.

Fourth, a sandwiched all-solid-state Ag/AgCl RE (S^3RE) was developed to form real solid-state potentiometric sensors which has become an evitable trend in modern potentiometry due to the high demand in reliable, economical, simple and miniaturized ISE sensors. A thin

layer of mixture of polyvinyl butyral (PVB) and KCl was utilized as the ion-electron transductor and another thin layer of aromatic polyurethane (PU) was deployed as the protection layer. Good performance comparable with the traditional liquid state REs, in terms of stability, chloride susceptibility and working temperature and pH range was obtained for this present S^3RE. Further study remains to be done regarding its sensitivity to electrostatic, repeatability and lifetime. This presented S^3RE is likely to provide a novel insight for potentiometric measurement and extend its usage to some new applications. Therefore, two novel applications of potentiometric nitrate sensors based on our presented solid-state REs to continuously monitor the nitrate in soil and corn stalks were demonstrated. Both of the applications are aimed at improving the fertilizer management in agriculture to ensure the crop production and meanwhile sustain the environment. Our presented solid-state REs were proven to be able to provide a suitable RE for this kind of applications.

Lastly, the performance comparison between the four REs described in this thesis and those reported in other literatures is summarized in table 8.1.

Table 7.1 The performance of reference electrodes presented in this thesis in comparison with other silver/silver chloride reference electrodes reported in the literatures

Sensor type	Electrolyte	Sensor dimension (length× width× height, mm×mm× mm	Chloride susceptibility	Long-term stability	Response time (minutes)	Temperature effect (mV) (from 20 to 70 ºC)	pH effect (mV) (from 3 to 11)	Ref.
Gel state	Gelatin with 1M KCl saturated with AgCl	22 × 22 × 5	4.2 $mvdec^{-1}$	Stabilized for first 7.5 days 37 µV/hr	20 (high to low) 5 (low to high)	7	5	This work (RE with microfluidic channel)
Liquid state	3M KCl saturated with AgCl	4 × 4 × 5	3 $mVdec^{-1}$ ($KCl < 10^{-3}$)	0.52 mV/hr for first 5 days	5 (high to low) <1 (low to high)	10	8	This work (RE with micro - channel)

Table 7.1 (continued)

Double junction	Inner: gelatin with 1M KCl saturated with AgCl Outter: 0.1M CH_3COOLi	30 × 18 × 7	0.22 $mVdec^{-1}$	Stabilized for first 10 days -75 µV/hr	10 (high to low) <1 (low to high)	9	0.72	This work (planar RE with double junction)
All-solid state	PVB with 3M KCl saturated with AgCl	10 × 25 × 0.5	5 $mVdec^{-1}$	104 µV/hr	3 (high to low) <1 (low to high)	30	25	This work (S^3RE)
Solid state	PDMS with saturated KCl	12 × 28	N/A	Stable for 70 days	120	N/A	N/A	[1]
All-solid state	Crystalline KCl melt	N/A	N/A	1mV drift for 3 months	A few minutes	N/A	3 mV (from 1.68 to 9.18)	[2]
Gel state	Agar with 0.1M KCl	N/A	N/A	20 µV/hr	N/A	N/A	N/A	[3]
Solid state	PVB with NaCl and $AgNO_3$	N/A	<1 $mVdec^{-1}$	90±33 µV/hr	N/A	N/A	0.18 mV/pH (from 4 to 10)	[4]
All-solid state	PVC with ionic liquid	5 × 5 × 0.5	±8 mV change (10^{-6} < KCl <10^{-2})	0.25-0.45 mV/hr for 14 hours	N/A	N/A	N/A	[5]
All-solid state	Protective paste with KCl	4 × 24	105 mV change (10^{-6} < KCl <10^{-2})	0.2-0.6 mV/hr	N/A	N/A	2 mV (from 2 to 13)	[6]
Liquid state	1M KCl	N/A	N/A	3-0.03 mV/day for 15 days	1.1±0.5 s in acidic 2.9±1.7 s in alkaline	N/A	500 mV (from 4 to 10)	[7]
Solid state	Ag/AgCl paste	N/A	-51.12±0.45 $mVdec^{-1}$	Stable for 6 months	N/A	N/A	N/A	[8]
Solid state	PVC with KCl	N/A	N/A	-9.1±0.6 mV within 13 hrs	N/A	N/A	N/A	[9]
Solid state	PEDOT	N/A	50-60 mV change 0.1M < KCl < 1M	3.5-4.5 mV/hr	N/A	N/A	4.1 mV deviation (from 7 to 4.1)	[10]

References

1. Shitanda, Isao, Hiroyuki Kiryu, and Masayuki Itagaki. "Improvement in the long-term stability of screen-printed planar type solid-state Ag/AgCl reference electrode by introducing poly (dimethylsiloxane) liquid junction." *Electrochimica Acta* 58 (2011): 528-531.

2. Vonau, W., et al. "An all-solid-state reference electrode." *Sensors and Actuators B: Chemical* 144.2 (2010): 368-373.

3. Simonis, Anette, et al. "Miniaturised reference electrodes for field-effect sensors compatible to silicon chip technology." *Electrochimica acta* 51.5 (2005): 930-937.

4. Guinovart, Tomàs, et al. "A reference electrode based on polyvinyl butyral (PVB) polymer for decentralized chemical measurements." *Analytica chimica acta* 821 (2014): 72-80.

5. Mamińska, Renata, Artur Dybko, and Wojciech Wróblewski. "All-solid-state miniaturised planar reference electrodes based on ionic liquids." *Sensors and Actuators B: Chemical* 115.1 (2006): 552-557.

6. Tymecki, Łukasz, Elżbieta Zwierkowska, and Robert Koncki. "Screen-printed reference electrodes for potentiometric measurements." *Analytica Chimica Acta* 526.1 (2004): 3-11.

7. Zevenbergen, M. A. G., et al. "Solid state pH and chloride sensor with microfluidic reference electrode." *2016 IEEE International Electron Devices Meeting (IEDM). IEEE*, 2016.

8. Cranny, Andrew, et al. "Screen-printed potentiometric Ag/AgCl chloride sensors: Lifetime performance and their use in soil salt measurements." *Sensors and Actuators A: Physical* 169.2 (2011): 288-294.

9. Dam, Van Anh T., Martijn Goedbloed, and Marcel AG Zevenbergen. "Solid-Contact Reference Electrode for Ion-Selective Sensors." *Multidisciplinary Digital Publishing Institute Proceedings*. Vol. 1. No. 4. 2017.

10. Zuliani, Claudio, Giusy Matzeu, and Dermot Diamond. "A liquid-junction-free reference electrode based on a PEDOT solid-contact and ionogel capping membrane." *Talanta* 125 (2014): 58-64.

APPENDIX A. HOME MADE DATALOGGER

A.1 Overview Design

The datalogger was designed for both indoor and outdoor applications. It consists of four modules: power module, read-out circuit module, micro-controller module and data transmission module. The physical photo of the homemade datalogger is shown in Figure A.1, and its flow chart is shown in Figure A. 2. In this figure, the orange arrows represent power transmission, the blue arrows represent data transmission and the black arrows represent general connection. The power module provides the power for the whole system. The read-out circuit capture the electrical voltage potential coming from the sensor electrodes, and then transmits the signal to the micro-controller for data processing. The processed data can be either stored into a micro SD card or be wirelessly transmitted by Bluetooth. The user can directly see the data through their smart devices, such as cell phone or iPAD. Each module will be described in the following sections.

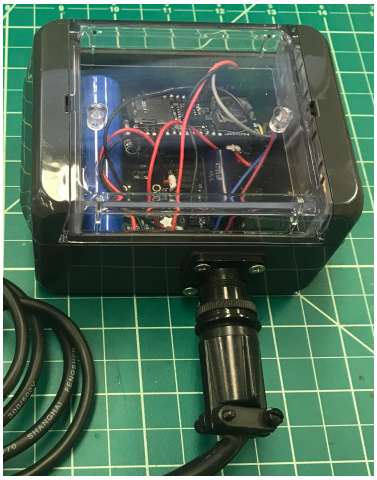

Figure A.1 *Physical photo of the home-made datalogger.*

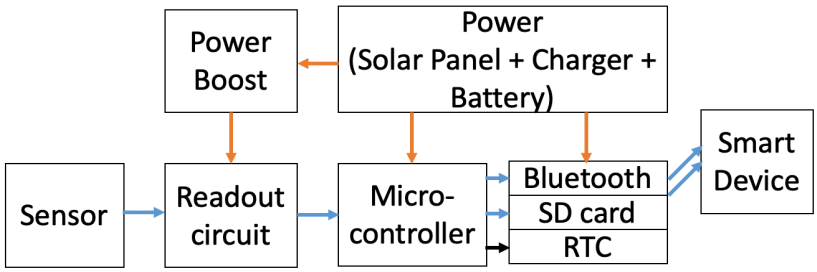

Figure A.2 *Flow chart of the electrical system used for home-made datalogger.*

A.2 Power Module

For portable and outdoor devices power management is one of the most significant considerations. Thus, the power module is designed to provide enough and consecutive power for the entail system. It is made up of four individual parts, including solar panel (Voltaic Systems -6V 2W), battery (Lithium Ion Battery Pack - 3.7V 6600mAh), charger (Lithium Ion Battery Charger v2 from Adafruit) and power boost (Power Boost 1000 Basic -5V). By using the solar panel, on one hand it is friendly to the environment, and on the other hand it is not necessary to charge the battery indoor anymore. Thus, it is perfect for outdoor projects, especially with the help of the Lithium Ion battery charger. This charger is produced by Adafruit Inc, and it can be easily used to charge 3.7V/4.2V Lithium battery with 5-6 DC, USB or 6V solar panel. This charger is a unique design, for example, when the charger is connected to a good power source, such as strong sunshine or from a USB port, the load current goes directly from the input voltage to the output. If the current required is higher than what the panel or USB port can provide, the current is supplemented by the Lithium battery, up to 1.8A, while if the current required is lower than what the panel can provide, the current goes to charge the battery, so that you do not lose efficiency form charging/discharging the battery. Another very important component for this power module is the power boost. The voltage coming out

from the Lithium battery is 3.7V, however, the voltage required by the read-out circuit, introduced later, is 5V. Thus, a power boost 1000 is selected to get the required power. This little DC/DC boost converter can run from 1.8V batteries or higher and convert that voltage to 5.2V DC for running 5V projects. Therefore, the designed power module is perfect for power-hungry portable device.

A.3 Read-Out Circuit Module

The read-out circuit is used to capture the electrical voltage potential coming out from the sensor electrodes, and then transmit it to the microcontroller for data processing and transmission. The schematic of this readout circuit is shown in Figure A. 3.

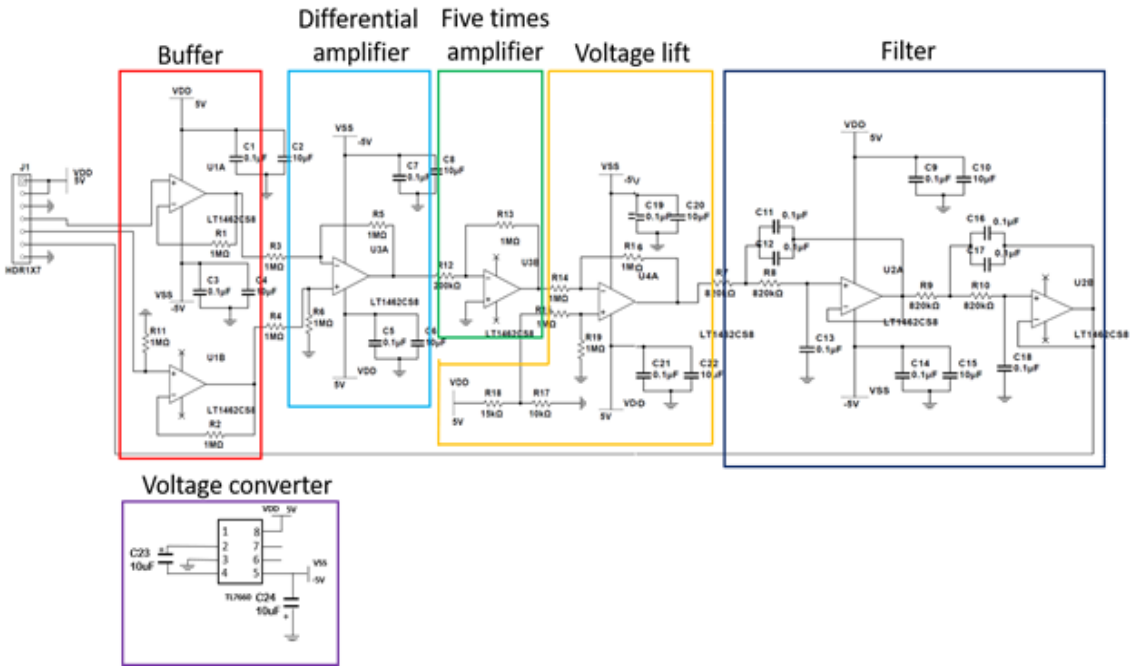

Figure A.3 *Schematic of the read-out circuit.*

This readout circuit consists of five stages and one voltage converter. The first stage is two buffer circuits used to insulate the inputs coming from the sensor electrodes with the

following stages. The second stage is one differential amplifier with one magnification factor to get the required electrical voltage potential of the sensing unit. The third stage is an inverting amplifier to amplify the voltage potential, and its magnification factor can be changed by adjusting the values of R11 and R12. The fourth stage is a voltage lift circuit made of a differential amplifier with one magnification factor. The reason why we need this stage is that the voltage potential from the sensors can be either positive or negative, however, the microcontroller can only read positive voltage. To capture all the data, we need to lift the voltage to prevent the losing of negative data. The voltage value lifted by the fourth stage can be changed by adjusting the values of R17 and R18. The fifth stage is a two-order filter with 1 Hz cut-off frequency. The last part of the circuit is a single negative voltage converter, which converts 5 V to -5 V used as the negative power supply for the amplifier.

The input range for this read-out circuit with all the components' values shown in Figure A. 2 is from -400 mV to 400 mV. This range can be changed by adjusting the magnification factor of the third stage and the lift value of the fourth stage. It is quite flexible.

A.4 Micro-Controller

Adafruit Feather 32u4 is selected to work as the micro-controller board in this device based on the following factors: firstly, the dimension of this board is small, 51mm x 23mm x 8mm. Secondly, its power consumption is low. So, it is suitable to build portable device. Last not least, it has a build in Bluetooth module, which is required for data wireless transmission introduced later. The micro-controller chip for this board is ATmega32u4 @8MHz with 3.3 logic/power. This chip has 20 GPIO pins, 10 analog inputs, hardware serial, hardware I2C, and hardware SPI support. These functions are enough to meet our requirements for the micro-controller.

A.5 Data Transmission

There are two options for the data storage. The first way is to directly save all the data into a micro SD card. To do that, a SD add-on board (Adalogger FeatherWing - RTC + SD Add-on For All Feather Boards) is needed. The good thing for this add-on board is that it can be directly added on the top of the Adafruit Feather 32u4 board. So, no additional wiring up is needed. Besides, this add-on board has a real-time clock (PCF8523), thus, it can provide timestamp for every data. This function is very helpful for data tracking. However, there is one disadvantage for this option. Because all the data are directly saved into the SD card, unless the user take out the SD card, he or she cannot view the data. Thus, this way is usually used as data backup.

The second option for data storage is using the Bluetooth module to wirelessly transmit the data to user's smart devices. The APP installed on user's smart device can allow the real-time data observation and save data into their device or database. The disadvantage for this option is the higher power consumption compared with the first way. But thanks to the power module design in this device, the energy is enough to support the Bluetooth function.

APPENDIX B. POT-MOS$_2$ BASED NITRATE ELECTRODE

Table B.1. Values of potential drifts per second (ΔE/Δt) and capacitate for different electrode materials (POT, MoS_2 and POT-MoS_2)

Nitrate Selective Electrode materials	ΔE/Δt (μV/s)	C (μF)
POT	115.4	433
MoS_2	213.3	234
POT-MoS_2	95.0	526

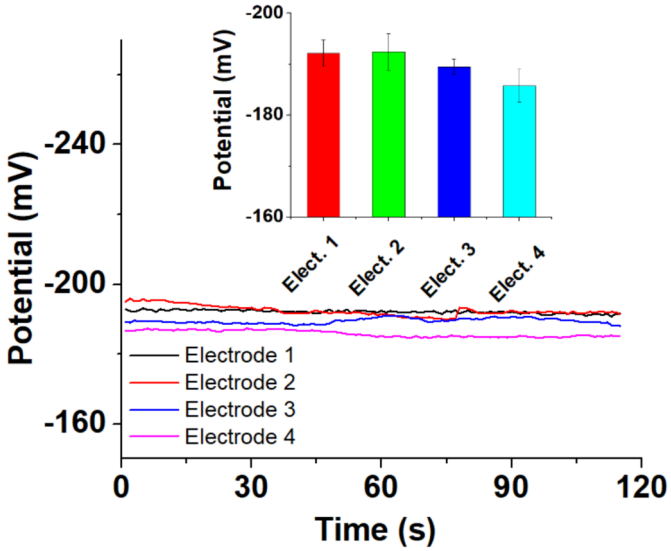

Figure B.1 *Reproducibility studies for POT-MoS_2 based sensor with individual identical copies of the electrode.*

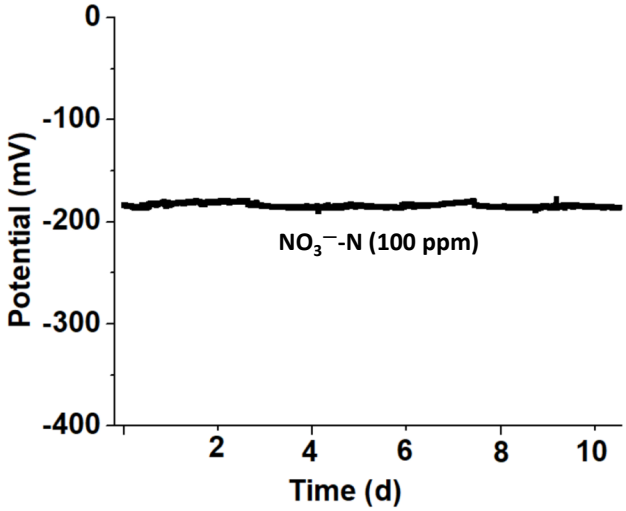

Figure B.2 *The potential stability of the sensor (ISM/POT-MoS_2) for nitrate-nitrogen detection. In this measurement, the ISM/POT-MoS_2 electrode was conditioned for 3 d at high concentration of nitrate-nitrogen (1500 ppm) and inserted an open vial filled with 100 ppm of nitrate-nitrogen for long-term stability measurement. Results show the initial potential (starting potential ~-184 mV) is almost matched after 10 days of potential measurement (end potential ~ -186 mV). However, it has been seen the there is a potential variation of 0.2 mV per day during continuous measurement.*

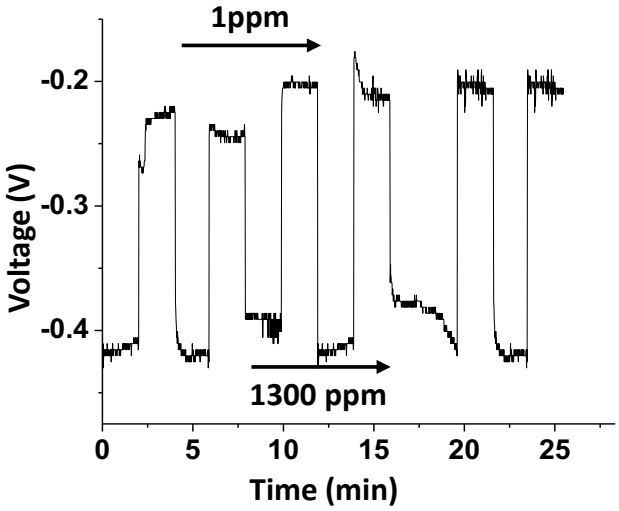

Figure B.3 *Activity of high (1300 ppm) and low (1ppm) concentration nitrate-nitrogen was performed to investigate the repeatability of the electrode.*